Université du Québec

Centre
Eau Terre Environnement

INRS Institut national de la recherche scientifique

THREE-DIMENSIONAL STOCHASTIC ASSIMILATION OF GRAVITY AND DC RESISTIVITY DATA AT THE LALOR VOLCANOGENIC MASSIVE SULPHIDE DEPOSIT, MANITOBA, CANADA

Par

Shiva Tirdad

Thèse présentée pour l'obtention du grade de
Philosophiæ Doctor, Ph.D.
en sciences de la Terre

Jury d'évaluation

Président du jury et examinateur interne	Nicolas Pinet Commission géologique du Canada
Examinateur externe	Gilles Bellefleur Commission géologique du Canada
Examinateur externe	Pejman Shamsipour GoldSpot Discoveries
Directeur de recherche	Erwan Gloaguen INRS-ETE Université du Québec
Codirecteur de recherche	J. Christian Dupuis Dép. de géologie et génie géologique Université Laval

ACKNOWLEDGEMENTS

First of all, I would like to thank my supervisor, Erwan Gloaguen; Thank you for helping me to push myself beyond what I thought I was capable of and for supporting me and caring throughout these years. It was a true pleasure working with you.

I would also like to thank my co-supervisor Christian Dupuis, for all the discussions, comments and corrections. I greatly appreciate your advice and wisdom during my PhD studies.

Thank you to the members of the jury Nicolas Pinet, Gilles Bellefleur and Pejman Shamsipour for accepting to take a critical look at my work, for the time you spent reading and judging this thesis so constructively.

I would also like to thank Abderrezak Bouchedda for all the discussions we had about the data and the models. Thank you for your help and collaboration.

A big thank you also to Martin Blouin for allowing me to use the code that he developed for the Bayesian sequential simulation algorithm.

I am also very thankful to Ble Jean Fidele Yrro for all the help with the gradual deformation method and GOCAD.

I also want to thank my office friends and colleagues, Cecilia, Mafalda, Maria Isabelle, Simon, Nicolò, Pier Paolo, Guilleume and Marie-Amélie. These years were most enjoyable next to you.

I would also like to express my gratitude to Hudbay Minerals Inc and Mira geoscience for providing us with the data of the Lalor deposit and Antoine Caté for providing the geological surfaces of the study area. I would also like to acknowledge the Canada Chair in stochastic data assimilation for 3D geological modeling and FRQNT program for partnership with the mining sector.

Finally, a big thanks to my family; my parents and my siblings who have always supported me unconditionally. All of this would have been simply impossible without you. Thank you to Ali, my rock, my companion, my best friend for your unwavering support, your continuous encouragement and your patience throughout these years.

ABSTRACT

We propose a new numerical workflow based on stochastic data integration where we merge a conceptual geological model, the drillhole geophysical and geological logs as well as surface and borehole geophysical data to compute a unified numerical model of a volcanogenic massive sulphide (VMS) deposit. The first step of the workflow consists in building a 3D numerical conceptual model of the geology by a geologist. This conceptual model as well as geological logs are then used to generate multiple equiprobable scenarios of the geology by means of multiple-point simulation (MPS). The MPS method studies high-order statistics in the space of a numerical conceptual model making it possible to reproduce complex geological structures. We then use conventional conditional sequential Gaussian simulation, which is a method based on a node-by-node sequential process to stochastically populate the geological grid with densities. For this purpose we use available density logs to simulate multiple equiprobable spatial distributions of the density at high spatial resolution within each geological unit separately. The stochastic high-resolution density models are iteratively combined by the gradual deformation method in order to minimize the difference between measured Bouguer anomaly data and the data computed on the combined realizations of density. Application of the proposed method to the Lalor deposit, a VMS in Manitoba, Canada, produces a density model that honors the geology of the deposit and the Bouguer anomaly data. The optimized density models and borehole conductivity logs are then fed to Bayesian sequential algorithms to compute 3D conductivity models that can explain the field measurements. The conductivity model goes through another gradual deformation optimization step where the objective function is to minimize the difference between raw and computed electrical potentials. The unified petrophysical model built with our method is geologically meaningful and considers the spatial variability so as the uncertainty inherent to each method. It has the advantage to include all the available information (geological and geophysical logs and surface and borehole geophysics) at scales appropriate for mining applications.

Keywords Stochastic inversion, Data assimilation, Gravity data modeling, Multiple-point simulation, Bayesian sequential simulation, DC resistivity modeling, Gradual deformation method

RÉSUMÉ

Nous proposons un nouveau flux de travail numérique reposant sur l'intégration stochastique de données dans lequel nous combinons un modèle géologique conceptuel, les diagraphies géophysiques et les descriptions géologiques sur les carottes, ainsi que les données géophysiques de surface et de forage pour obtenir un modèle numérique unifié d'un gisement sulfure massif volcanogéne. La première étape du flux de travail consiste en l'élaboration d'un modèle conceptuel numérique 3D de la géologie par un géologue expert de la zone à l'étude. Ce modèle conceptuel ainsi que les diagraphies géologiques sont utilisés pour produire cent scénarios équiprobables de la géologie au moyen de la simulation multipoints (SMP). La méthode SMP est utilisée, car elle permet de tenir en compte les statistiques d'ordre supérieur dans l'espace du modèle numérique conceptuel, rendant ainsi possible la reconstitution de structures géologiques complexes. Nous utilisons ensuite la simulation séquentielle gaussienne conditionnelle classique, une méthode basée sur un processus séquentiel noeud-par-noeud pour peupler de manière stochastique la grille géologique par des valeurs de densité hétérogènes. À cette fin, nous utilisons des diagraphies de densité disponibles pour simuler différentes distributions spatiales équiprobables de la densité à haute résolution spatiale dans chaque unité géologique. Les modèles de densité stochastiques de haute résolution sont itérativement combinés par la méthode de déformation graduelle afin de minimiser la différence entre les données d'anomalie de Bouguer mesurées et les données obtenues des réalisations combinées de la densité. L'application de la méthode proposée au gisement de Lalor, un gisement de sulfures massifs volcanogènes au Manitoba (Canada), produit un modèle de densité qui reflète bien la géologie du gisement et les données d'anomalie de Bouguer. Les modèles optimisés de densité et les conductivités de forage sont ensuite transmis aux algorithmes séquentiels bayésiens afin de calculer des modèles 3D de conductivité pouvant expliquer les mesures de champ. Le modèle de conductivité passe par une autre étape d'optimisation de la déformation graduelle dans laquelle l'objectif est de minimiser la différence entre les potentiels électriques bruts et calculés. Le modèle pétrophysique unifié construit avec notre méthode est géologiquement réaliste et prend en compte la variabilité spatiale ainsi que l'incertitude inhérente à chaque méthode. Il présente l'avantage de l'intégration et le couplage de toutes les informations disponibles (diagraphies géologiques et géophysiques et les mesures géophysiques en surface et en forage) à des échelles convenant à des applications minières.

Mots-clés Inversion stochastique, Assimilation de données, Modélisation de données gravimétriques, Simulation multipoints, Simulation séquentielle bayésienne, Modélisation de la résistivité en courant direct, Méthode de la déformation graduelle

SOMMAIRE RECAPITULATIF

Introduction

À travers le monde, 60% des projets miniers ne rencontrent pas leurs objectifs financiers après cinq ans d'exploitation et ont une production inférieure à 70% des capacités estimées (Vallée, 2000). Pour un projet minier, la première étape après la découverte consiste à réconcilier les données de forages entre elles, ainsi qu'avec les données géophysiques, géochimiques et géologiques afin de construire un modèle géologique unifiant le plus de connaissances possibles. Les experts de l'industrie associent l'échec financier des projets miniers à l'inexactitude des modèles géologiques et à l'ignorance de l'incertitude inhérente aux données disponibles. Les lacunes principales sont la compartimentation des expertises lors de la construction des modèles, l'utilisation d'outils non appropriés pour l'interpolation des mesures en forage et l'absence d'utilisation d'algorithmes d'assimilation quantitative des données géologiques et géophysiques. Les méthodes géophysiques ne sont souvent utilisées qu'à des fins d'exploration et ne sont pas ou peu prises en compte lors de la construction des modèles géologiques. La raison principale est due au design d'acquisition des données géophysiques qui n'est pas optimisé pour l'estimation des ressources, mais aussi au traitement même des données qui sur-lisse les images des propriétés physiques (Fullagar et al., 2008). Cet effet de lissage fait en sorte que les modèles géophysiques n'ont plus la résolution et la corrélation suffisantes pour être comparés aux propriétés mesurées en forages ou sur carottes (Dubreuil-Boisclair et al., 2012). L'objectif de ce projet est l'amélioration de l'assimilation quantitative de toutes les informations disponibles (géologie, propriétés physiques, géophysiques) pour construire un modèle pétrophysique plus fiable d'un gisement qui honore, le mieux possible, toutes les données disponibles. En effet, les méthodes conventionnelles d'inversion conjointe ne permettent pas d'intégrer de manière optimale des données de sources multiples ayant des résolutions différentes. Dans les faits, le modèle final d'une inversion conjointe est un modèle ayant la résolution proche de la résolution de la méthode ayant la plus basse résolution et il n'a souvent aucun sens géologique (Doyen, 2007). Dans le domaine pétrolier, plusieurs de ces problématiques ont été résolues récemment (Doyen, 2007). À cette fin, tous les experts agissent de concert à toutes les étapes de la construction des modèles géologiques et d'hydrocarbure en place (Dubrule, 2003).

De plus, les mesures géophysiques (sismique réflexion) sont acquises de manière à répondre aux exigences de l'exploration, mais aussi afin de pouvoir estimer de manière précise les propriétés physiques. De plus, lors des forages d'exploration, un ensemble de diagraphies est toujours mesuré afin d'établir les relations statistiques entre les paramètres physiques et les paramètres géologiques d'intérêt. Une fois modélisées, ces relations entre les propriétés physiques et géologiques mesurées aux puits pourront éventuellement être utilisées pour traduire les mesures géophysiques en propriétés géologiques en dehors des forages (Doyen, 2007). Cependant, les mesures géophysiques de surface et de puits n'ont pas la même résolution, ne mesurent pas les phénomènes à la même échelle et ont des erreurs de mesure différentes. C'est la raison pour laquelle, depuis une dizaine d'années, de nouvelles méthodes d'assimilation de données ont été développées dans le domaine pétrolier (Dubreuil-Boisclair et al., 2012; Claprood et al., 2013) mais aussi en environnement (Ruggeri et al., 2013). Bien que les systèmes de déposition des gisements miniers soient généralement plus complexes que dans le domaine pétrolier, il y a de nombreuses méthodes développées en modélisation des réservoirs qui peuvent être adaptées pour la caractérisation des sites miniers. Par exemple, Perozzi et al. (2012) ont montré qu'il était possible d'utiliser les données de tomographie sismique entre forages afin d'estimer les teneurs en Ni, Cu, Co du gisement de Voysey's Bay. De manière plus prosaïque, mon projet de doctorat consistait à développer un algorithme d'inversion stochastique de gravité et conductivité électrique contraint par les données géophysiques en forages et de surface et par le modèle géologique conceptuel construit par des géologues. Une des raisons majeures de la non-utilisation des modèles géophysiques dans le modèle de teneur est leur manque de résolution spatiale. Ce manque de résolution est dû à deux causes : la résolution intrinsèque des méthodes géophysiques utilisées et le lissage dû au processus d'inversion (passage de la mesure géophysique au modèle 3D de la propriété physique associée). L'effet de lissage est d'autant plus grand que la profondeur du gisement est importante (ex : le gisement de Lalor est situé de 570 m à 1170 m de profondeur). Certaines solutions proposent de faire de l'inversion contrainte par les diagraphies. Cependant, les résultats sont souvent complexes à analyser (la résolution augmente lorsqu'on s'approche des forages et diminue plus on s'en éloigne s'il n'y a pas de contrôle structural), ces inversions impliquent des hypothèses très fortes sur les effets d'échelles entre la mesure en forage et la résolution géophysique et elles reposent sur une hypothèse de stationnarité stricte des propriétés physiques, ce qui est irréaliste dans le cas de gisements (changements brusques des propriétés entre les zones minéralisées et les zones non-minéralisées). De plus, comme ces inversions sont réalisées de manière indépendante, la plupart du temps, elles ne respectent ni

le modèle géologique ni les relations pétrophysiques. À cette étape, nous proposons d'adapter la méthode d'inversion stochastique bayésienne qui a été développée pour le domaine pétrolier par Dubreuil-Boisclair et al. (2012). Le point de départ de cette méthode est le modèle géologique conceptuel 3D (en accord avec la géologie régionale et les relations pétrophysiques). Ce modèle est utilisé comme modèle de base pour générer de manière stochastique plusieurs scénarios géologiques 3D respectant les données géologiques en forage, mais aussi le modèle conceptuel. Ensuite, chaque unité géologique est peuplée par des propriétés physiques respectant les relations pétrophysiques. Cette étape permet de produire des modèles pétrophysiques à la résolution des diagraphies. La modélisation des mesures géophysiques de surface est calculée sur chaque modèle pétrophysique associé et comparée aux données géophysiques mesurées (mesures électriques DC, gravimétrie). Il est à noter que cette méthodologie ne requiert aucune inversion déterministe et que chaque modèle pétrophysique est à très haute résolution. Comme nous calculons uniquement des modèles directs, il n'y a pas de problème de compatibilité entre les résolutions et les échelles des différentes mesures. En revanche, il se peut que, localement, les modèles simulés soient inadéquats. C'est pourquoi la dernière étape consiste à combiner de manière globale ou locale les différents modèles afin de minimiser l'écart entre les mesures géophysiques de surface et de forage calculées et mesurées.

Objectifs

Mon projet de doctorat a consisté à développer de nouveaux outils numériques de modélisation stochastique pour l'assimilation de données de sources multiples afin d'améliorer la justesse des modèles pétrophysiques en trois dimensions et d'en évaluer leur incertitude. L'objectif technique de ce travail a été d'étudier les relations pétrophysiques entre les données de forages et de construire des modèles pétrophysiques stochastiques. Ces modèles sont contraints par (1) le modèle conceptuel, (2) les données géochimiques (puisque le modèle conceptuel est construit en utilisant les données géochimiques), (3) les données géophysiques à haute résolution mesurées en forages et (4) les mesures géophysiques de surface. Ils consistent donc en un ensemble de modèles unifiant toutes les connaissances sur le gisement à un moment donné d'un projet.

Contributions

Les différentes problématiques abordées dans ma thèse ont nécessité des développements théoriques, méthodologiques et algorithmiques. Ces trois aspects sont indissociables; les méthodes d'acquisition des données sur le terrain doivent être guidées par les connaissances géologiques, les développements théoriques et algorithmiques doivent répondre à des problématiques géologiques et tous les modèles numériques résultants doivent impérativement respecter les concepts géologiques. Même si ces affirmations semblent triviales, elles constituent des défis scientifiques importants pour lesquels il n'existe que peu de réponses actuellement. L'innovation de mon projet de recherche concerne l'intégration et le couplage de plusieurs mesures géophysiques et géologiques ayant des résolutions spatiales très différentes par le développement de méthodes géostatistiques novatrices, en vue de maximiser la justesse et la précision des modèles de propriétés physiques d'un gisement SMV (sulfures massifs volcanogènes). Bien que la méthodologie ait été développée pour ce type de gisement en raison de l'acquisition de données physiques en forages pour la caractérisation du gisement SMV de Lalor, la méthodologie est générale et peut être transposée à de nombreux gisements. En plus des répercussions dans le domaine minier, les avancées scientifiques ont des applications dans la réhabilitation des aquifères contaminés et dans la gestion et la protection des ressources en eau souterraine et des systèmes d'approvisionnement en eau, l'optimisation des opérations pétrolières et la connaissance du potentiel de stockage du CO_2 dans les couches géologiques profondes du Québec. Ces retombées constituent une contribution importante, non seulement pour l'avancement des connaissances, mais aussi pour le transfert de nouvelles technologies vers les milieux de pratique. Durant ma thèse, j'ai publié un article dans le numéro spécial sur la géophysique minière au Canada dans le journal Canadien des Sciences de la Terre (Tirdad et al., 2019). J'ai aussi écrit quatre articles de conférences.

Contexte géologique

Le gisement de sulfures massifs volcanogènes (SMV) paléoprotérozoïque de Lalor est situé dans le camp minier de Snow Lake à environ 700 km au nord de Winnipeg, Manitoba. Le gisement est exploité par Hudbay Minerals Inc. Dans le bassin du Chisel (la partie plus épaisse dans la séquence de Chisel au sud-ouest de la ville de Snow Lake), une anomalie au nord de bassin

et l'autre au sud ont été détectées par Hudbay Minerals lors d'un levé électromagnétique de surface dans le domaine temps en 2003. Le levé était conçu pour cibler les conducteurs profonds. Cependant, l'anomalie sud a recoupé une mineralisation à la chalcopyrite, la pyrite et la pyrrhotite non économiques. Hudbay Minerals a mené la première campagne de forage en 2007 pour tester l'anomalie électromagnétique du nord et le premier forage (DUB168) a montré une largeur rentable de sulfures massifs riches en zinc (Newton et al., 2017). Le gisement est situé entre 570 et 1500 m sous la surface. Il s'étend sur une longueur d'environ 900 m dans la direction nord-sud et sur une largeur de plus de 700 m est-ouest. Les lentilles minéralisées de Lalor sont divisées en trois groupes dépendant de la minéralisation, soit zinc, or et or-cuivre. Figure 3.3 montre les zones minéralisées du gisement. La présence d'or dans divers types de minerais à Lalor à des teneurs supérieures à la moyenne pour un SMV ainsi que la grande taille du gisement font de Lalor un gisement SMV unique dans la région de Snow Lake (Galley et al., 2007; Mercier-Langevin et al., 2011; Caté, 2016).

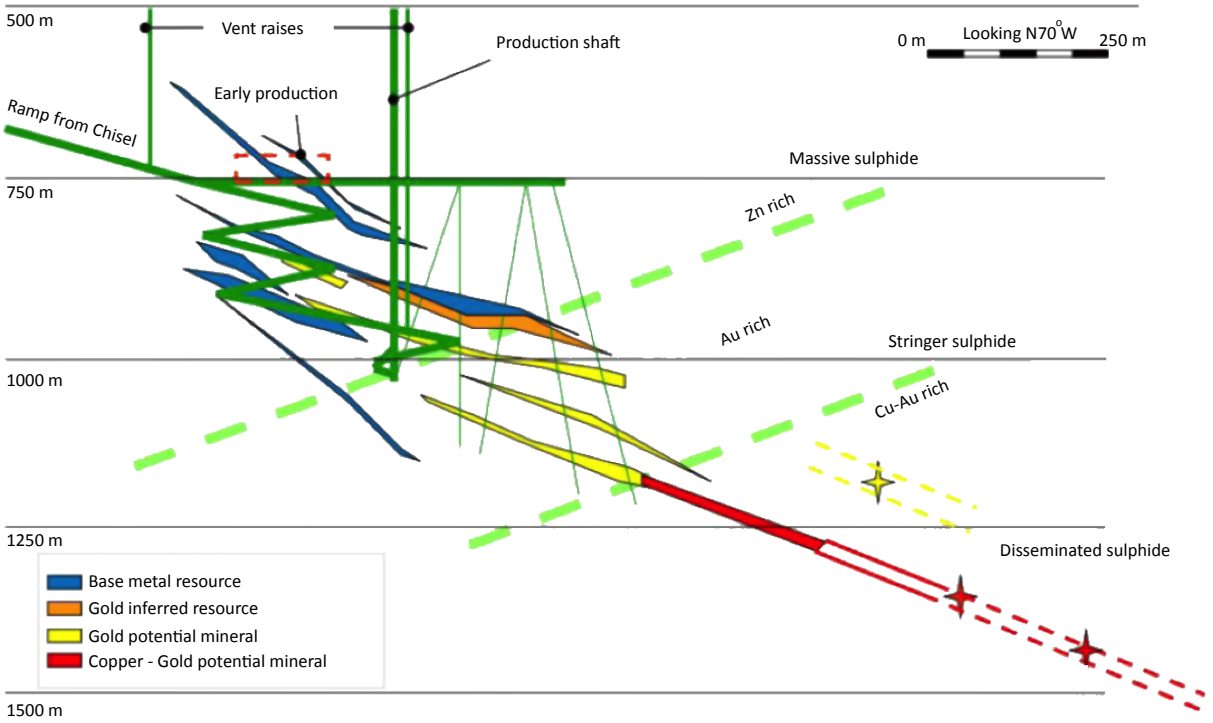

FIGURE 3.3 : Vue horizontale des zones minéralisées du gisement Lalor en direction nord-ouest

Méthodologie

Cette section présente en détail les étapes de la méthodologie proposée dans ce projet (Figure 3.1). Le modèle géologique conceptuel 3D original du gisement Lalor a été construit par un étudiant au doctorat en géologie de notre groupe de recherche (Caté et al., 2015). On entend ici par modèle géologique conceptuel, un modèle numérique dépeignant de manière générale la disposition spatiale des unités géologiques. Il n'est pas un modèle de ressources et ne repose que sur la connaissance géologique. Nous avons modifié ce modèle géologique original afin de regrouper les unités géologiques possédant des propriétés pétrophysiques similaires (étape 1). Ce modèle a ensuite été utilisé comme l'image d'apprentissage pour générer 100 scénarios géologiques stochastiques 3D équiprobables à l'aide de l'algorithme de simulation multipoints (MPS), tout en respectant les données des forages géologiques (étape 2). Ensuite, chaque unité géologique a été peuplée par les valeurs de densité considérant les relations pétrophysiques intrinsèques à chaque unité en utilisant l'algorithme de simulation séquentielle conditionnelle gaussienne ou SSCG (étape 3). Étant donné que les modèles de densité sont stochastiques, les modèles simulés seront précis et proche des données de conditionnement (mesures de diagraphies acquises le long des puits), mais perdront en précision en s'éloignant de ceux-ci. Par conséquent, l'étape suivante consiste à combiner les différents modèles stochastiques de densité afin de minimiser la différence entre les données gravimétriques calculées sur les modèles de densité stochastiques et celles mesurées à la surface et en forages (étape 4). Le modèle optimisé de densité et les conductivités électriques des diagraphies sont ensuite fournis à l'algorithme simulation séquentiel bayésien (SSB) afin de créer des modèles de conductivité 3D qui intègrent les mesures de champ gravimétrique, le modèle géologique conceptuel, les informations géologiques en forages et les diagraphies de densité et de conductivité électrique (étape 5). Ces modèles de conductivité passent ensuite par une autre étape d'optimisation de déformation graduelle dans laquelle l'objectif est de minimiser la différence entre les potentiels électriques bruts et calculés, ce qui permet d'obtenir un modèle de conductivité optimisé, qui intègre toute l'information à notre disposition (étape 6).

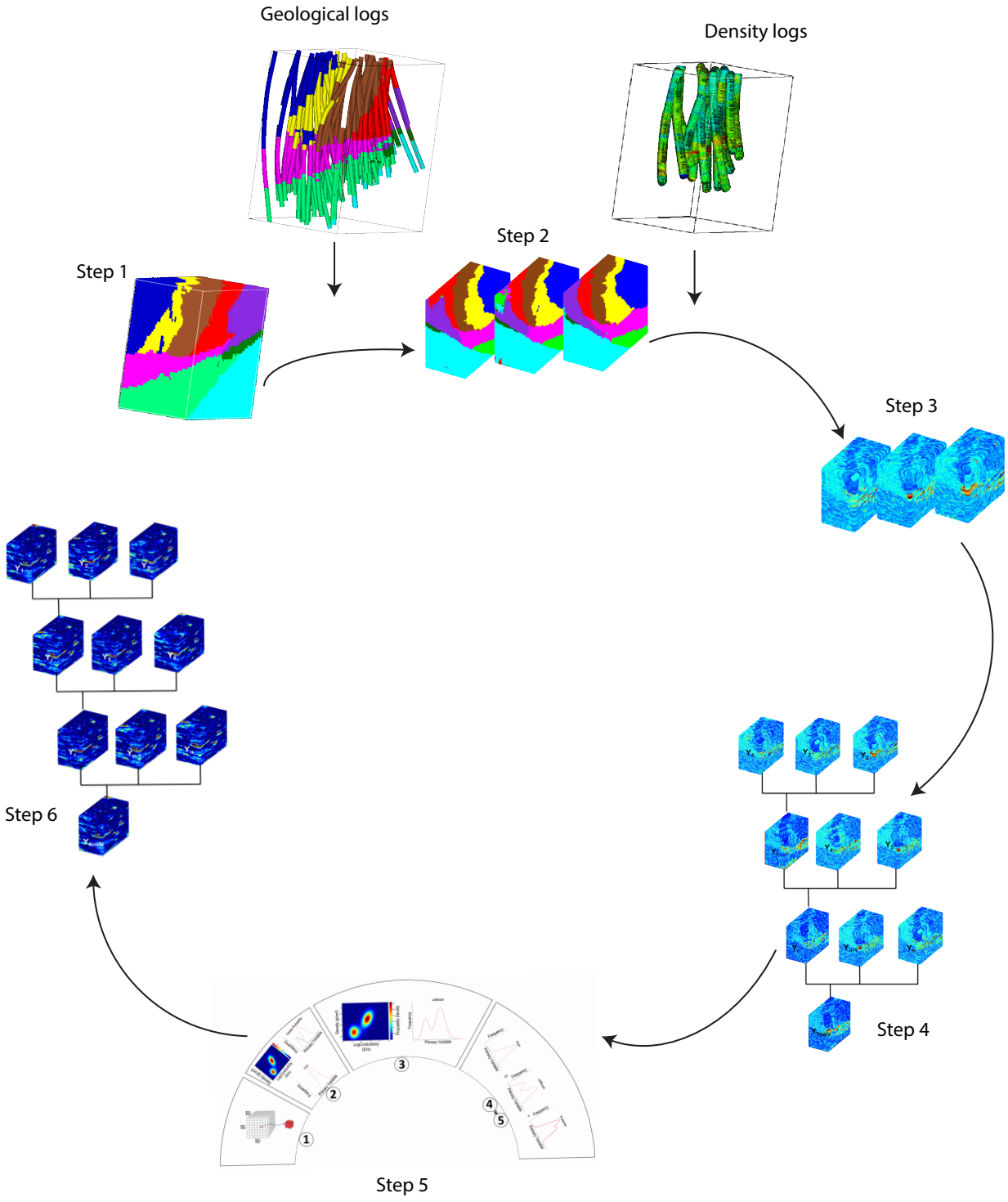

FIGURE 3.1 : Flux de travail

Modèle géologique

Parmi les études géologiques, le travail de Caté et al. (2015) est le plus récent sur Lalor et aussi celui qui résume toutes les descriptions précédentes. Les données complémentaires utilisées pour créer le modèle comprennent des descriptions détaillées des forages et des données géochimiques de Hudbay Minerals ainsi que des données recueillies par Caté et al. (2015). Le modèle a été construit à l'aide d'un algorithme de classification par apprentissage automatique pour distinguer les unités volcaniques et les types d'altération. Différents indices d'altération ont été utilisés pour modéliser la géométrie des zones d'altération. Pour notre étude, nous avons modifié la taille du modèle pour couvrir un volume plus important que seule la zone de la mine, soit une grille de dimension 974 m × 1929 m × 1663 m. Ce modèle contient 9 unités lighologiques incluant Balloch basalt, Ghost Lake rhyodacite, la FWHW1 qui contient la Lalor Powderfouse dacite, North Balloch rhyodacite, North Chisel dacite, Threehouse mafic unit, Upper Moore mafic unit, Upper Threehouse mafic unit et FWHW2 qui contient Western Powderhouse dacite. Les lentilles de sulfures massifs sont situées dans l'unité de FWHW1 et l'unité Upper Moore mafic unit, qui sont des unités volcanoclastiques felsiques et mafiques, respectivement (Caté, 2016).

Méthode de simulation multipoint (SMP)

La SMP permet de simuler des fonctions aléatoire catégoriques correspondant à des unités géologiques. La méthode SMP a été proposée et mise en œuvre par Guardiano et al. (1993) pour surmonter les limites des simulations géostatistiques classiques basées sur l'utilisation du variogramme. Les SMP utilisent une image d'apprentissage (TI), qui est un modèle géologique conceptuel en 3D et qui représente la structure spatiale *a priori* de la géologie sur laquelle les statistiques d'ordre supérieur à trois (ou à points multiples) sont calculées. Les statistiques multipoints prennent en compte la corrélation entre trois localisations ou plus, plutôt que de calculer uniquement le variogramme, qui calcule la dissimilarité entre les valeurs d'une fonction aléatoire entre seulement deux localisations. Par conséquent, en utilisant les SMP, il est possible de simuler des structures géologiques complexes (Strebelle, 2002). Dans notre cas, nous avons utilisé une version améliorée de l'algorithme appelée impala (Chugunova et al., 2008). Chugunova et al. (2008) présente une version complètement parallèlisée et optimisée de l'algorithme initial. Il utilise une méthode hybride

de calcul des statistiques d'ordre supérieur en cours de calcul et de stockage de celles-ci dans un arbre de recherche. Un arbre de recherche est une structure de données dynamique constituée d'un ensemble de nœuds qui correspondent aux patrons (patterns) particuliers pour stocker les statistiques de points multiples à partir de l'image d'apprentissage. À l'aide des SMP, un ensemble de 100 réalisations de modèles géologiques 3D est d'abord calculé en utilisant le modèle géologique 3D conceptuel modifié de Caté et al. (2015) qui prend en compte les unités géologiques identifiées sur des carottes de forages dans un volume de 974 m × 1929 m × 1663 m.

Méthode de simulation séquentielle conditionnelle gaussiennes (SSCG)

Dans cette section, un aperçu pratique de l'algorithme SSCG est présenté. Une revue théorique complète peut être trouvée dans Goovaerts (1997). La méthode SSCG permet de générer des réalisations stochastiques gaussiennes de variables continues (Journel et al., 1978). L'algorithme de simulation séquentielle conditionnelle gaussiennes consiste à:

— 1- Vérifier si le modèle de la fonction aléatoire suit la loi de distribution gaussienne (ou normale). Dans le cadre de cette étude, les données sont transformées en une distribution gaussienne.

— 2-Appliquer l'algorithme de simulation séquentielle qui exige la définition d'un chemin aléatoire pour visiter chacun des noeuds de la grille à simuler. Effectuer le krigeage simple à ces points à partir des points de mesures. Afin de reproduire le modèle de covariance, les valeurs précédemment simulées sont aussi utilisées ainsi que les données d'observation comme valeurs conditionnantes pour le calcul du krigeage. À la fin de la simulation, une transformation inverse est nécessaire pour garantir la reproduction du variogramme des données d'origine.

Pour chaque unité géologique des 100 modèles géologiques simulés à l'étape SMP, cinq réalisations différentes et équiprobables de densité sont calculées, générant ainsi 500 modèles de densité 3D. Avant d'utiliser les valeurs de densité du forage de conditionnement pour la simulation, les densités sont classifiées selon les unités géologiques existantes, puis normalisées. Les distributions des données de densité brutes ne sont pas gaussiennes et, étant donné que nous utilisons l'algorithme SSCG pour calculer les réalisations de la densité, la distribution des données brutes doit être d'abord normalisée par anamorphose gaussienne (Goovaerts, 1997).

Méthodes de Déformation graduelle (DG)

Les modèles générés précédemment intègrent les connaissances conventionnelles (modèle géologique conceptuel et données de forages). Ils ne sont pas contraints par les mesures géophysiques abondantes sur les camps miniers ou les zones en exploration avancée. Il est possible d'utiliser ces mesures géophysiques brutes afin de combiner de manière optimale l'ensemble des 500 réalisations stochastiques de haute résolution générées par SMP et SSCG. La méthode de combinaison géostatistique qui est adoptée dans la présente étude est la méthode de déformation graduelle proposée par Hu (2000). L'idée principale de cette technique est que la combinaison linéaire de deux fonctions aléatoires gaussiennes indépendantes permet d'obtenir une nouvelle réalisation de la même fonction aléatoire gaussienne tout en préservant leur structure spatiale et leurs moyenne et variance (e.g. covariance). L'algorithme de DG consiste à optimiser un seul paramètre de déformation (r) qui indique le poids relatif de chacune des réalisations. En faisant varier le coefficient de déformation dans un processus itératif, la méthode cherche à minimiser la différence entre les données géophysiques calculées sur une combinaison de modèles de densité et celles mesurées. Plusieurs développements ont permis d'adapter le principe de déformation graduelle pour des réalisations avec des distributions non gaussiennes (Hu, 2000) et pour les réalisations conditionnelles (Hu, 2002). Dans mon projet, j'ai utilisé une version modifiée de la méthode de déformation graduelle multidimensionnelle. Comme Ying et al. (2000) l'ont montré, cette version, appelée conditionnement graduel, de DG peut être directement appliquée aux réalisations conditionnelles aux données observées, permettant d'ajuster parfaitement les mesures de densités mesurées en forages. La Figure 3.21 résume la méthode de la déformation graduelle impliquant la combinaison graduelle de trois réalisations. Afin d'appliquer le conditionnement graduel, nous devons calculer la modélisation directe de gravimétrie g causée par la distribution spatiale de densité (ρ) dans le sous-sol afin de les comparer avec l'anomalie résiduelle mesurée. Le volume souterrain 3D est discrétisé en une grille de 19,8 m × 39,4 m × 33,9 m le long des axes x, y, et z, respectivement. Le domaine 3D est donc divisé en 50×50×50 = 125000 cubes. Contrairement à l'inversion déterministe ou stochastique conventionnelle, la déformation graduelle permet d'utiliser plusieurs types de normes dans la fonction objectif. Nous avons testé deux types de norme, soit L1 et L2. La fonction objectif de norme-L1 (valeur absolue de la différence entre les données calculées et mesurées) est moins sensible aux mesures qui présentent une grande variabilité par rapport aux données mesurées (données dites aberrantes) en comparaison avec des normes supérieures. La

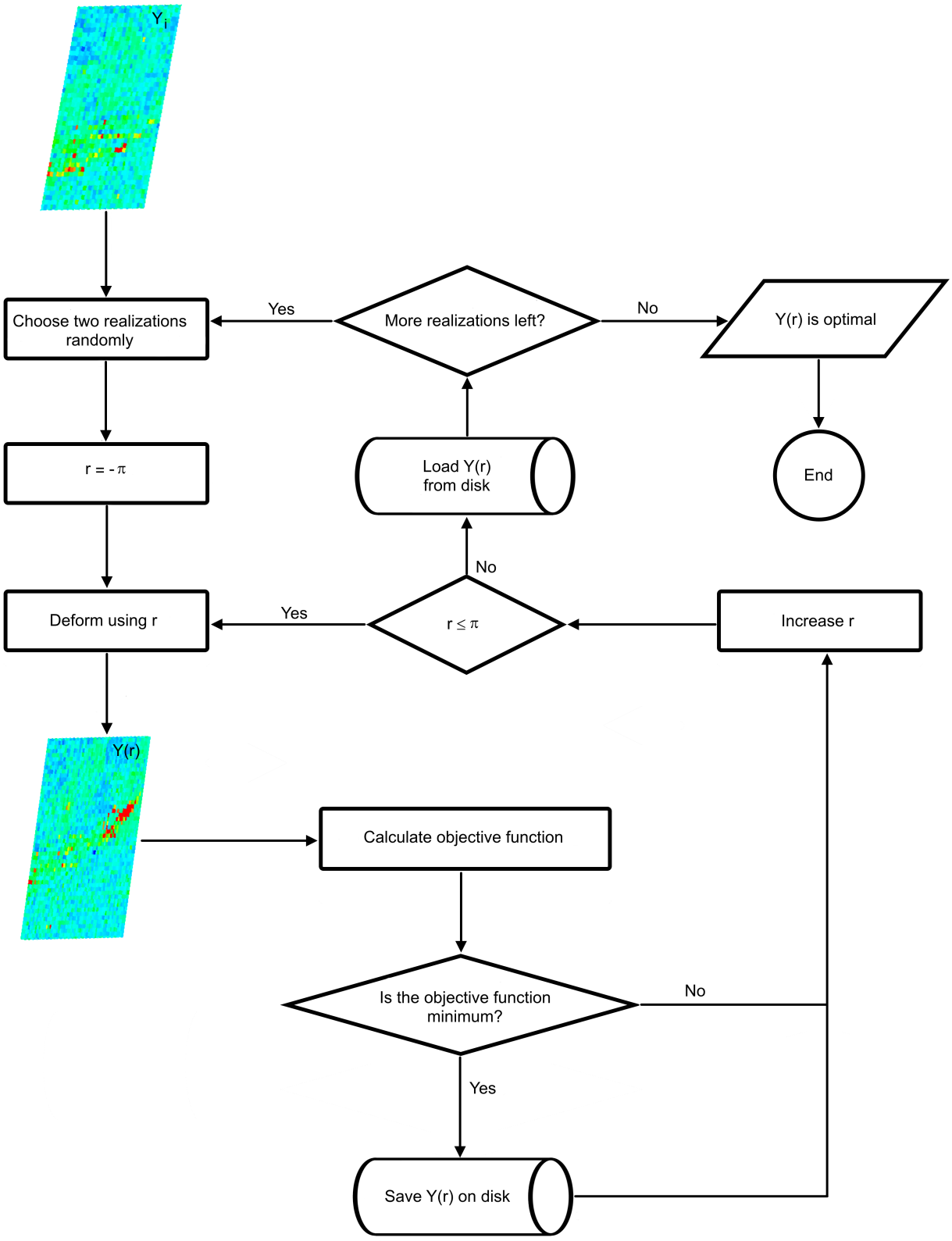

FIGURE 3.21 : Workflow de l'étape de déformation graduelle

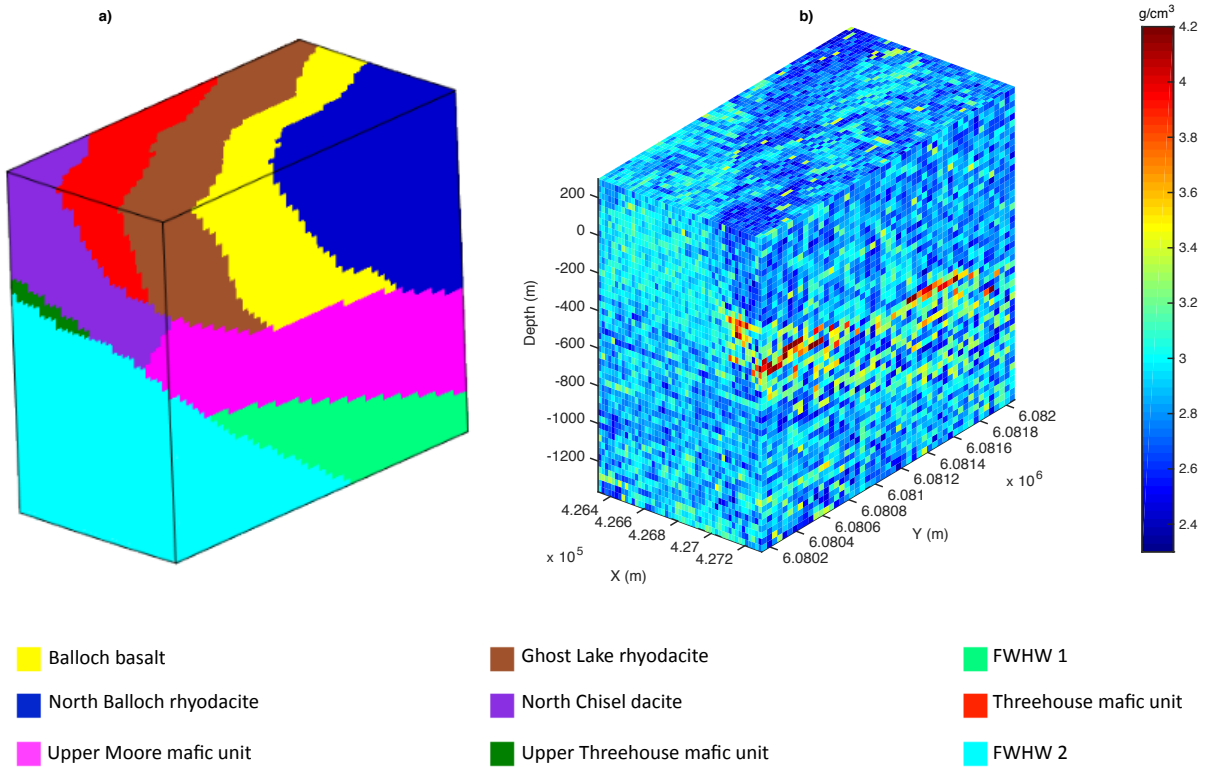

FIGURE 3.26 : a) Modèle géologique 3D, b) Modèle de densité 3D optimisé par inversion stochastique par la fonction objectif norme-L2.

fonction objectif de norme-L1 dans l'optimisation de la déformation graduelle de tous les modèles de densité simulés converge plus rapidement que la fonction objectif de norme-L2. Toutefois, l'erreur quadratique moyenne de la norme-L2 a une valeur de convergence inférieure à l'erreur calculée pour l'autre fonction objectif. Le modèle de densité obtenu à l'aide de la fonction objectif L2 est illustré dans Figure 3.26-b. L'examen de modèle de densité montre, il existe une correspondance claire entre les unités lithologiques du modèle géologique (Figure 3.26-a) et les contrastes de densité du modèle de densité (Figure 3.26-b), en particulier la zone à haute densité correspondant à l'unité Upper Moore mafic unit.

Méthodes SSB

La simulation séquentielle bayésienne (SSB) est basée sur le paramétrage du théorème de Bayes en présence d'une variable corrélée avec une variable d'intérêt, et mesurée ou estimée en tous points de l'espace. Le SSB a été proposé pour l'interpolation et l'extrapolation des données

lithologiques contraintes par des attributs sismiques non linéaires (Doyen et al., 1996). L'implémentation du SSB comporte 5 étapes (Dubreuil-Boisclair, 2013):

- 1- Un chemin aléatoire doit être défini pour visiter chaque voxel de la grille (une fois seulement). Ce chemin est unique pour chaque réalisation.
- 2- Le voxel choisi passe par une étape de krigeage simple à fin d'obtenir la distribution *a priori*. Étant donné que les données de densité et de conductivité montrent une distribution bimodale, il convient de déterminer statistiquement à quelle famille le voxel de la grille à simuler appartient. La famille 1 correspond aux valeurs de conductivité et de densité hautes et la famille 2 correspond aux valeurs basses de conductivité et de densité. Dans ce but, la méthode des modèles de mélanges gaussiens (GMM) est utilisée. Pour obtenir la distribution *a priori* des données de conductivité, le variogramme et la moyenne de la famille choisie sont utilisés pour le krigeage simple des données de conductivité mesurées et simulées précédemment.
- 3- Dans cette étape, la relation pétrophysique statistique entre la densité et la conductivité est déduite et la distribution conjointe est estimée à l'aide de la méthode du noyau développée par Rosenblatt (1956) et par Parzen (1962).
- 4- La distribution a posteriori est calculée en mettant à jour l'*a priori* en la multipliant avec la vraisemblance dans le cadre du théorème de Bayes. Les relations spatiales des valeurs de conductivité et de densité qui sont elles-mêmes conditionnées aux densités et lithologie de forage sont prises en compte dans la distribution a posteriori.
- 5- Cette dernière étape consiste à tirer de manière aléatoire une valeur de conductivité à partir de la distribution a posteriori et à l'attribuer à la cellule choisie. Cette valeur de conductivité simulée est prise comme une valeur mesurée (connue) pour les prochaines itérations de la simulation. Si toutes les cellules sont visitées l'algorithme arrive à sa fin sinon elle répart de la première étape et une nouvelle cellule est choisie.

L'avantage de la SSB est que la relation statistique entre les données peut être de toute nature, comme dans notre cas une relation non linéaire et hétéroscédastique. La Figure 3.31 présente six réalisations 3D de conductivité parmi les 100 réalisations générées par SSB.

Afin de calculer les potentiels électriques causés par une distribution spatiale de conductivités électriques en présence d'une source de courant, une modélisation directe est nécessaire. La modélisation est effectuée sur une grille de cellules rectangulaires, dont chacune a une valeur constante de conductivité. Les emplacements des électrodes peuvent se trouver n'importe où dans

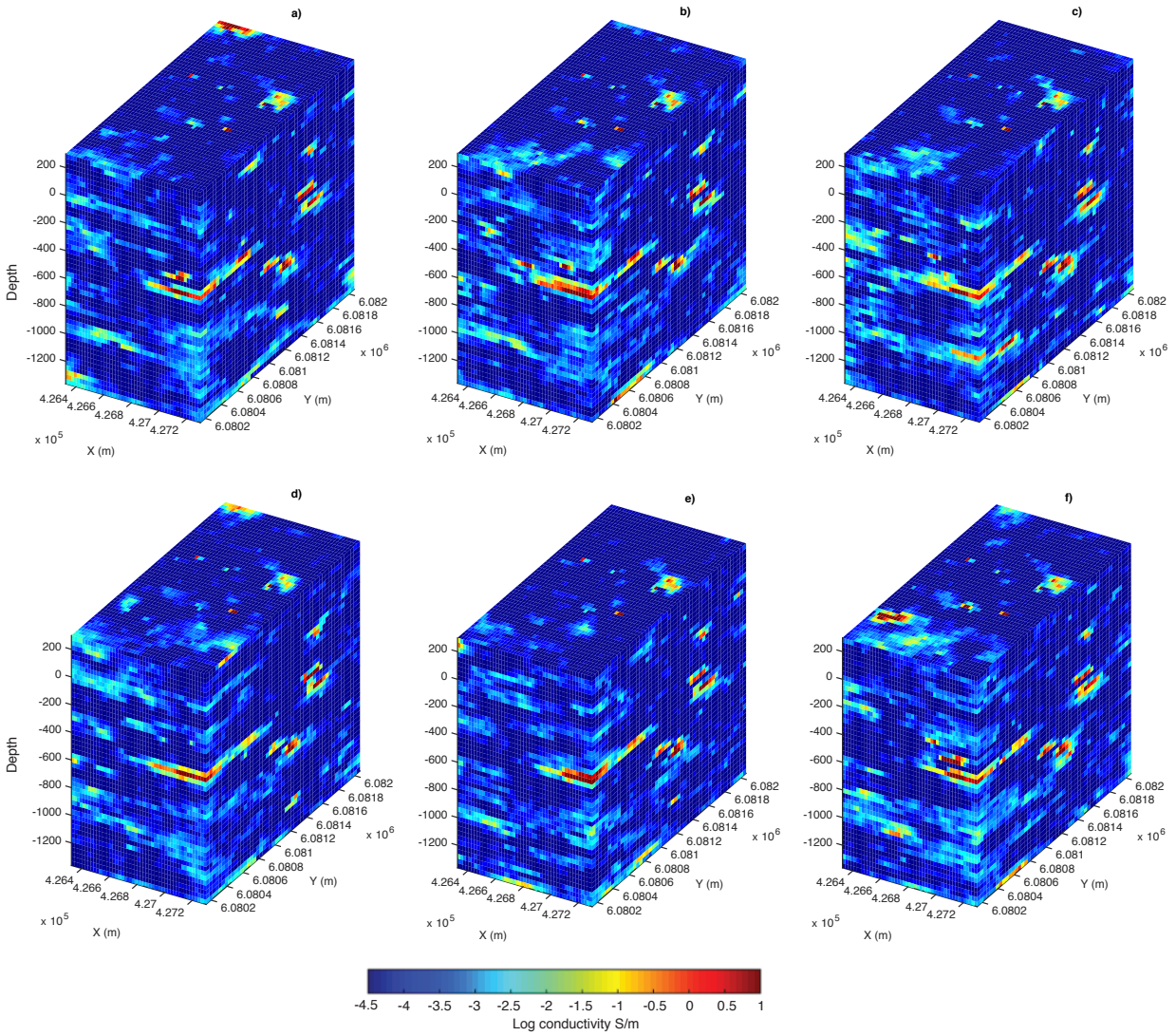

FIGURE 3.31 : Le modèle de conductivité généré par l'itération a)1 **b)**20 **c)**30 **d)**60 **e)**80 **f)**100

le volume du modèle. La grille a les mêmes dimensions que dans la modélisation gravimétrique. Les équations DC sont résolues en utilisant la méthode des volumes finis (Dey et al., 1979). La Figure 3.33 montre le modèle de conductivité simulée optimisé après 100 itérations.

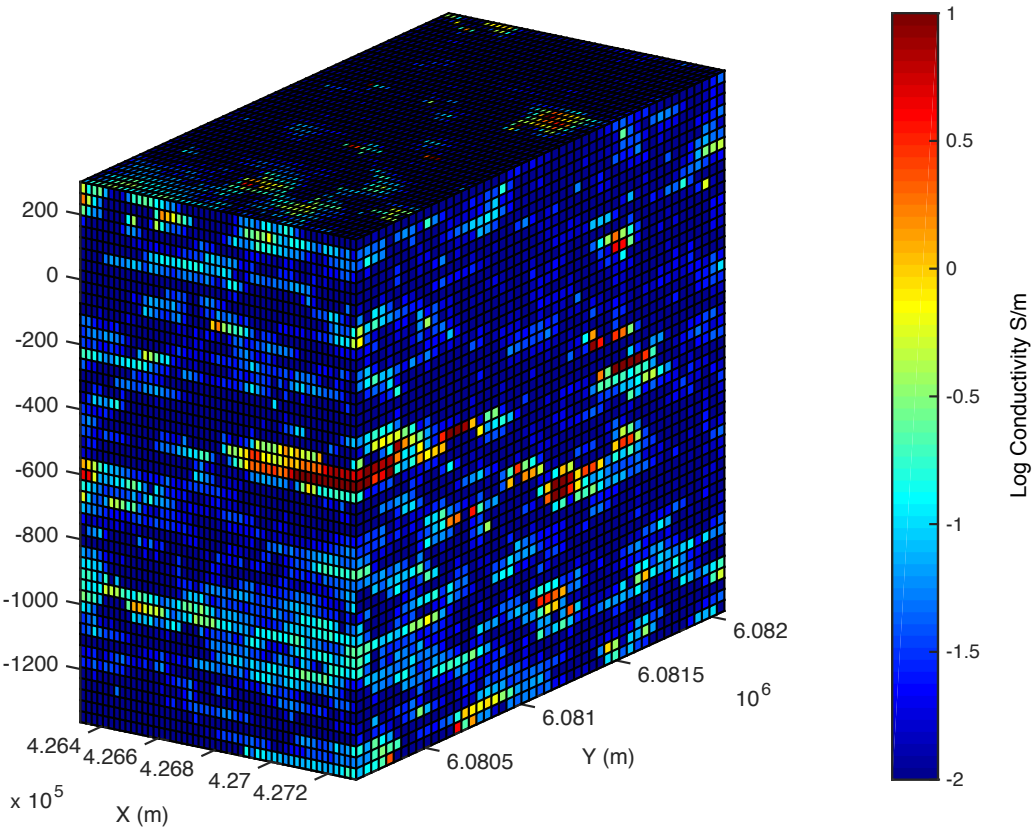

FIGURE 3.33 : Modèle de conductivité optimisé après 100 itérations

Discussion

L'assimilation stochastique des données gravimétriques a montré une diminution significative de la difference entre l'anomalie gravimétrique calculée et mesurée et une amélioration de réalisme géologique par rapport à l'inversion par moindres carrés. Cela démontre l'avantage et l'applicabilité de la méthodologie proposée pour construire de meilleurs géomodèles. Il permet également de valider le modèle géologique *a priori*. L'un des principaux avantages de cette méthode est de construire un jumeau numérique unifié du gisement. Cela signifie que le regroupement de toutes les données disponibles dans un modèle numérique permet de détecter des incohérences dans le modèle géologique. Le modèle géologique est peuplé par les propriétés physiques mesurées et après le calcul de la modélisation directe, il est possible de comparer ces données calculées avec les données géophysiques mesurées. Malgré les efforts considérables déployés pour construire le modèle géologique, il existe encore des incohérences entre le modèle géologique fourni et les

modèles géophysiques, notamment en ce qui concerne les propriétés physiques. En effet, les unités géologiques qui ont été classées dans la même catégorie présentent des réponses variables dans les données géophysiques. Cela a un impact sur les résultats de la méthodologie proposée. Dans le cas de la modélisation stochastique de la résistivité, les données de diagraphie étaient de mauvaise qualité. Il n'était pas possible de s'en remettre à elles de la même façon que pour les données de densité. Ceci est certainement dû à des problèmes d'étalonnage des outils utilisés sur le terrain. Cependant, nous avons quand même décidé de suivre la méthodologie avec les données dont nous disposions. Les résultats montrent clairement que nous diminuons la fonction objectif indiquant qu'à partir de la forme générale du modèle de densité, nous continuons à améliorer le modèle numérique du gisement en intégrant des données haute résolution. Le modèle final intègre dans le même modèle numérique 3D, le modèle conceptuel géologique, la lithologie géologique des forages, les levés gravimétriques de surface et de forage et les données de résistivité de surface et de diagraphie. L'algorithme bayésien a l'avantage de pouvoir incorporer des relations fortement non linéaires entre les données dans la simulation (Doyen, 2007).

Conclusion

À fin de vérifier l'efficacité de cette méthodologie, elle a été appliquée à un cas réel. Les résultats montrent que le flux de travail proposé permet d'obtenir un modèle optimisé final qui montre une meilleure correspondance géophysique avec le modèle géologique initial. La première étape, qui consiste à simuler des unités géologiques, est suivie par une étape permettant de peupler ces unités de propriétés continues, ici les densités afin d'obtenir des modéles géologiquement réalistes et intégrant les mesures pétrophysiques associées à chacune des unités. La deuxième phase de cette étude qui inclut la méthode SSB, permet d'intégrer les données provenant de la géophysique de surface et en forages dans le cadre de la mise à jour des modèles par optimisation heuristique, ici par déformation graduelle. Contrairement à l'inversion conjointe, cette approche a l'avantage de pouvoir utiliser conjointement plusieurs mesures géophysiques ayant des résolutions spatiales très différentes et donnant accès à des propriétés physiques différentes dans la construction d'un modèle pétrophysique unifié. Cette approche donne aussi accès à l'incertitude sur l'estimation des propriétés en incluant explicitement l'incertitude reliée à chaque mesure géologique et géophysique (en forage ou de surface). En perspective, une fois que des relations statistiques ou empiriques sont développées entre les mesures physiques et de teneurs, nos modèles pourront servir de

base à l'estimation des ressources comme c'est le cas dans le domaine de la caractérisation des réservoirs.

TABLE OF CONTENTS

LIST OF FIGURES

LIST OF TABLES

1 INTRODUCTION

1.1 General introduction

The project that is described in this work is not directly associated with the mineral exploration phase, but rather once the presence of mineralization has already been established. The objective of this project is to improve the quantitative assimilation of all the information available (e.g. geology, physical properties, etc.) to build a more reliable petrophysical model of a deposit that honours, as best as possible, all of the data available. The accuracy of the appraisal of a deposit is critical to the technical and economic success of a mining project. A quality appraisal helps to reduce the sources of uncertainty and financial risks that are often associated with over-simplification of a deposit that arise from a number of simplifying assumptions that had to be made during the appraisal stage. The impact of this over-simplification is illustrated by industry statistics that show that 60 percent of the mining projects around the world do not meet their financial objectives after five years of operation. Furthermore, these projects ultimately produce less than 70 percent of the estimated reserves (Vallée, 2000). The research on productivity of gold mines in Canada of Knoll (1989) and Clow (1991) showed that very few mines were operating according to their original mine design. In Clow's study only 3 out of 25 gold operations had met their production schedule (dos Santos et al., 2014). Another study showed that out of 35 Australian gold projects, only 2 achieved their predicted recovery grades (Burmeister, 1988). Dominy et al. (2002) review on performance of the Australian gold operations concluded that recoverable grade over-estimation is the root cause of error. Over time, the technical problems that plague the development of profitable mining projects will undermine the confidence of investors and will limit the future mining capital available to new projects.

The estimation of the resources of a deposit that will be mined over time is a complex task. It includes several milestones that adapt to the maturity of the projects. Figure 1.1 shows the general workflow of stochastic resources modeling inspired from reservoir characterization workflows (Dubrule, 2003):

— 1- Data processing and analysis: It is important to note, the data come from multiple sources, from conventional drill-holes, geological a priori and geophysical data. The first step after the

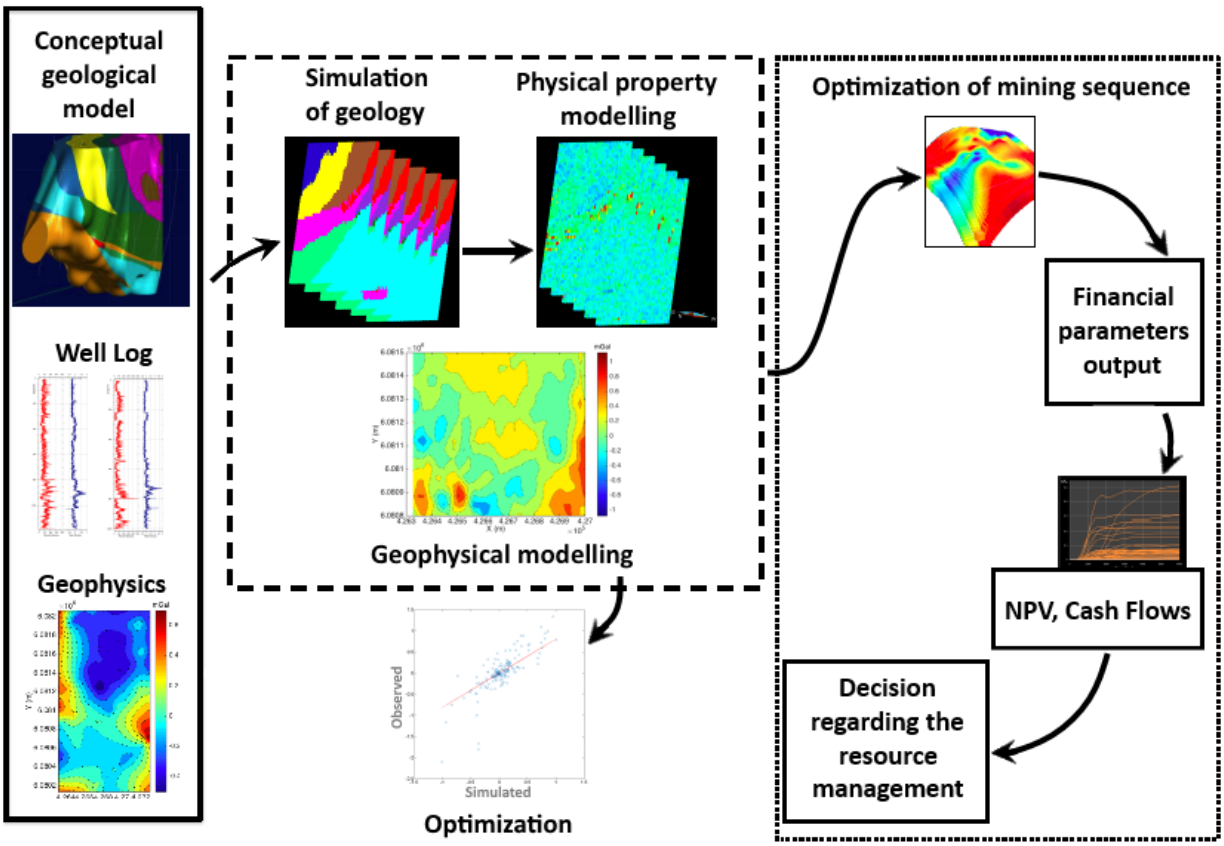

FIGURE 1.1 : Workflow schematizing the steps of modelling the mining project; We focus on the first two rectangles from the left.

discovery is to reconcile the different data that have led to the discovery (e.g. geophysical, geochemical, petrophysical and geological data).

- 2- Building of a numerical geological/structural model that honours the data.
- 3- Building stochastic numerical petrophysical models of the mineralized zones
- 4- Applying geophysical modelling to the stochastic petrophysical models
- 5- Stochastic models are combined in order to minimize the absolute difference between computed and measured geophysical data.

A consensus is emerging amongst experts in the industry that financial failure of mining projects is underpinned by the failure of the geological models to accurately represent the complexity of the deposits. Geo-models often ignore the uncertainty inherent to the data available (Dimitrakopoulos et al., 2002) and are only based on geological a priori and core data. Indeed, the most important causes for this deficiency are (1) the compartmentalization of expertise in the construction of the models, (2) the use of unsuitable tools for interpolation of the drilling data and (3) the lack

of algorithms for quantitative assimilation of geological and geophysical data that allows for their variability to be honoured in the models.

The current state of the art for grade interpolation requires the definition of envelops or wireframe within which the mean and the variance of the metal grades are constant. This step is largely influenced by the conceptual model of the deposit envisioned by the geologists guiding how the wireframe is constructed. The limits of the envelopes defined on the grid are thus deterministic and do not allow for the evaluation of the risk associated with inherent data uncertainty. The over or under estimation of the wireframe's volume will definitely have a deleterious impact on the inferred resources.

Geophysical surveys have played a critical role in mineral exploration (Bishop et al., 1992) however they are often considered only during the exploration phase to define targets and to determine the geometry of a deposit. Geophysical methods are not generally considered during the construction of geological and grade models. This is mainly due to the absence of a simple relationship between petrophysical data and grades, the design of geophysical data acquisition that is not optimized for the estimation of resources, and also because data processing over-smooths images of physical properties. This over-smoothing does not allow the use of inverted geophysical data for quantitative resource estimation (Fullagar et al., 2008). The smoothing imposed by traditional inversion methods causes geophysical models to have insufficient resolution to correlate with the measured properties in boreholes (Dubreuil-Boisclair et al., 2012). This means that the smoothing is responsible, at least in part, for the elimination of the correlation between the true geometry of the geology and the measured grades along boreholes. One possibility to overcome this problem is to use stochastic inversion and cooperative inversion in order to avoid a degradation of the resolution of the original dataset.

In the oil and gas industry, many of these issues have been studied (Doyen, 2007). The main reason that motivated these studies was the development of reliable petrophysical relationships between geophysical and reservoir data. This integration allows all of the experts to work together at every stage of the construction of geological model and for the estimation of the hydrocarbon in place (Dubrule, 2003). As an example, geophysical measurements (seismic reflection) acquired in order to meet exploration objectives are later leveraged to accurately estimate physical properties within the sedimentary basins. Well-logs acquired during drilling of the wells are used to determine the statistical relationships between the physical parameters and geological parameters of interest

(porosity, saturation). Once modelled, the relationship between the measured physical and geological properties at the wells are used to interpret geophysical measurements based on geological properties outside boreholes, to constrain the seismic inversion and to built in-situ statistical relations between reservoir and physical properties (Doyen, 2007).

Geophysical surface measurements and well-logs do not have the same frame of reference and their spatial resolution are significantly different. Physical properties that contribute to these measurements are not considered at the same scale and the same is true with the uncertainties associated with each measurement. Also, joint inversion fails to take into account geophysical data depending on different physical properties and of varying resolutions (Dubrule, 2003). This is why, for ten years, new data assimilation methods have been developed in the petroleum industry (Dubreuil-Boisclair et al., 2012; Claprood et al., 2013) and for environmental projects (Ruggeri et al., 2013). For example, Figure 1.2 shows the results of a synthetic multi-resolution stochastic inversion experiment. Figure 1.2-C, 1.2-D and 1.2-E show three model realizations that integrate high-resolution electrical well-logs and low-resolution surface electrical measurements (Ruggeri et al., 2013). The texture of the simulated models is well reproduced (compared to the target model Figure 1.2-A) and the smoothing effect of the deterministic inversion (Figure 1.2-B) has disappeared.

The use of this stochastic inversion approach allows us to use all of the geophysical measurements and drillhole data for the construction of the petrophysical models. It also provides a quantification of the uncertainties related to the physical parameters and, ultimately, the reserve estimates by explicitly including the uncertainties related to the measurements.

In Bouchedda et al. (2016) the authors proposed an approach to estimate a small-scale conductivity model by inverting DC resistivity and logged data. They considered an objective function which contains a conventional DC resistivity data fitting term and a second term which forces the inverted resistivities to respect the semivariogram of logged resistivity data. To solve this problem, they used a derivative-free gradient stochastic algorithm. In another study Yrro (2018) proposed an approach to jointly inverse the time-domain electromagnetic (TDEM) and helicopter-borne time-domain electromagnetic (HTEM) data to obtain an optimized two-dimensional high-resolution stochastic electrical resistivity model.

These types of multi-resolution and multi-parameter quantitative assimilation approaches are becoming more wide spread. Indeed, around the world and in Quebec, deposits are increasingly sought in deeper and more complex geological environments. The investment risks increase

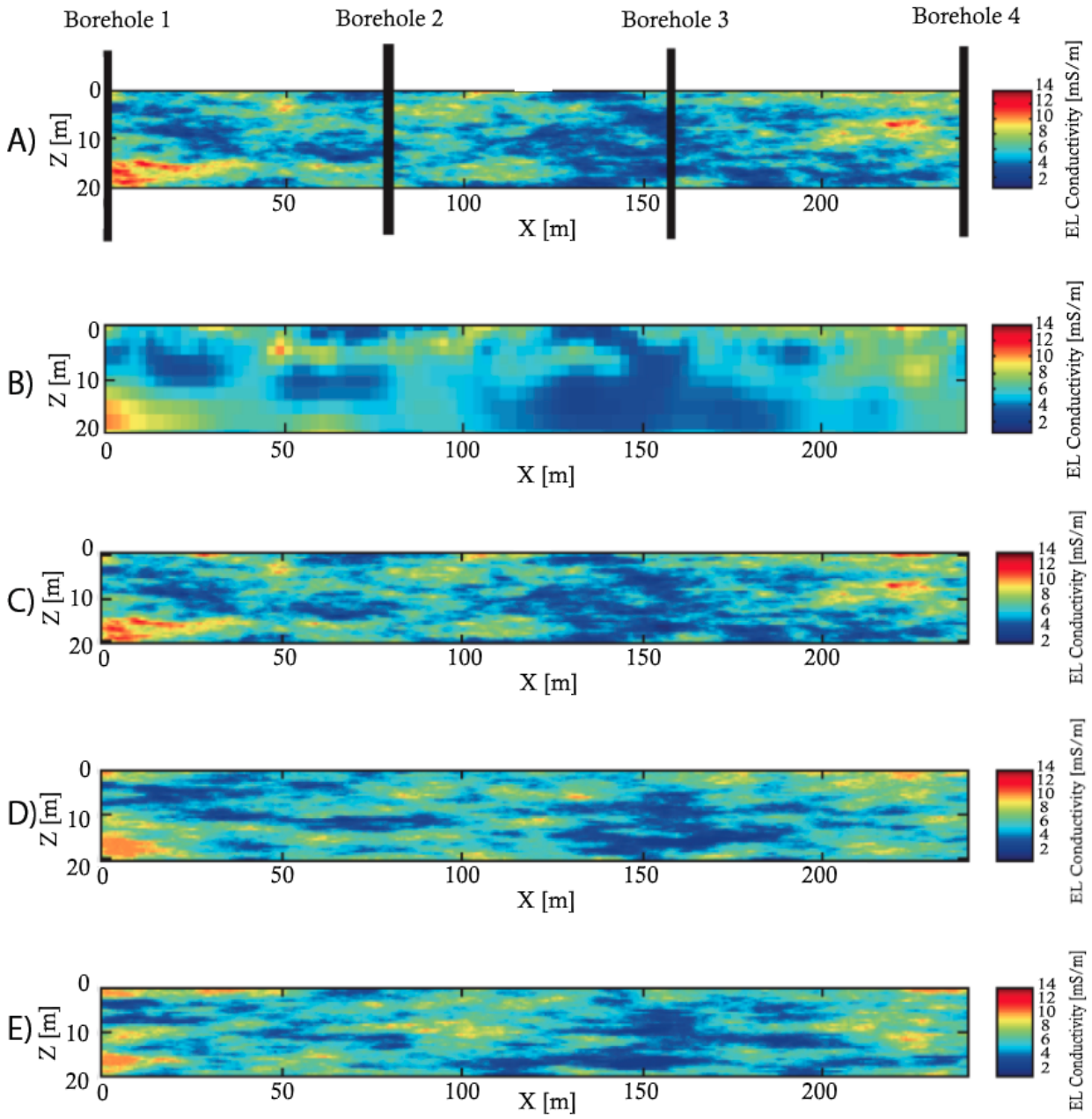

FIGURE 1.2 : (A) Original high-resolution hydraulic conductivity field (B) deterministic inversion resulting in smoothing effect, (C, D, E) three realizations that integrate physical measurements in boreholes and surface electrical measurements, from (Ruggeri, 2014).

significantly as well as the possibility of failure (e.g. economic and environmental). It is therefore crucial to develop new methodologies to optimize the use of all of the available information in order to efficiently characterize the deposits and quantify the associated uncertainty.

1.2 Objectives

The objective of this study is to develop a new stochastic quantitative data assimilation framework for multiple sources of data to improve the characterization of a mineral deposit, in terms of geophysical and geological models. Our work uses the working hypothesis that geophysical data can be used to better estimate the physical properties across a deposit and that these can be linked to the abundance of economic minerals.

We developed a workflow for petrophysical modelling that is constrained by geological data knowledge and geophysical data measured at surface and in boreholes (the two left rectangles in Figure 1.1). This workflow is applied to a real-data example from a mining site (Lalor deposit in Manitoba).

The focus of this work is to study the petrophysical relations along boreholes and build 3D stochastic petrophysical models. These models are constrained by (1) the conceptual model, (2) geochemical data (since the conceptual model is built using the geochemical data), (3) high-resolution geophysical logs and (4) surface and downhole geophysical data.

The Lalor deposit, in the Snow Lake camp, was chosen because it provides a well characterized 25 Mt deep ore deposit (Bellefleur et al., 2015a). It has been surveyed with magnetic, seismic, gravimetry, airborne electromagnetic (VTEM, ZTEM) and electrical resistivity measurements. Furthermore, geophysical logs (Sonic, density, electrical resistivity and magnetic susceptibility) were also acquired in seventeen diamond drill-holes where the geology was also logged. Geochemical assays are also available for these cores. This measurements set is unique in Canada and this project could not have been done without this data-rich environment. The results of this work are easily generalizable and do not only apply to the Snow Lake camp. We show that the Lalor site is an ideal laboratory to gain a better understanding of the signatures and the characteristics of volcanogenic massive sulphide deposits (VMS). A better understanding of the footprint of these deposits is very important for the improvement of our exploration strategies and how these deposits are appraised. This is especially valuable for the province of Quebec where many VMS deposits are known and more are likely to be discovered.

1.3 Contributions

The contributions of this thesis can be characterized as methodological improvements and application of multi-resolution stochastic inversion to a real dataset. From a methodological standpoint, the development of algorithms and implementation of the workflow contribute to the efficient use of geophysics in geological modelling. The methodology does not require conventional least-squares inversion and each model (geologic, geophysical) retains its inherent resolution (e.g. smoothing artefacts are avoided). The forward modelling approach that is used means that there are no compatibility problems between resolution and scale of the different datasets. The stochastic approach aims to ensure that all sources of uncertainty are considered through generating multiple realizations. The goal is to have quality appraisal and ultimately be able to make better decision during the exploration phase by quantifying the risk of a mining operation.

The second innovative aspect of this study is the application of modified stochastic algorithms for Lalor volcanogenic massive sulphide. Using this stochastic approach, several equiprobable scenarios of the geology and petrophysical models are generated while honouring statistically related data. During my thesis, I published an article in the special issue entitled “Geophysics Applied to Mineral Exploration” in the Canadian Journal of Earth Sciences (Tirdad et al., 2019). I have also written four conference papers.

2 THEORETICAL OVERVIEW

In this chapter, an overview of the geophysical and geostatistical methods used in the proposed stochastic inversion workflow is given to provide context for the third chapter: "Application of the methodology on real data: the Lalor case study".

2.1 Geophysical methods

Geophysical measurements consist in recording the response of the ground physical properties to the passage of a natural or controlled field. These measurements integrate the induced field between the sources and receivers and do not inform directly on the spatial distribution of physical properties in the ground. The iterative process of reconstructing physical properties of subsurface is called geophysical inversion which is an optimization problem (Meju, 1994; Menke, 2018; Aster et al., 2018). An inverse problem includes at least three variables: the data (geophysical measurements), the parameters (physical property of interest in the ground) and a forward operator linking the data to the parameters. A problem that is said to be well-posed meets the three following requirements: (1) A solution must exist, (2) the solution must be unique and (3) it must continuously depend on the data (Le Ravalec-Dupin et al., 2007). Unfortunately, the solution to a geophysical inverse problem does not often depend continuously on the geophysical measurements and thus makes inversion an ill-posed problem.

The geophysical inverse problem seeks to recover the distribution of physical properties such as density and electrical conductivity from data that were measured. The measurements that are most often available are magnetic susceptibility, gravity and electrical conductivity. The geophysical problem is ill-posed because there are many more spatial variations in parameters that can be estimated from the data available. In order to compute the solution to the inverse problem, the measured data must be described using a model for a given spatial distribution of parameters. These models, that describe the spatial distributions of parameters, are important to understand the subsurface geology because variations in physical properties can identify important geological information that are associated with local enrichment of metals sought.

2.1.1 Gravity methods

Ore minerals with high-density values, sulphides, iron oxides, and other metallic ores will be associated with excess mass which will be reflected on the local gravity field. Conversely, regions where significant geological processes have altered the rock-mass and hence increased its porosity will be associated with a mass deficit and will be reflected by a localized decrease in the earth's gravitational field. The variations in the earth's gravitational field can be used to map density variations that are associated with these different geological structures to help exploration or to constrain deposits.

2.1.1.1 Measurements

The measurement of the earth's gravitational field is based on Newton's law of gravitation: the force of attraction between two masses is directly proportional to the two masses, and inversely proportional to the square of the distance between them. For decades gravity surveys have been used in different mineral exploration contexts (Paterson et al., 1985) and in engineering and environmental studies (Hinze, 1990). Surface gravity surveys capture the variations of density near the surface. When the deposit of interest is situated at greater depth, the resolution of the surface gravity measurements are limited by the quadratic decay of the attractive force between the mineralized target and the instruments (Schetselaar et al., 2015).

Small changes in density close to the sensor can mask the response of deeper and denser geo-bodies. To circumvent this shortcoming, great efforts have been made to develop reliable borehole gravimeters that can be positioned closer to the geo-bodies. Borehole gravimetry (BHGM) for exploration was pioneered by Smith (1950). The principles of a borehole gravimeter are the same as a surface gravity meter. Gravity measurements are collected through a series of stops and readings at discreet intervals at depths that are pre-selected. It is shown by several studies that these measurements are not affected by casing or formation damage caused by drilling (Smith, 1950; Jageler et al., 1976; Beyer, 1987). According to Nind et al. (2013) in the early stages of exploration it is possible to obtain quantifiable information on the detection and estimation of mineralization tonnage from a few boreholes using a borehole gravity survey. This results in reducing time and hence exploration cost. An other application of BHGM is to determine the in-situ apparent density

of different lithologies. Inversion of borehole gravity measurements acquired from three or more boreholes is useful in building a general 3D representation of the body (Wasylechko et al., 2014; Newton et al., 2017). The first borehole gravimeter was introduced by LaCoste and Romberg in the early 1960s. Figure 2.1 shows a LaCoste-Romberg gravimeter. This gravimeter uses a hinged beam that carries a mass attached to its free end and is supported by a zero-length spring. The combination of the tension in the spring and an electrostatic force keeps the beam balanced. The spring is said to be zero-length because the tension in the spring is proportional to actual length, rather than to extension from unstressed length. In practice this means that the spring extension is directly related to the acceleration due to gravity. This means that an increase in the acceleration due to the gravity will cause an increase in the weight of the beam. This first generation of borehole gravimeters were only suitable for large-diameter boreholes and that were near vertical; conditions only found in the petroleum industry. Further information on these first generation borehole gravimeters can be found in McCulloh (1965, 1967); LaFehr (1983) and Popta et al. (1990). Since then, a second generation of gravimeters has been developed by Scintrex. The new gravity sensor is based on fused quartz technology (Nind et al., 2007). In this system the basic sensor technology has been miniaturized and equipped with self-leveling capabilities. The associated electronics modules have been packaged to fit into a narrow diameter borehole probe. The specifications of Gravilog include logging inside NQ diameter (47.6 mm) drillholes to a depth of 2500 m, with a sensitivity of better than $5\mu\mathrm{Gals}$. These new sensors can also be deployed in inclined boreholes from -30° to vertical (Nind et al., 2013).

2.1.1.2 Modelling gravity

In a gravity survey the vertical component of the gravity field caused by anomalous mass can be described as:

$$g_z(r_0) = \gamma \int_V \rho(r) \frac{z - z_0}{|r - r_0|^3} dv \tag{2.1}$$

where V is the anomalous mass volume and γ is the gravitational constant ($6.67 \times 10^{-11} Nm^2/Kg^2$). Also $r = (x, y, z)$ and $r_0 = (x_0, y_0, z_0)$ are the source and observation locations respectively.

For gravity modelling the subsurface is discretized into a set of 3D rectangular prisms using a 3D-mesh with constant density contrast values within each cell. Several analytical formulations for rectangular prism gravity response can be found in Li et al. (1998). In our case, we used the

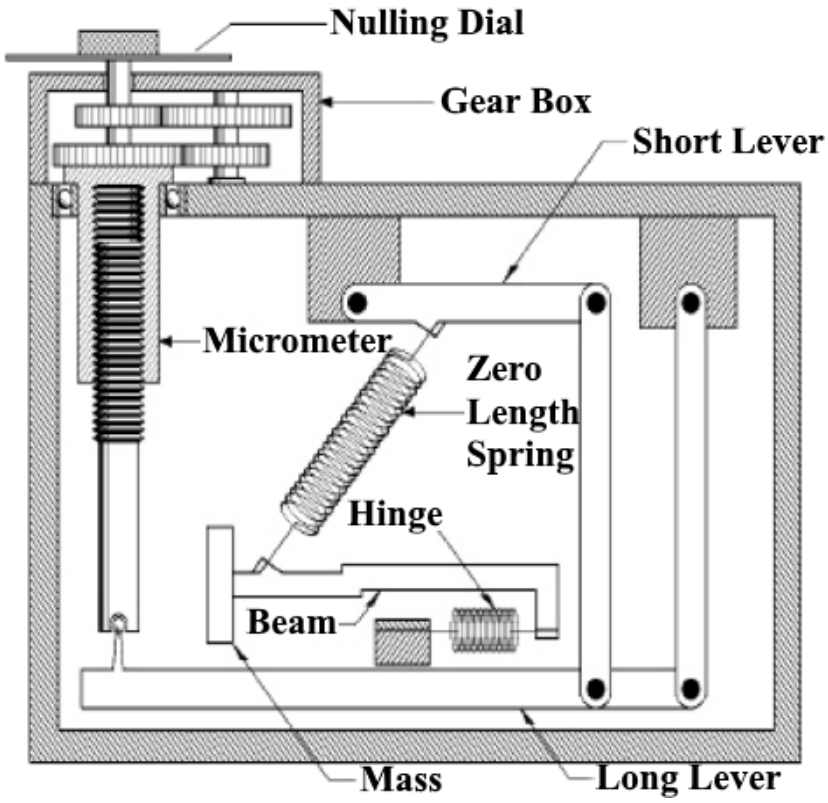

FIGURE 2.1 : Geometry of the Zero Length Spring, LaCoste-Romberg gravimeter (Crossley et al., 2013).

formulation in equation 2.2 of Haáz (1953), which is valid for all observation points at any location. Calculating the gravity response of a complex body is based on the principle of superposition since gravimetry is a linear problem. The gravimetric response of a body can be discretized into rectangular prisms and calculated by summing the contribution of each of these prisms (Li et al., 1998) following equation 2.3.

$$g(x_0, b_l, \rho_l) = -\gamma\rho_l \sum_{i=1}^{2}\sum_{j=1}^{2}\sum_{k=1}^{2} \mu_{ijk}[x_i \ln(y_j + r_{ijk}) + y_j \ln(x_j + r_{ijk}) - z_k \arctan(\frac{x_i y_j}{z_k r_{ijk}})] \qquad (2.2)$$

where,

$$x_i = x_0 - \xi_i, \quad y_j = y_0 - \eta_j, \quad z_k = z_0 - \zeta_k \quad i, j, k = 1, 2$$

$$r_{ijk} = \sqrt{x_i^2 + y_j^2 + z_k^2}$$

$$\mu_{ijk} = (-1)^i (-1)^j (-1)^k$$

and ξ, η, ζ define the eight corners of the prism b_l. The response at the observation point is caused by all of the m prisms such that:

$$g(x_0) = \sum_{l=1}^{m} g(x_0, b_l, \rho_l) \tag{2.3}$$

2.1.1.3 Corrections applied to gravity measurements

In order to isolate the anomalies caused by local density variations from other fields, gravity measurements require a series of corrections (Blakely, 1996). These corrections include Bouguer and terrain corrections (effect of normal mass above sea level), motion due to a moving platform (Eotvos), free air (effect of elevation above sea level), and tidal (time dependent variations). In BHGM, for correcting the drift in measurements it is recommended to do the acquisition from the bottom to the top of the borehole without any reversals of directions. Measurement points should be visited at least three times to obtain enough data for analysis (Nind et al., 2013). For free-air correction which is to compensate for the increase in gravity with depth due to the free-air-effect, the free-air gradient is computed using equation 2.4.

$$F = -(0.3087691 + 0.0004398 \sin^2 \phi)h + 7.2125 \times 10^{-8} h^2 \tag{2.4}$$

where ϕ is the latitude at the borehole and h is the depth of the stations in meters. The Bouguer effect takes into account the mass surrounding the gravimeter. This effect must be removed from the measurements to obtain the anomaly corresponding to the target density zone because the free air anomaly does not take into account the densities of the formations intersected by the borehole (Nind et al., 2013).

$$BE = -4\pi G \rho h \tag{2.5}$$

where ρ is the slab density. The Bouguer anomaly is then calculated as (Schetselaar et al., 2015)

$$G_B = G_{obs} - F - BE \tag{2.6}$$

Regional anomaly should also be removed from the measurements where there are substantial regional effects caused by large geologic features. This anomaly can be obtained using methods such as upward or downward continuation, using measurements at a lower or higher elevation respectively to extrapolate values at a common level.

2.1.2 Direct current resistivity methods and modelling

In a Direct Current (DC) resistivity forward modelling problem the electrical potentials are described as a function of conductivity in the ground, electrode geometry and input current. To this end potential electrodes pairs are placed in a line or a grid to measure a series of potential differences due to the injection of a fixed current intensity at another pair of electrodes. In a resistivity survey, several ways of arranging the current and potential electrodes exist. This configuration of electrodes (array) and the spacing between them are important parameters in a survey as the depth of investigation and the vertical and lateral resolutions depend on them (Roy, 1972; War, 1988). Arrays that are frequently used are illustrated in Figure 2.2. DC resistivity surveys have been used in a wide range of investigation problems such as mapping of groundwater contamination (Klefstad et al., 1977; Ross et al., 1990), evaluation of groundwater resources and aquifer parameters (Schwartz et al., 1977), exploration of hydrocarbons (Yungul, 1962) and also in mining exploration. Mapping of massive and disseminated ore deposits using resistivity or induced polarization techniques has been shown successfully by Leney (1966) and Maillot et al. (1966). The basic principal for DC resistivity experiment is the expression relating the current density J $(A.m^2)$ and the current intensity I (A) injected into the ground at locations $r_s = (x_s, y_s, z_s)$ (equation 2.7) (Dey et al., 1979).

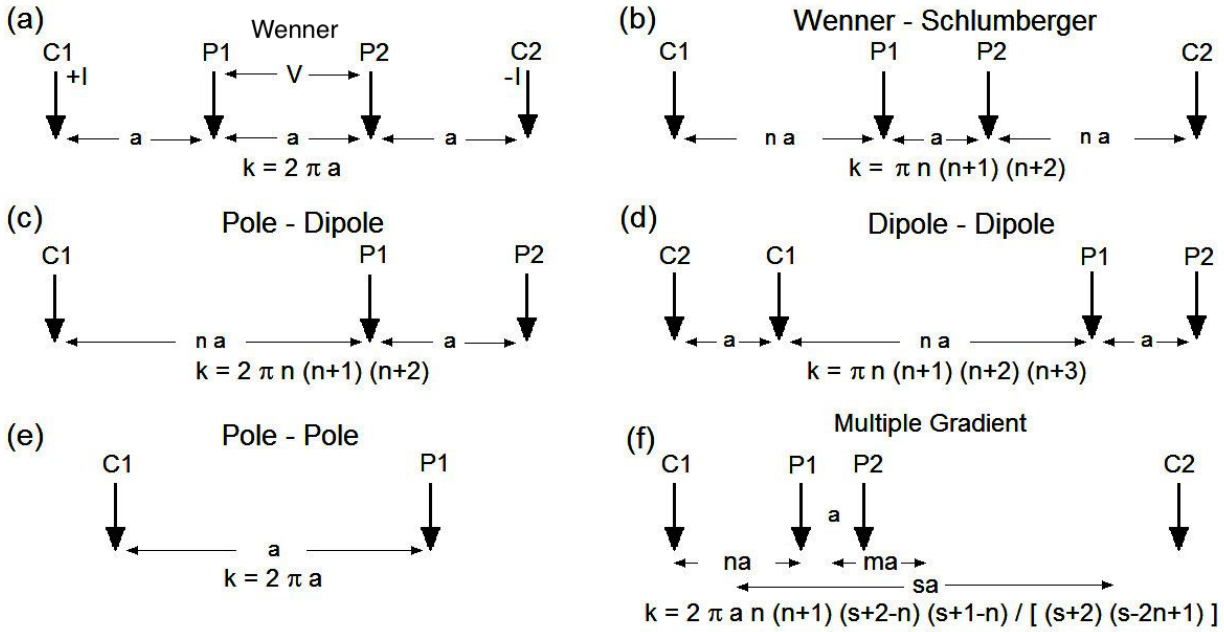

FIGURE 2.2 : Electrical resistivity arrays commonly used in resistivity profiling (Loke et al., 2013).

$$\nabla.J = (\frac{I}{\Delta V})\delta(x - x_s)\delta(y - y_s)\delta(z - z_s) \tag{2.7}$$

where

$$J = \sigma E \tag{2.8}$$

and

$$E = -\Delta\Phi \tag{2.9}$$

therefore

$$J = -\sigma\Delta\Phi \tag{2.10}$$

where σ is the electrical conductivity in (S/m) and Φ is the potential (V). The basic equation to be solved as the forward problem to calculate the potential distribution in the ground is the equation 2.11 as following:

$$-\nabla.[\sigma(x, y, z)\nabla\Phi(x, y, z)] = (\frac{I}{\Delta V})\delta(x - x_s)\delta(y - y_s)\delta(z - z_s) \tag{2.11}$$

Equation 2.11 can be solved by a finite volume method (Dey et al., 1979) or finite element method (Bing et al., 2001; Wu, 2003).

2.2 Geophysical inversion

The geophysical methods used in our case study were briefly described in the geophysical methods section. In order to compute the spatial distribution of the density and resistivity in the ground, the geophysical data acquired using these methods needs to be inverted. It should be mentioned that the same methodology can be applied on other types of geophysical data. There are several academic references on geophysical inverse theory (Menke, 1984; Sen et al., 1991; Parker et al., 1994; Oliver et al., 2008). The conventional approach uses deterministic least-squares algorithm providing, by construction, a single smooth and low-resolution 3D model of the spatial variability of the physical property in the ground. The downside is that the least-squares approach over samples the mean while under sampling the extreme low and high values that are the most important in resources evaluation. Then, this deterministic model can only be used for exploration and does not have the resolution required for further use in the mine design. To overcome this

problem, the direct stochastic approach seeks the posterior probability density of the parameters, unlike the conventional inversion where a single model is sought. For a simple well-posed linear system $Ax = b$ the normal equation is (Menke, 1984):

$$x = (A^T A)^{-1} A^T b \tag{2.12}$$

If the data or parameters are contaminated with noise, or there are more parameters than data or the A operator is only approximative, or any other cause of ill-posedness conditions, the normal equation must be adapted. Depending on the field where those equations are applied, they have different names. In geophysics, they are known as damped least-squares (Menke, 1984) and they include diagonal covariance matrices of the data (C_b) and of the parameters (C_x). With no lack of generality, if x and b are centered variables (zero mean):

$$x = \bar{x} + (A^T C_x^{-1} A + C_b^{-1})^{-1} A^T C_x^{-1} (b - A\bar{x}) \tag{2.13}$$

The damped least-squares, as their names indicates, are suitable to find the best average value of the parameters and fail to infer the lower and upper tails of the "true" or a posteriori distribution of the parameter x. Indeed, in engineering and geostatistics, these equations are known as BLUE (Best Linear Unbiased Estimator) or cokriging, respectively (Gloaguen et al., 2005). In addition to the smoothing effect of the damped least-squares, the optimization step in real applications in inversion can be computationally expensive which is the main restriction of inversion techniques. Another limitation of these approaches is that the final model could depend on the initial model, as the solution of the inverse problem could have local minima. Also different optimized models with the same response could be achieved using different initial models (Grana et al., 2012).

2.2.1 Stochastic inversions

A lot of efforts have been put into stochastic inversion methods to deal with limitations of conventional inversions algorithms in the past few years. Even if they are generally more computationally intensive, in many cases, they are found to be effective to approximate the full distribution of the parameters under study (Gloaguen et al., 2005). There are several approaches, all being different versions of the same goal that is to mimic at best the posterior distribution of the parameters by randomly sampling it. Hence, stochastic inversion will not only provide the best estimate of the

parameters, but also provide an ensemble of equiprobable models of parameters which, in return, give access to the uncertainty of these parameters. There is a large body of literature on stochastic inversion methods (Franklin, 1970; Mosegaard et al., 1995; Eidsvik et al., 2004; Tarantola, 2005) and their application on geophysical data (Haas et al., 1994; Torres-Verdin et al., 1999; Asli et al., 2000; Chasseriau et al., 2003; Gloaguen et al., 2005; Bosch et al., 2006; Hansen et al., 2006; Giroux et al., 2007; Shamsipour et al., 2010, 2011a, 2012).

2.2.2 History matching methods and ensemble methods

In this section, the described techniques are related to the present work in terms of sourcing the motivation behind it.

2.2.3 History matching

History matching is a rich optimization group of techniques that aims to integrate time dependent non-linear forward modelling of a secondary variable to improve the knowledge on a primary variable that varies in time and-or space. For example, in oil and gas reservoir characterization, well information such as pore pressure and oil production are simulated using water and oil flow modelling and then compared to measured ones in order to improve the understanding of petrophysical properties (pore oil saturation, permeabilities) (Le Ravalec et al., 1999). Recent advances in history matching allow for a complete update of geological features like faults, lithology, porosity as well as for the fluids features (pressure, oil saturation) by integrating 4D seismic and well production data (Skjervheim et al., 2005). History matching can be deterministic or stochastic. This concept is further discussed in the optimization section 2.4.

2.2.4 Ensemble methods

A very convenient way to compute stochastic history matching is to use ensemble methods as proposed by Evensen (2003). Ensemble methods rely on stochastic modelling of the variables under study such as oil saturation, permeability. As a starting point, we need to generate multiple models of the reservoir primary variables. These models are sent to a reservoir forward modelling algorithm that calculates the secondary information (pore pressure, production rates) on each stochastic

model allowing for experimental covariance computation. Then, measured secondary information, typically at wells, are used linearly to update the primary variables on all models over time.

These two techniques inspire the entire workflow of this thesis in the sense that we aim to attain history matching between petrophysical properties and geophysical data. As any history matching algorithm, it starts with stochastic modelling of the variables under study. This involves integrating knowledge on geology, petrophysics, geostatistics and geophysics in a nested workflow. In the following sections we present the geostatistical tools used to generate the starting stochastic models.

2.3 Geostatistical methods

Geostatistics provides a series of tools for interpolating or simulating variables using the spatial correlation between data. These methods were initially developed in 1960s for the purpose of reserves evaluation in mining deposits (Goovaerts, 1997). Nowadays geostatistic methods have vast applications in mining, petroleum, hydrogeology, environmental studies and several other disciplines. In traditional orebody modelling, grade control and ore reserve calculations are carried out using only grades measured on assays from diamond drill-holes. Once the geology is defined in the form of the mineralized areas with stationary grade mean and variance, the grades are interpolated within the wireframe using kriging or simulation algorithms.

2.3.1 Kriging

Kriging, a least-squares linear regression method was proposed by Matheron (1963) and was named after the pioneer work of Krige (1951). The method was further promoted by Blais et al. (1968) and David (1969). The basic idea of kriging is to estimate the value of a function based on the weighted average of its known values in the neighbourhood and is similar in every point as the BLUE algorithm in engineering. Detailed descriptions of the kriging method can be found in Journel et al. (1978), Isaaks et al. (1989), Armstrong (1998) and Kelkar et al. (2002). Kriging involves computing the experimental variogram of the data, fitting it with an admissible theoretical model, computing the relevant variances and finally the kriging estimate and kriging variance calculations (David, 2012). The main characteristic of kriging is to minimize the variance estimation, making it the best unbiased linear interpolator. However while minimizing the estimation variance since the method is

a least-squares estimator of the mean, it suffers from a smoothing problem. The smoothing effect causes kriging to underestimate large values and overestimate the average values (Journel et al., 1978). Also the smoothing is not uniform meaning that close to data locations it is small and it increases farther away from the measurement locations. An other disadvantage of kriging is that it returns a single estimation of the parameter of interest precluding the quantification of uncertainty of the process (Goovaerts, 1997). These shortcomings in conventional grade modelling approach caused by the smoothing effect can result in spatial variability decrease (David, 2012). According to Monjezi et al. (2013) several studies do not recommend the application of smoothing method in the grade modelling (Deutsch et al., 1998; Sinclair et al., 2006; Webster et al., 2007) as all resources estimations rely on tonnage of ore above a given cut-off. More precisely, it means that the resources estimation depends on our capability to accurately estimate all the quantiles of the "true" grade distribution.

2.3.2 Simulations

To address the limitations of the conventional method and the orebody uncertainty, stochastic simulation method is proposed (Journel, 1974; Journel et al., 1978; David, 1988; Dimitrakopoulos, 1990; Journel, 1992; Dimitrakopoulos, 1994; Fouguet et al., 1994). Simulation algorithms generate a set of possible responses (realizations) for a set of measured data and their variogram instead of a single output as it is the case in kriging estimation. In these techniques the data values are honoured resulting in conditional realizations, conditioned to the data values. Also the histogram and the covariance model of the sample data are reproduced from the simulated values. The simulation techniques can be classified based on the type of the variable to be simulated. Algorithms suitable for continuous variables are sequential Gaussian simulation, indicator simulation, LU decomposition, p-field simulation and simulated annealing. Algorithms that can be used to simulate categorical variables include Boolean and object-oriented algorithms; single or multiple truncations of a Gaussian field; indicator-based algorithms; simulated annealing and p-filed simulation (Goovaerts, 1997). Some techniques such as multiple-point simulation methods can be used for both continuous and categorical variables (Mariethoz et al., 2010).

According to Halton (1970) conditional simulation is a sort of Monte Carlo techniques which constructs grade distribution realizations with equal probability (Chiles et al., 2009; Deutsch et al., 1998; Dimitrakopoulos, 1998). The method has been used to associate the grade uncertainty

with the orebody modelling in open pit mining (Ravenscroft, 1992; Dimitrakopoulos, 1998; Smith et al., 1999; Kumral et al., 2001). Several studies have been carried out throughout the years on improving and applying the method, which resulted in important remarks such as the deviation from the project objective due to planning with a single kriged orebody model while applying the conditional simulation (Dimitrakopoulos et al., 2002), finding the best simulation model for the deposit (Dimitrakopoulos et al., 2007) and application of conditional simulation to obtain the maximum net present value (NPV), (Ramazan et al., 2018).

According to Isaaks (1992) the optimum classification in grade control would not be achieved by kriging since it does not account for the uncertainty in grade estimation and the map of blast hole grade values showing the ore-waste or ore block boundaries would be over-smoothed (Verly, 2005). Verly's paper (2005) concentrates on two estimation-based grade control methods, the simple polygonal interpolation and the ordinary kriging approach (David, 1977; Journel et al., 1978; Isaaks et al., 1989) along with four simulation based methods. From this study he concludes that simulation is advantageous over kriging for reasons such as better integration of geological input, soft information and spatial trends, not smoothing the maps like the kriging methods and handling the problem of change of support. Other benefits of simulation methods (Isaaks, 1992; Gómez-Hernández et al., 1993; Verly, 1993; Goovaerts, 1997) include better quantifying the risk with probability maps and finding the tonnage that exceeds the cut-off grade.There are several simulation techniques which all have their pros and cons, but all try to reproduce the joint probability density function (pdf) of a generating random function. The simulations can be :

- non conditioning (turning bands (TUBA), fast Fourier transform moving average (FFT-MA) ...) or self-conditioning (sequential Gaussian simulation, LU, ...)
- continuous (turning bands, FFT-MA, ...) or discrete (sequential indicator simulation, multiple-point, truncated Gaussian, ...)
- order two (FFT-MA, LU, ...) or high-order (multiple-point, wavesim, ...)

All these algorithms provide a series of tools that can be used depending of the task to be completed.

2.3.3 Sequential simulation methods

One of the best known ensemble of simulation techniques is the sequential simulation. This method is not the fastest or the easiest to use, but it has the advantage of being self conditioning

and sequential, making it very convenient to integrate multiple variables. The method makes use of the fact that any joint probability distribution function of the model parameters can be exactly approximated by a sequential product of conditional pdf. Practically speaking, this means that, at each node of a grid, a conditional pdf is computed using conditional measured data including the values previously simulated (Goovaerts, 1997). There are two categories of sequential simulation methods, which are based on two-point or multiple-point statistics. Two-point statistics considers the spatial variability of model parameters through a covariance model. An example of this category is the Gaussian model, which involves a mean and a covariance model under the assumption of a normal distribution of the model parameters (Ruggeri, 2014). According to Journel (1994) the sequential algorithms that are used in practice consist of Sequential Gaussian Simulation (SGS), that is based on simple kriging technique, as well as sequential indicator simulation (SIS) which is based on indicator kriging approach (Alabert, 1987).

2.3.4 Sequential Gaussian simulation (SGS)

In this section, as SGS is a well known simulation technique, we only present a practical overview of SGS algorithm. A complete theoretical review can be found in Goovaerts (1997). Sequential Gaussian simulation is referred to the implementation of the sequential principle under the multi-Gaussian random function (RF) model. SGS involves the following steps: 1-Check for the appropriateness of the multi-Gaussian RF model. Here, the data are transformed to a Gaussian distribution using the normal score transform. 2-The sequential simulation is then performed on the transformed data. This step includes defining a random path to visit all the nodes of the grid (only once). Next the conditional mean and variance are estimated using simple kriging and the normal score semivariogram model. The simulated values are sampled from a Gaussian probability distribution and are subsequently used as input data in the simulation at following points. All simulated values are then back-transformed to the original data space, which requires the inverse of the normal score transform (Goovaerts, 1997; Deutsch et al., 1998; Doyen, 2007). In SGS process more realizations are obtained by repeating these steps with a different random path. A theoretical extension to Gaussian sequential simulation is shown by Xu et al. (1994) where the values are simulated without any prior normal score transformation. In this method called direct sequential simulation (Dssim), continuous variables can be simulated with their variograms reproduced, if the simulated values are taken from a distribution whose parameters (mean and variance) are estimated

by simple kriging Journel (1994). However in order to reproduce the histogram a post processing step is necessary since Dssim does not control the histogram of simulated values (Goovaerts, 1997).

2.3.5 Multiple-point simulation (MPS)

The MPS is a pixel-based stochastic facies modelling technique commonly used in oil and gas geological modelling to simulate complex geological structures (Guardiano et al., 1993; Journel et al., 2006). The method was first proposed and implemented by Guardiano et al. (1993) to overcome the limitations of conventional geostatistical simulations based on the study of the variogram of the lithology measured along drill-holes (two-point statistics). Specifically, two-points algorithms (like indicator kriging, indicator simulations) can only reproduce simple geology in space (for example uniformly distributed lenses with similar shapes) and fail to mimic more complex geology (Journel, 1993; Caers et al., 1998; Strébelle et al., 2000; Strebelle, 2002; Caers et al., 2004). MPS uses a training image (TI), which is a 3D conceptual geological model representing the a priori spatial structure of the geology on which high-order (or multiple-point) statistics are computed. By multiple-point statistics we mean taking into account the correlation between three or more spatial locations rather than only computing the variogram, which calculates the dissimilarity of a variable between only two locations. The training image depicts only the conceptual geological structures of the simulated phenomenon. This implies spatial continuity similar to the actual phenomenon but does not provide precise spatial information (Arpat et al., 2007; Maharaja, 2008). As described in Arpat et al. (2007), the dimensions of these training images are different from the study area. They could be obtained from the available data such as outcrops or from an unconstrained realization of an object-based simulations method. In Guardiano et al. (1993) approach a new scan of the complete training image is required at each simulated node, which made it computationally inefficient (Wu et al., 2008). During the two last decades several MPS algorithms were developed to improve the computational performance of the original algorithm. These algorithms however, propose different simulation methods, termed snesim (Strebelle, 2002), filtersim (Zhang et al., 2006; Wu et al., 2008), simpat (Arpat et al., 2007), and hosim (Mustapha et al., 2010) or Direct Sampling (Mariethoz et al., 2010). All of them are based on stationary training images. The stationarity of the training images is based on the principle of similarity and repetition of patterns in space. Different descriptions of the stationarity are given in literature but a simple definition would be the zones that have approximately

the same mean, variance and/or other statistical moments (Deutsch et al., 1998; Arpat et al., 2007; Chiles et al., 2009). Caers et al. (2004) describe the stationarity as having the data originating from one population (a zone of stationarity) and being able to pool these data to calculate the bivariate and multiple-point statistics. In the original MPS algorithm, the stationarity of the training image cannot be respected when geological heterogeneity exists. To overcome this problem, Arpat et al. (2007) proposed the simpat algorithm in which the simulation method of the original algorithm is modified by adding other a priori information in the form of simple geometric rules, such as rotation and dilatation. Vries et al. (2008) proposed another solution by dividing the training image into stationary sub-zones. Other developments in multiple-point simulation algorithms include Markov Random Field approach (Daly, 2005; Tjelmeland et al., 2005), the kernel approaches (Scheidt et al., 2008) and multi-scale simulations based on the wavelet decomposition of training images (Chatterjee et al., 2009; Gloaguen et al., 2009). In our case, we used the impala algorithm, which is an improved version of the Chugunova et al. (2008) algorithm. The latter applies auxiliary constraints to distinguish patterns by storing the values of one or several secondary variables in the search tree, which is a dynamic data structure consisting of an ensemble of nodes corresponding to particular patterns to store the multiple-point statistics from the training image. To improve its computational efficiency, Straubhaar et al. (2011) proposed the impala algorithm, an improved parallel MPS algorithm using a "list approach", where the search tree is replaced by a list which not only makes the simulation less random-access memory (RAM) demanding but also deals with non-stationary training images. The list contains the data events and their occurrence for each geological unit. The advantage of this parallelization approach is that rather than simulating several realizations at the same time (Vargas et al., 2008; Mariethoz et al., 2010), it tends to parallelize the computation of the conditional probability density function at every node, speeding up this step which is the most time consuming one (Straubhaar et al., 2011). In impala algorithm in order to assign a facies at a node u on the simulation grid, we need to retain the nodes v that are in the training image and have the same components of data event $d(v)$ as those of $d(u)$. In order to calculate the conditional probability distribution function (CPDF), the occurrences of all the facies at the nodes v are then calculated. This CPDF is then used to randomly draw a facies at node u. The probability to draw the facies k at the node u is obtained from equation 2.14, where n is the number of components in $d(u)$, in positions $i_1 < ... < i_n$, with $0 \leq n \leq N$. Also the $u + h_{i_1}, ..., u + h_{i_n}$ are the simulated nodes in the

data event $d(u)$ centered at u.

$$P(s(u) = k|d(u)) = \frac{\#\{v \in TI : s(v + h_{i_j}) = s(u + h_{i_j}), 1 \leq j \leq n \quad and \quad s(v) = k\}}{\#\{v \in TI : s(v + h_{i_j}) = s(u + h_{i_j}), 1 \leq j \leq n\}} \tag{2.14}$$

2.3.6 Bayesian sequential simulation

The Bayesian sequential simulation (BSS) is a two-point geostatistical algorithm and it is based on parameterization of Bayes theorem (Bayes, 1763). Bayesain cokriging was first proposed to deal with interpolation of lithological data constrained by non-linear seismic attributes (Doyen et al., 1996). After, this algorithm was modified to generate multiple feasible realizations of the spatial distribution of the primary variable conditioned to a secondary variable (Ruggeri, 2014). The BSS technique considers and quantifies the uncertainty and like all geostatistical sequential simulation methods, the procedure of generating each stochastic realization is done iteratively. At each iteration, the previously simulated values are considered as known values for the following steps (Goovaerts, 1997; Deutsch, 2002). This technique makes it possible to integrate different types of data, while taking into account the non-linear links existing between them. It also makes it possible to include any previously known information on the variable under study (Dubreuil-Boisclair, 2013). This concept is expressed in terms of conditional probabilities as shown in equation 2.15.

$$p(A_i|B) = \frac{p(B|A_i)P(A_i)}{\sum_{j=1}^{k} p(B|A_j)P(A_j)} \tag{2.15}$$

where $A_1, ..., A_k$, are k events from the sampling space considered as primary variable, B is an observed event (i.e. secondary variable), $p(.)$ denotes a probability distribution. The a priori probability representing the previously known statistical information on the phenomena of interest is shown by $p(A_i)$. The probability $p(B|A_j)$ is called Bayesian likelihood function and is determined by estimating the joint probability density. The update of the a priori once the event B observed is called posteriori probability and it is denoted by $p(A_i|B)$. BSS allows finding petrophysical properties from observations, as long as a certain statistical relationship exists between them causing the technique to be often described as an inversion method (Dubreuil-Boisclair, 2013). Collocated data are usually used to empirically model this statistical relationship (Ruggeri, 2014). The aim of Bayesian inverse methods is to obtain samples of the posterior density probability function (Caers et al., 2006). This approach has been successfully used for reservoir (Gastaldi et al., 1998; Doyen,

2007; Dubreuil-Boisclair et al., 2012) and hydrological characterization (Bosch et al., 2010; Dubreuil-Boisclair et al., 2011; Ruggeri et al., 2013). We propose to adapt the Bayesian stochastic inversion method, which has been developed for gas hydrate grade estimation (Dubreuil-Boisclair et al., 2012). This stochastic approach allows incorporating all available data including geological and geophysical data while taking into account their respective uncertainties. It is due to the non-linear nature of the relationships between the physical properties including conductivity and density of the measurement points at the deposit under study that makes this approach suitable for characterization purposes. Figure 2.3 shows the BSS workflow adapted in the present study.

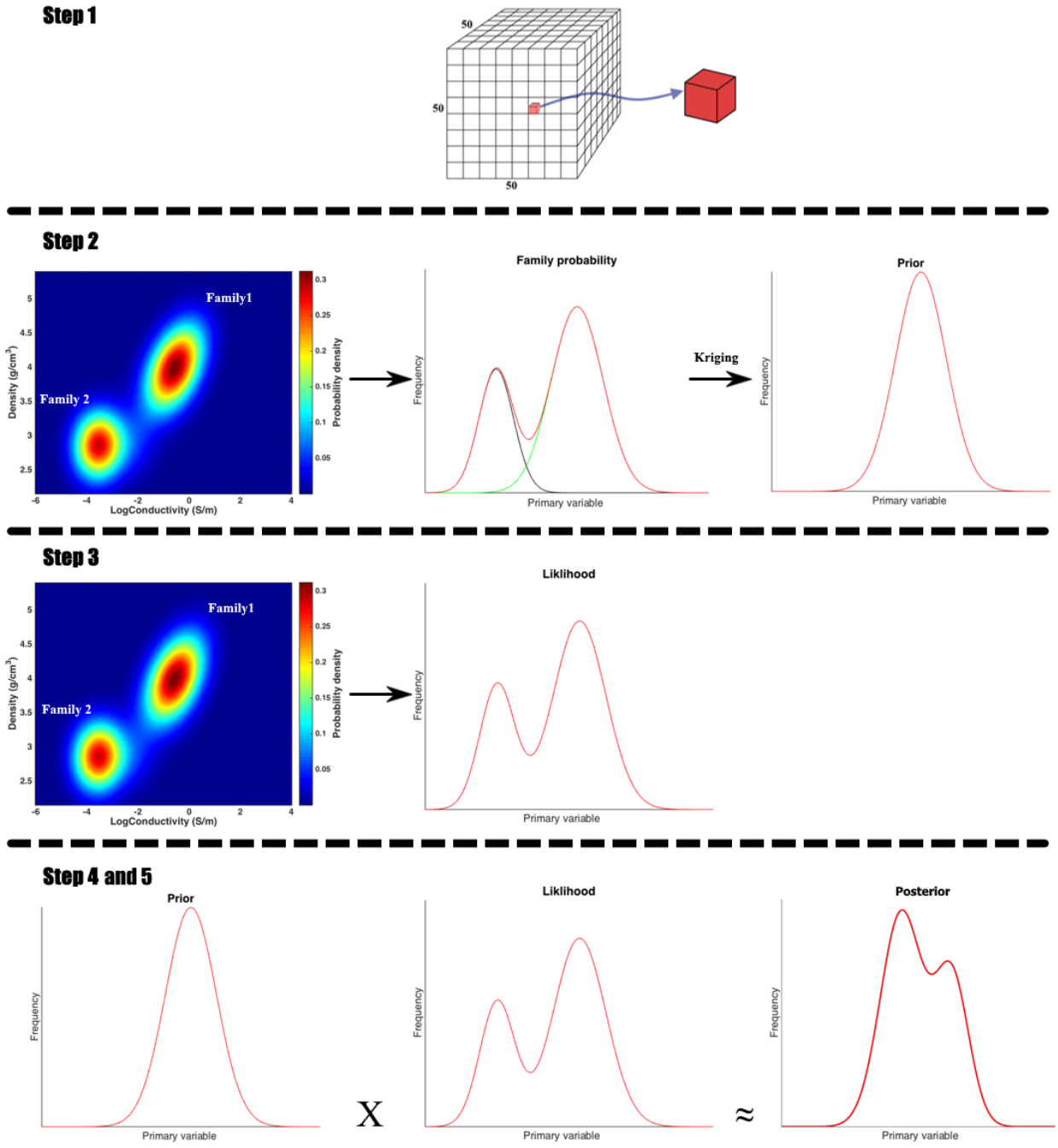

FIGURE 2.3 : Bayesian sequential simulation algorithm

2.3.6.1 Kernel estimation

The concept of the kernel estimator is very similar to that of the histogram but in a multi-dimensional way. Indeed, rather than estimating the probability density of a point x by adding the number of observations included in a bin of fixed width h, the kernel method replaces the bin with a continuous distribution function, called kernel. This can take several forms including a normal distribution, centred in x, of variance h_2. Thus, the closer an observation gets to this point, the more important it is. The final probability density is obtained by the sum of each of these contributions, which is then normalized to obtain a density function. In a multivariable case, this function will be obtained by multiplying the probability densities corresponding to each of the random variables. Among the most common kernels (uniform, triangle, epanechnikov, quadratic, cubic, Gaussian, and circular), it is the Gaussian kernel (zero mean and variance of one) that has been retained because it best corresponds to the shape of the marginal distributions and eliminates abrupt variations. It is routinely used for continuous variables. This is expressed by the following formula:

$$K(u) = \frac{1}{\sqrt{2\pi}} \exp^{-\frac{1}{2}u^2} \tag{2.16}$$

The simplest solution for combining all of the kernels to form the multidimensional kernel, $K(u) = K(U_1, ..., U_d)$, is to multiply them to determine the joint probability density of the d random variables (Epanechnikov, 1969; Wand et al., 1995). Therefore for two random variables such as conductivity (σ) and density (ϕ), equation 2.17 follows:

$$f(\sigma, \phi) = \frac{1}{nh_1h_2} \sum_{i=1}^{n} K(\frac{\sigma - \sigma_i}{h_1}) K(\frac{\phi - \phi_i}{h_2}) \tag{2.17}$$

where h_1 and h_2 control the amount of smoothing applied to data and are the smoothing parameters called kernel bandwidths and K is the kernel function. For Gaussian kernel the bandwidth is calculated using three methods proposed by Silverman (2018) as shown in equation 2.18, the equation 2.19 referenced to as the Rule of thumb by Deheuvels (1977) and the formulation by Bowman et al. (1993) in equation 2.20:

$$h = 0.9An^{-\frac{1}{5}} \tag{2.18}$$

where A is the minimum of the standard deviation and the inter-quantile rank divided by 1.34.

$$h = 1.06\sigma n^{-\frac{1}{5}} \tag{2.19}$$

$$h = \sigma n^{-\frac{1}{6}} \tag{2.20}$$

Other than these empirical equations, another way to choose the smoothing parameter is to plot several curves and choose the one most concordant with the ideal probability density function. This visual selection of bandwidth is specifically suitable where there are only two variables under study. It should be noted that a bandwidth that is too large leads to too much smoothing therefore it decreases the resolution of the relationship between variables. For example, it might smooth away the bi-modality structure of the relationship between variables. However, an insufficient bandwidth leads to an unstable relationship between variables (Wand et al., 1995; Dubreuil-Boisclair, 2013).

2.3.7 Gaussian mixture model (GMM)

A mixture model is used as a probabilistic model to determine the subpopulations within an overall population without knowing which observed data belongs to which subpopulation. Therefore, the method is used in the present study to cluster the log data to infer the family clusters for each cell being visited in the BSS process. A specific type of mixture models is a Gaussian mixture model (GMM) (McLachlan et al., 1988). A continuous random function Z with a normal or Gaussian distribution with the notation of $Z \sim N(\mu, \sigma^2)$, where μ and σ^2 are the mean and the variance of the distribution, has a probability density function as following:

$$p(x) = \frac{1}{(2\pi)^{\frac{1}{2}}\sigma} \exp[-\frac{1}{2}(\frac{Z(x) - \mu}{\sigma})^2] \tag{2.21}$$

A continuous random function with a Gaussian mixture distribution has the following pdf:

$$\begin{aligned} p(x) &= \sum_{m=1}^{M} \frac{c_m}{(2\pi)^{\frac{1}{2}}\sigma_m} \exp[-\frac{1}{2}(\frac{Z(x)-\mu_m}{\sigma_m})^2] \\ &= \sum_{m=1}^{M} c_m N(Z;\mu_m,\sigma_m^2) \\ &(-\infty < z(x) < \infty; \sigma_m > 0; c_m > 0), \sum_{m=1}^{M} c_m = 1 \end{aligned} \tag{2.22}$$

2.4 Optimization

The process of iteratively comparing data and changing the model is termed history matching. There are two categories for history matching, 1) by gradient methods and 2) by stochastic methods. Gradient method algorithms include Quasi-Newton, Conjugate Gradient and Levenberg-Marquardt and they require computing the Jacobian (partial derivative of the parameters) (Gill et al., 1981). The calculation of these derivatives (gradients) to define the direction and the amount to change in the parameter is still an active area of research. There is a tendency in these methods to converge quickly in pure convex parameter space however they are sensitive to local minima. Therefore the initial guess needs to be selected close to the optimum. In the present study, when we talk about stochastic methods, we are referring to techniques that do not involve calculating gradients and they only require the evaluation of a forward-model. This excludes the stochastic gradient methods (Hinton et al., 2012) but eases the understanding of the document. The optimization methods such as simulated annealing and genetic algorithms belong to the category of stochastic methods (Hoffman, 2005). These methods are theoretically able to converge to the global minimum and not likely to be trapped in local minima as in gradient methods.

2.4.1 Definition of objective function

The goal is to find a parameter m that minimizes the norm of the mismatch between measured data d_{obs} and calculated data $g(m)$, where $g()$ is the transfer function between data and parameters.

$$y(m) = \frac{1}{2} \left\| g(m) - d_{obs} \right\|^2 \tag{2.23}$$

Another approach to define the objective function is to use the norm of sum of these mismatches, however a limitation due to the units of measurement arises. In the case where the data have different units, a normalization step can be applied to the equation. The weights for the normalization are calculated from the error of the observed data. Equation 2.23 is usually used when the number of parameters to be estimated are less than the number of observed data, in other words, when the problem is over-determined (Feraille et al., 2003). In practice, however, this is usually not the case. When dealing with large number of parameters, a second term is typically added to the objective function to make the response of the model geologically plausible. There are several studies that have discussed the addition of this second term to equation 2.23 to penalize the differences between the calculated and the a priori model of parameters or to apply a weighted norm to measure the smoothness of the function (Tikhonov et al., 1977; Lee et al., 1986; Makhlouf et al., 1993). Such objective function can be written as:

$$y(m) = \frac{1}{2} \|g(m) - d_{obs}\|^2 + \alpha \|m - m_0\|^2 \tag{2.24}$$

where α is the coefficient of regularization that controls the deviation of the final model from the initial model and smoothing of the optimal model.

2.4.2 Minimization of objective function

There are different algorithms to minimize an objective function. The algorithms that are based on gradient-based approaches use Gauss–Newton or quasi-Newton methods for minimization. Gradient-based methods allow a fast descent to the closest minimum and are practical when dealing with smooth functions. Unfortunately they fail to pass beyond a local minimum if the function has several minima. To avoid these limitations, stochastic global optimization techniques can be used. These techniques generate random trajectories until a satisfactory minimum is reached (Mantica et al., 2001). Some of the global optimization methods include evolutionary techniques such as genetic algorithm (GA), simulated annealing (SA) which applies a probabilistic mechanism that enables the search procedure to escape from local minima (Kirkpatrick, 1984; Dekkers et al., 1991) and Hybrid approach which combines neural networks with SA method (Ouenes et al., 1994).

In order to overcome time constraints, stochastic parameterization techniques can be used. A good parameterization technique must preserve the variability of the stochastic models while

ensuring a fast convergence of the optimization algorithm by reducing the parameter space (Hu, 2000). The optimization problem in the case of gradual deformation reduces to a one dimensional minimization problem of determining the value of α (Oliver et al., 2011). In the present study, the objective functions are minimized using Matlab's *fminbnd* optimization function which allows minimizing a non-linear function to a bounded interval (Brent, 1973; Forsythe et al., 1977). The algorithm is based on golden section and parabolic interpolation. The limitations of Matlab's *fminbnd* function are that the function to be minimized must be continuous, the solutions obtained are local, and the algorithm may exhibit slow convergence to even divergence when the solution is on one of the limits of the interval where the function is evaluated (Yrro, 2018). The golden-section search is an efficient way to progressively reduce the interval to locate the minimum. The algorithm maintains the function values for point triplets whose distances form a golden ratio. This minimization involves a prob step to construct a new narrower search interval that is guaranteed to contain the minimum value of a convex function.

The line-search algorithm is another method to achieve this minimization. Line-search starts by finding the direction and then identifying an appropriate distance known as the step length. The method is used as part of a larger optimization algorithm. At each step of the main algorithm the line-search method searches along the line containing the current point parallel to the search direction, which is a vector determined by the main algorithm (Nocedal et al., 2006; Fletcher, 2013). In order to obtain global convergence not only the step lengths must be well chosen but also the search directions have to be appropriately selected. Since, in theory, the GDM is based on set of realizations and each are randomly drawn according to the same a priori probability, we are able to escape the local minima. Therefore, the minimum reached by GDM is theoretically the global minimum but, it depends on the initial set of realizations and the way they are iteratively integrated.

2.5 Gradual deformation method

The parameterization method which is the one adapted in the present study is the gradual deformation method proposed by Hu (2000). Several variations of the gradual deformation method (GDM), first developed by Roggero et al. (1998) for history matching purposes, have been tested (Hu, 2000, 2002; Hu et al., 2001; Le Ravalec et al., 2012). This parameterization technique seeks a better match between the computed and measured data through generating gradual and continuous perturbations of a set of initial prior realizations (Caers, 2007). The original deformation method

allows to respect the following three characteristics: (1) The deformed model must remain a realization of the stochastic model. (2) It must yield a regular objective function so as to be processed by an efficient optimization algorithm (e.g. a gradient based algorithm). (3) The deformation must allow one to cover the whole solution space.

The method gradually combines two independent Gaussian realizations of the physical property ($y_1(r)$ and $y_2(r)$ in equation 2.25) through a linear combination of variable r and computes the geophysical response on the new combined model $y(r)$. The combination in equation 2.25 results in a Gaussian random model that has, by design, the same mean and covariance as the two initial models (Feller, 2008). The combinations are parameterized with a single parameter, which results in the reduction of the high dimensional optimization problem to a much simpler 1D space. The corresponding weights in the combinations allow the gradual modification of the models between the poles formed by the original models and prevent geologically unrealistic responses.

$$y(r) = y_1 \cos r + y_2 \sin r \tag{2.25}$$

The sequence built to achieve the realizations honouring the statistical properties is the exploration path within the realizations space. The trigonometric expression above is characteristic of a hyper-ellipsoid whose dimensions are the number of components of y realizations in an iteration and it is centred at y_0 the mean realization (Figure 2.4). In minimization with gradual deformation, the

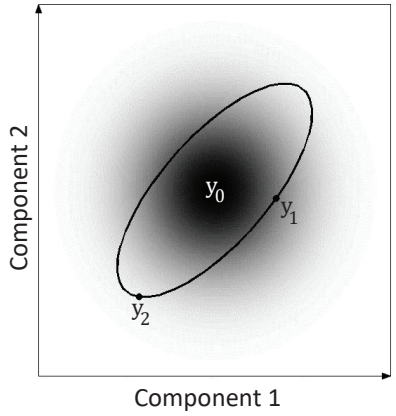

FIGURE 2.4 : Sequence of realizations developed by gradually combining the realizations y_1 and y_1. y_0 is the mean realization (Le Ravalec-Dupin, 2011)

hyper-ellipsoids built from the successive optimization processes are explored. The goal is to find the realization that minimizes the objective function. Gradually, the ellipses are oriented towards the minimum until it is reached (Figure 2.5).

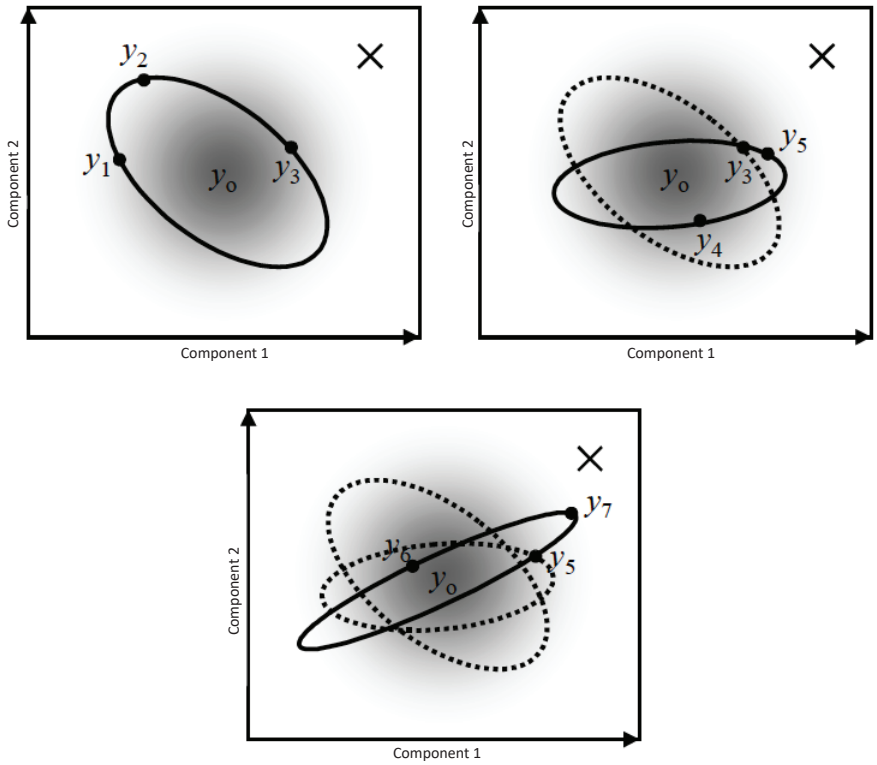

FIGURE 2.5 : y_0 and the cross symbols represent the mean realization and where the minimum is sought, respectively (Le Ravalec-Dupin, 2011).

2.5.1 Multidimensional gradual deformation

It is possible to use several independent realizations to generalize the deformation algorithm and create a multidimensional process of independent realizations. The weights (α_i) are still applied to preserve the variance of the model.

$$y(r_1, r_2, ..., r_m) = \sum_{i=0}^{m} \alpha_i y_i \tag{2.26}$$

where

$$\sum_{i=0}^{n} {\alpha_i}^2 = 1$$

with

$$\alpha_1 = \prod_{i=1}^{m} \cos r_i$$

$$\alpha_i = \sin r_i \prod_{j=i+1}^{m} \cos r_j (i = 1, m-1)$$

$$\alpha_m = \sin r_m$$

Introducing this generalization of GDM, Hu (2000) allows to solve an optimization problem for m deformation parameters $r_1, r_2, ..., r_m$. This optimization leads to an improved fit to the observed data. In summary the advantages of GDM are (Le Ravalec-Dupin, 2011):

— 1- Realizations discretized on very large size grids can be deformed using only a few deformation parameters therefore the number of parameters are reduced.

— 2- The adequacy between the deformed model and the a priori model can be qualified by analyzing the hyper-ellipsoid on the average realization. The mean, variance and the covariance are preserved for all the realizations on this hyper-ellipsoid.

— 3- The minimization problem is well simplified due to the consistency of GDM with regard to the a priori constraint. This consistency allows for not integrating the a priori constraint as a term in the objective function.

3 APPLICATION OF THE METHODOLOGY ON REAL DATA: THE LALOR CASE STUDY

3.1 Introduction

In this chapter, the proposed workflow (Figure 3.1) of our stochastic inversion method and the results of its application on the Lalor case study are presented. The original 3D conceptual geological model of the Lalor deposit was built by a Ph.D. student in geology in our research group (Caté et al., 2015). We modified this original geological model in order to group geological units with similar petrophysical properties (Step 1 in Figure 3.1). This model was then used as the training image to generate 100 different 3D stochastic geological scenarios using the multiple-point simulation (MPS) algorithm, while at the same time respecting the geological borehole data and the conceptual model (step 2 in Figure 3.1). Each geological unit was then populated by density values from their intrinsic petrophysical relationships using the conditional sequential Gaussian simulation (CSGS) algorithm (step 3 in Figure 3.1). In conventional inversion workflow, as local scale borehole measurements provide the physical data at a high-resolution and considering that geophysical least-squares inversions have low to very low resolution, it is challenging to integrate them without losing the high resolution of downhole data. However, as our methodology involves only forward modelling, there is no problem of compatibility between the resolution and the scale of different measurements. However, as the density models are stochastic, the locally simulated models are likely to be inadequate with regards to the geophysical data far from the boreholes. Therefore, the next step is to combine the different petrophysical models to minimize the difference between the calculated and measured gravity data (step 4 in Figure 3.1). The optimized density model and borehole conductivity logs are then fed to Bayesian sequential simulation algorithms to stochastically build 3D conductivity models (Step 5 in Figure 3.1). Next, the conductivity models go through another optimization step where the objective function is to minimize the difference between raw and computed electrical potentials resulting in an optimized conductivity model (Step 6 in Figure 3.1). In the following sections, we will describe in detail each step of the workflow.

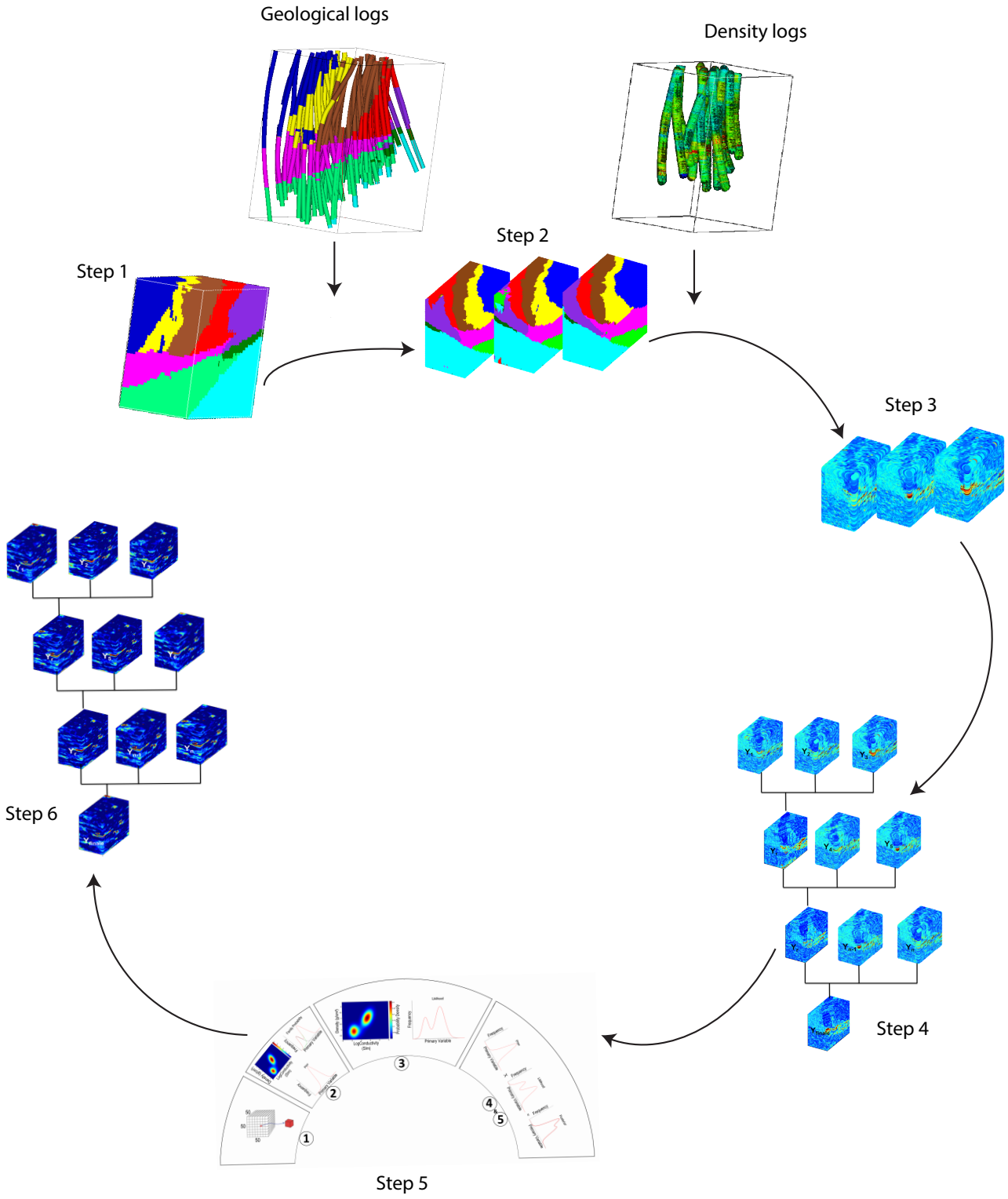

FIGURE 3.1 : Workflow of the proposed approach. Step 1: building the geological model. Step 2: applying MPS on the 3D initial geological model. Step 3: applying CSGS on a hundred 3D geological realizations. Step 4: performing GDM. Step 5: computing BSS. Step 6: GDM application on conductivity realizations

3.2 Description of the Lalor deposit

The study is carried out on the Lalor volcanogenic massive sulphide (VMS) deposit, which is located near Snow Lake, Manitoba, Canada (Figure 3.2). It sits approximately 700 km north of Winnipeg and lies within the Chisel Basin sequence of the Proterozoic Flin Flon Greenstone Belt (Blakley et al., 2008). In the Chisel Basin a north and a south anomaly were detected by the company Hudbay Minerals during a surface time-domain electromagnetic survey in 2003. The survey was designed to target deep conductors. However the south anomaly intersected non-economic stringer chalcopyrite, pyrite and pyrrhotite after drilling. Hudbay Minerals conducted the first drilling campaign in 2007 to test the north electromagnetic anomaly and the first borehole drilled (DUB168) showed a profitable width of zinc-rich massive sulphides (Newton et al., 2017). In Geological Survey of Canada's phase 4 of the Targeted Geoscience Initiative (TGI-4) several geophysical surveys were carried out on the Lalor site, including seismic, passive seismic interferometry, electrical resistivity tomography (ERT) and gravity surveys. Through different geophysical methods the extent of the depth projection of VMS deposit was studied. These methods include forward modelling of 3D seismic data, inversion of gravity and magnetic data and ERT (Bellefleur et al., 2015a). The lateral extent of the deposit is approximately 900 m in the north–south direction and 700 m in the east–west direction. It also dips shallowly to the northeast. The mineralization is found between 570 and 1500 m below surface. Several studies have been carried out on the deposit (Bailes, 2013; Yang et al., 2013; Bellefleur et al., 2015a; Caté et al., 2015; Duff et al., 2015; Schetselaar et al., 2015; Bouchedda et al., 2016; Caté, 2016; Duff, 2016; Caté et al., 2018; Schetselaar et al., 2018). Through an extensive drilling program, (2007–2012) which included the drilling of a total of 225 surface holes and wedges for a total of 200,081 m (Carter et al., 2012) three mineralization styles within the deposit were found including a sulphide rich mineralization called near-solid sulphide, which mainly contains pyrite and sphalerite with lesser amounts of chalcopyrite and pyrrhotite. The second mineralization style is the stringer sulphide with sulphide minerals such as chalcopyrite and lesser amounts of pyrite, sphalerite and galena. The third mineralization style is the disseminated sulphide mineralization which contains up to 20 percent sulphide minerals such as pyrite and small amounts of sphalerite and pyrrhotite (Taylor, 2014).

Three distinct mineralization zones were mapped from the drilling program: (1) zinc, (2) gold, and (3) gold–copper (Bellefleur et al., 2015a; Duff et al., 2015). Figure 3.3 shows a vertical section of the deposit. The Chisel sequence has been subdivided into lower and upper sequences (Bailes et al.,

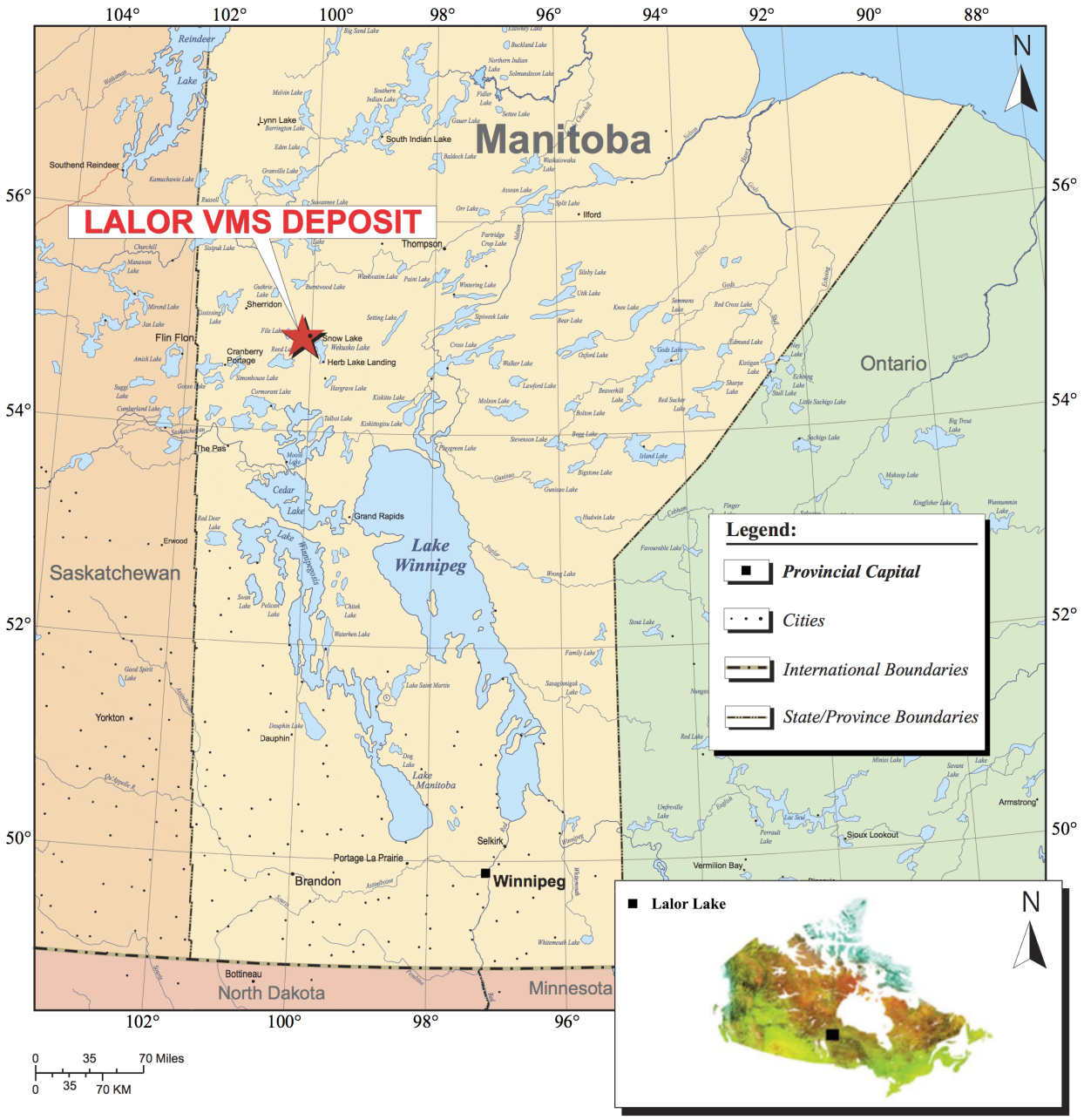

FIGURE 3.2 : Lalor VMS deposit, Snow Lake, Manitoba, Canada Blakley et al. (2008).

2007) which form the footwall and hanging wall of a structural contact, respectively. The sulphide ore lenses of the Lalor deposit lie 10–100 m beneath this contact. The hanging wall includes mafic and felsic volcanic rocks while the footwall consists of a thick zone of intensely metamorphosed hydrothermally altered rocks (Carter et al., 2012). This leads to a local transformation of volcanic and volcaniclastic rocks into schist and gneiss (Galley et al., 2007; Caté et al., 2013). Lalor is by far one of the largest metal deposits within the Flin Flon Greenstone Belt. Among the 25 Mt of reserves, resources and the exploited ore, the zinc-rich zones are the largest (15 Mt) and the shallowest,

and they consist of near-massive sulphide mineralization. The gold and gold–copper zones, which include 8.8 Mt of reserves and resources at 4.6 g/t Au, are disseminated and are composed of stringers of sulphide mineralization. The gold–copper zone consists of semi-massive and stockwork chalcopyrite and pyrrhotite. The average grade of Cu for this zone is 4.64% (Carter et al., 2012; Bellefleur et al., 2015a; Caté et al., 2015). An active exploration target at greater depths over the study area is the deeper part of the deposit where the gold–copper mineralization is assumed to continue (Bellefleur et al., 2015b). Overall the deep high-grade gold and gold-copper zones are the unique features of the Lalor deposit that have attracted further exploration at greater depths at this site (Schetselaar et al., 2015).

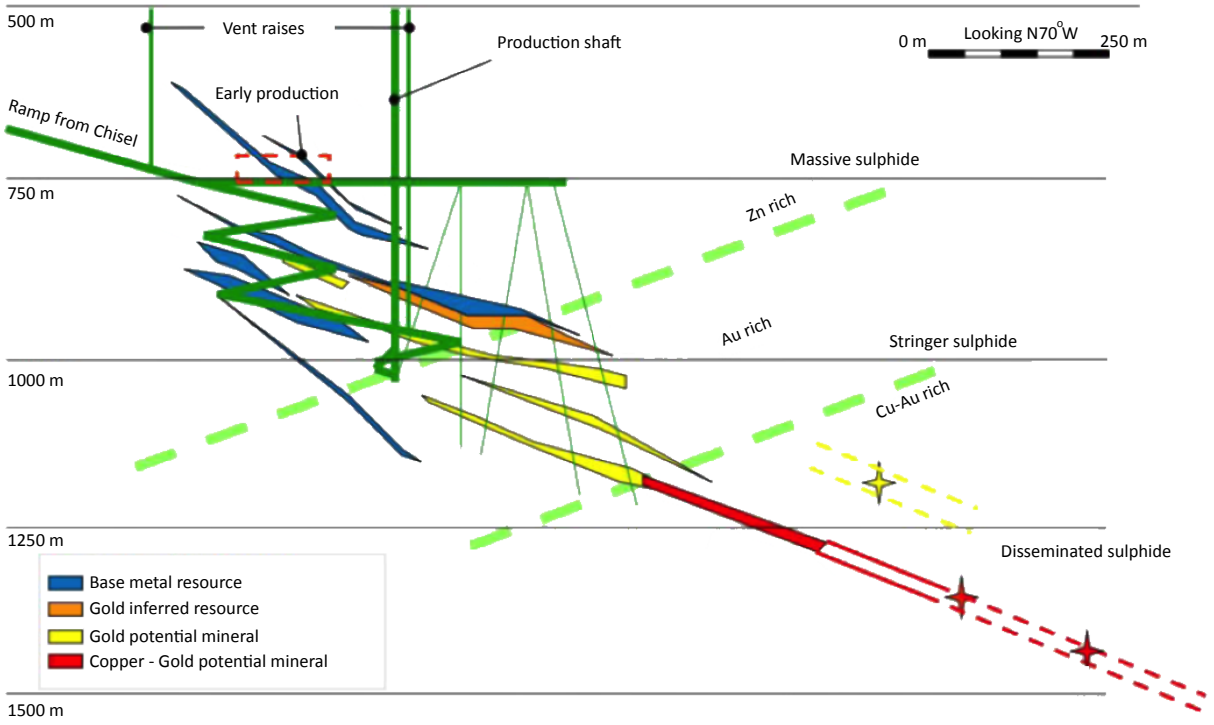

FIGURE 3.3 : Vertical section of the Lalor deposit showing Zn-rich, Au-rich and Cu-Au rich mineralized zones, from Bellefleur et al. (2015a).

3.3 Geological model

Among the geological studies and models, the work by Caté et al. (2015) is the most recent on Lalor and presents a summary of all the previous site descriptions. The complementary data used for creating the model include extensive drillhole descriptions and geochemical data from Hudbay Minerals as well as data collected by Caté et al. (2015). The model was built using a classification

machine-learning algorithm to distinguish volcanic units and alteration types. Various alteration indices were used to model the geometry of the alteration zones. For our case study, we have modified the size of the model to cover a volume of 974 m × 1929 m × 1663 m (Figure 3.4). This model contains 9 lithological units including Balloch basalt, Ghost Lake rhyodacite, FWHW1 which contains Lalor Powderhouse dacite, North Balloch rhyodacite, North Chisel dacite, Threehouse mafic unit, Upper Moore mafic unit, Upper Threehouse mafic unit and FWHW2 which contains Western Powderhouse dacite, as shown in the Figure 3.4. Massive sulphide ore lenses are located in the FWHW1 unit and the Upper Moore mafic unit, which are felsic and mafic volcaniclastic units, respectively (Caté, 2016).

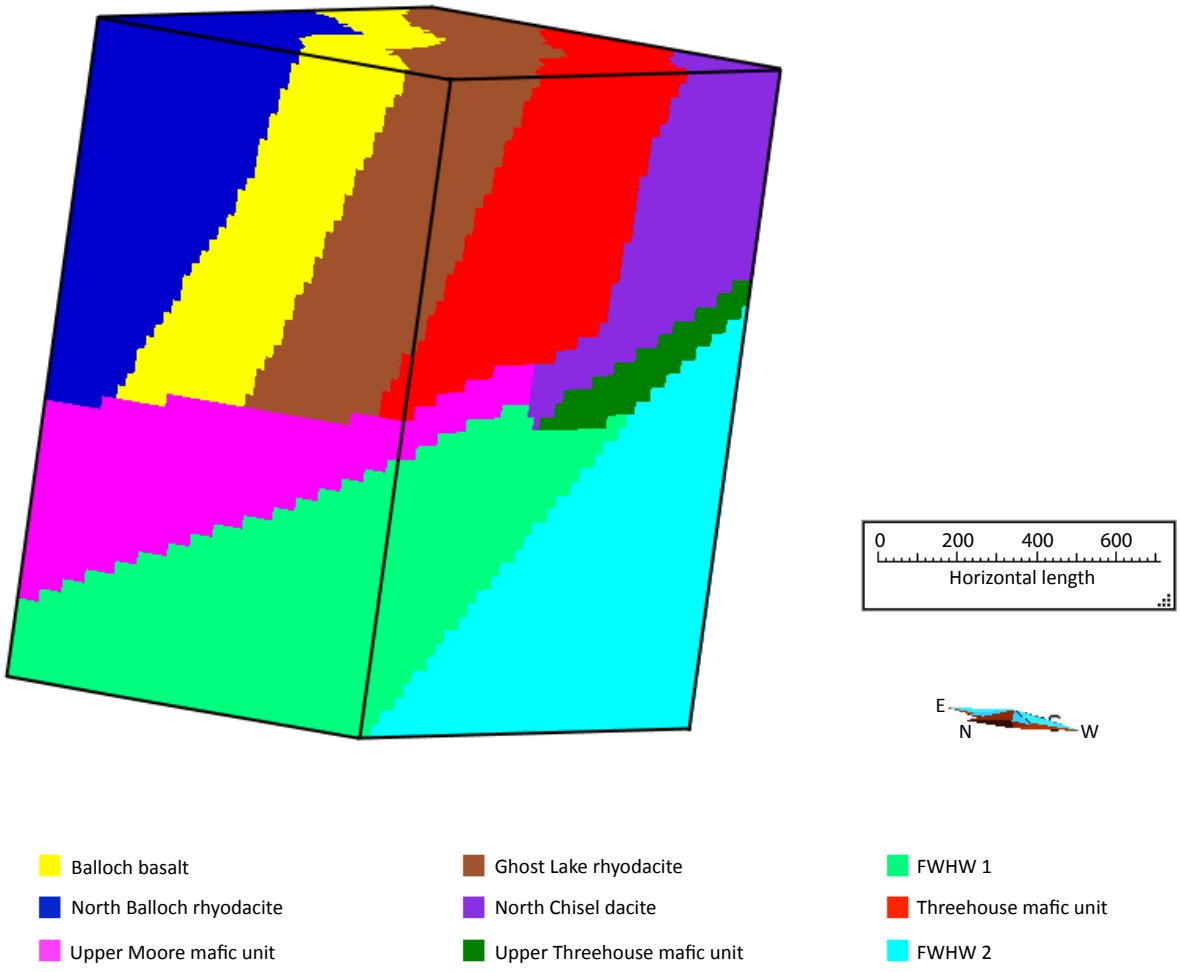

FIGURE 3.4 : Geological model of Lalor VMS area modified from (Caté et al., 2015).

3.4 Geophysical signatures of volcanogenic massive sulphide deposits

Volcanogenic massive sulphide (VMS) deposits typically show strong physical property contrasts with their host rocks. This contrast is due to the substantial differences in physical and chemical properties such as density, gravity and electrical resistivity between the deposits and the host rocks (Thomas et al., 2000). This makes geophysical techniques instrumental in the discovery of VMS deposits, especially when they are deeply buried (Newton et al., 2017). The geophysical signature produced by the orebody depends on its shape, depth and its sulphide content. Electric and electromagnetic (EM) methods are currently the most used techniques to detect VMS deposits. These surveys include airborne EM (with systems such as megaTEM), and DCIP (using for example Titan 24). These techniques are essentially used to target drill sites to help overcome the limits of detectable depth ranges (Morgan, 2012). In order to determine whether a conductivity anomaly is caused by a low-density graphite body or by a high-density sulphide mineralized zone at depth, gravimetric surveys can be used in conjunction with conductivity surveys (Thomas et al., 2000). The minerals found in VMS deposits including sulphide minerals (pyrite, pyrrhotite, chalcopyrite, sphalerite) and non-sulphide minerals (magnetite, hematite) have relatively high specific gravity values in contrast to those of sedimentary and volcanic host rocks. Gravimetric surveys are also used to detect and estimate the size of a body with excess mass at depth which may imply the existence of an orebody (Morgan, 2012). Several geophysical surveys have been conducted over the Lalor deposit. These surveys include airborne (VTEM, ZTEM, HELITEM, HeliSAM), surface (TDEM, AMT/MT, DCIP, Seismic, VLF) and logging (borehole EM, downhole gravimetry, petrophysical logging). Figure 3.5 shows HeliSAM and DPEM test survey grids and loops, the seismic receiver and shot line locations and borehole locations for BHGM survey over the deposit. The physical rock properties at Lalor are in general agreement with properties from elsewhere in the Flin Flon Belt (Fowler et al., 2005; White et al., 2012). As an example of geophysical survey, Yang et al. (2013) used airborne and ground electromagnetic (EM) data for their study. The ground survey covers a smaller area compared to the airborne survey but provides information about the deep targets through very late times. Therefore in order to build a model that is able to image the structure at the deposit scale and also covers the area at a regional scale they inverted the ground data with a smooth airborne model as the reference model for the three-dimensional (3D) inversion. Their study was focused on finding a common conductivity model between two models that resulted from individually inverting the two data sets. They concluded that although the ground EM data have

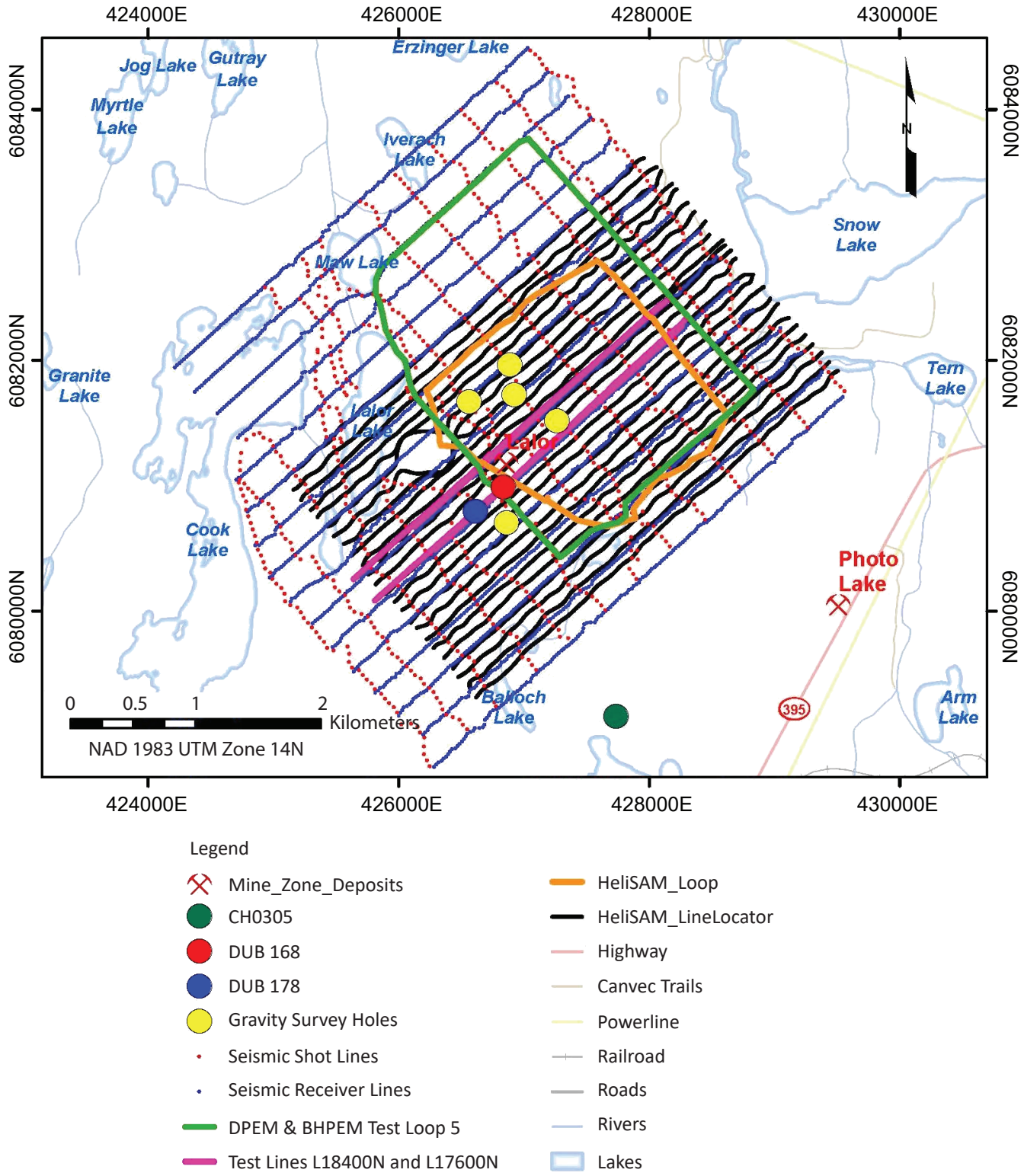

FIGURE 3.5 : Locations of HeliSAM and DPEM test survey grids, seismic receiver and shot lines and boreholes for BHGM survey shown over the deposit (Newton et al., 2017).

more signals from a potential deep orebody, there is a deficiency in the amount of information from these data that prevents fully delineation of the target geometry. This lack of information is due to the restriction of locations of measurements in the ground survey. Bellefleur et al. (2015b) studied the data from a 3D seismic survey over the deposit (Figure 3.5) in order to define the geometry and reflectivity of the orebody as well as integrating the seismic data with 3D geological information. The 3D geological model provided them with important information including the continuation of contacts away from the boreholes. The data used in their study were wireline logging data acquired in boreholes and measurements including V_p, V_s and density on core samples. It is shown from the physical rock properties that contacts between felsic and mafic volcanic rocks are the most likely cause of seismic reflections in the area. Bellefleur et al. (2015b) also show that zinc-rich massive sulphide zones have high acoustic impedances therefore prominent reflections can be produced when they are juxtaposed against any host rocks. Although this is not the case for the gold-rich zones. Cheraghi et al. (2015) analyzed passive seismic interferometry for exploration of the massive sulphide deposits in a complex crystalline rock environment. For this purpose they acquired ambient noise data over a subset of an active-source 3D three-component seismic grid over the Lalor mining area. The authors showed the applicability of the seismic data in depicting the boundaries of the orebody. The seismic methods are however, limited in mining industry due to the high cost of data acquisition, the limited number of case studies, the lack of economical discoveries in these case studies and the uncertainty in approaches to how the seismic data should be integrated with exploration data. In the case of Lalor VMS deposit the method may have been of questionable utility as it is not a direct ore finding method (Newton et al., 2017). It provides 3D structural information on deposits but reflectors cannot always be directly associated with mineralization. This interpretation can only be achieved through a proper understanding of the ore forming processes and the structural constraints (Yang et al., 2018). For this reason, 3D seismic has its most value in a brown field setting where it can help reduce the cost of drilling, not as a primary exploration tool. In Bouchedda et al. (2016), a small scale conductivity model was constructed from the Lalor dataset. The authors defined an objective function with two terms including conventional electrical potential data misfit and the misfit between experimental semivariograms of the inverted conductivity model and the logged resistivity data. Shamsipour et al. (2014) studied the use of structural orientation constraints in the stochastic inversion of gravity data from Lalor. The constraints were point pairs corresponding to massive sulphide ore which were extracted from a 3D seismic cube. The use of these structural constraints proved to be helpful in recovering the orientation of the deposit at depth. Schetselaar

et al. (2014) implemented the Common Earth Modeling (CEM) approach on Lalor data set to build a numerical grid model that reconciles 3D lithofacies models with 3D seismic data as well as 3D potential fields inversions. This makes it possible to corroborate the relationships between protoliths, hydrothermal alterations and their effects on geophysical responses (seismic and gravity). To this end they built a geological surface model of the deposit from drillhole logs and a geologic map of unit contacts. This surface model was used to build a curvilinear grid for the 3D lithological model and stochastic models of physical properties.

Tirdad et al. (2019) computed the least-squares gravity inversion on Lalor deposit. In this study, they discretized the 3D subsurface volume into a regular grid of $31 \times 31 \times 16$ cells along the x, y, and z-axis, respectively. The size of the cells within the grid determines the resolution of the model. The cell size was chosen to be 100 m in proportion to the distance between the gravity measurements. The authors used Tikhonov regularization parameter equal to 0.1 to overcome the instability of the solution. In addition, 248 density measurements in drill holes were used to constrain the output model. Figure 3.6 shows this output density model after 35 iterations. The resolution of this model is too low and its distribution overrepresents the mean while not reaching the extreme values measured along boreholes.

In the next section, we present in more details the data used in this study. While, there would be an interest in integrating all the above data, we had to choose the most valuable data for the available downhole physical data. The focus of the present study is on using the gravity, DC resistivity, density and resistivity logs for data integration.

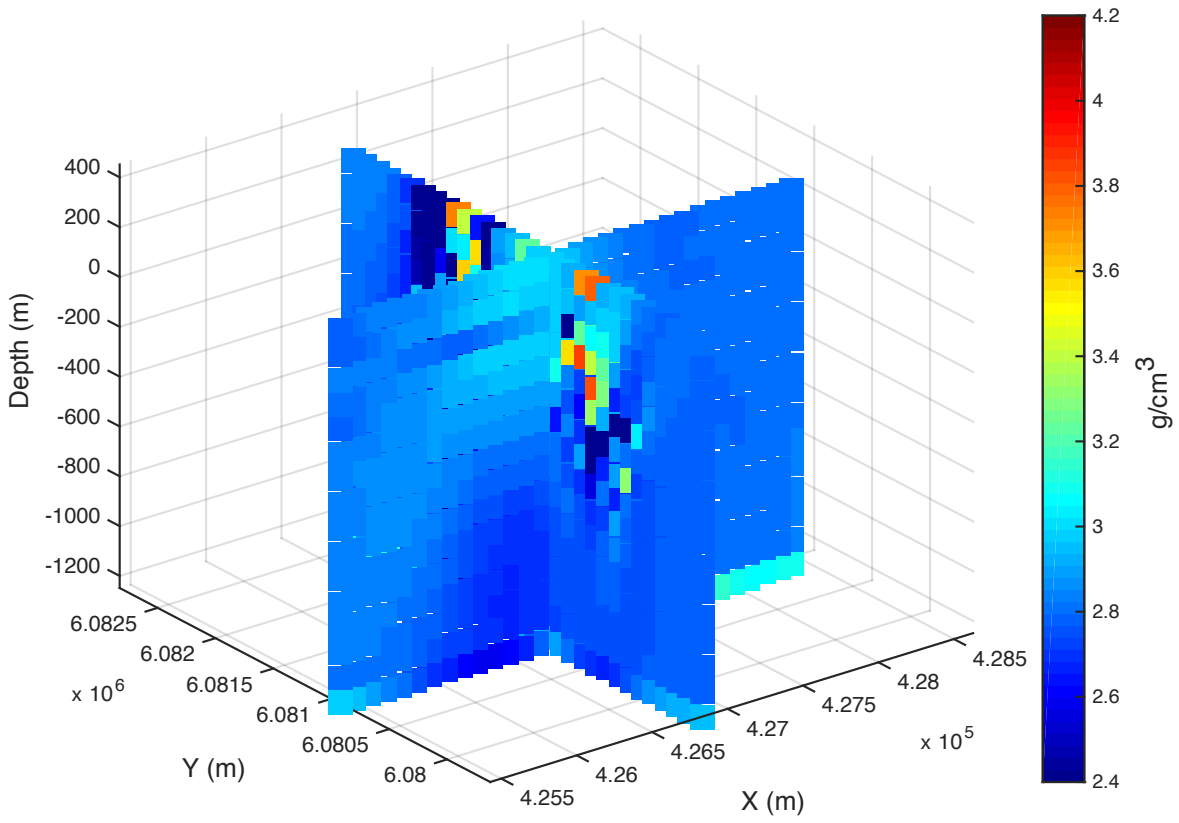

FIGURE 3.6 : Sections of density model obtained from borehole Tikhonov regularized least-squares inversion (Tirdad et al., 2019).

3.5 Well logs and geophysical data

Contrary to the practice in the petroleum industry, only a few studies have tackled the problem of defining petrophysical relations in mineral exploration. One of the main reason is the very high number of drillholes available in mining projects compared to that available in the oil and gas industry. Also, the geological settings are more complex in the mining environment, rendering the application of petrophysical relations non-trivial. However, as a work hypothesis, we claim here that petrophysical data would help geophysical inversion and geological modeling. At the Lalor deposit, only 17 boreholes were logged with geophysical tools to provide collocated information on the host lithology, orebodies, and geophysical parameters. In this study, 13 boreholes are selected as they are located within the grid of our geological model. This type of data are key to translate physical properties into geological properties and vice versa. The logging of physical rock properties was carried out by DGI Geoscience for Hudbay Minerals. A total of 15 physical properties were recorded in the boreholes at a vertical spacing between 10 and 20 cm. In this dataset, a significant

number of measurements for each of these rock properties was considered as “no data value”. This was particularly the case for conductivity measurements where about 93% of the readings are NAN since no strong signal was detected in the conductivity at these points (Caté et al., 2017). In addition to geophysical logging, lithology along all boreholes was conventionally logged by geologists. Figure 3.7 shows the density logs along with lithology for boreholes DUB260, DUB253, DUB245, DUB202, DUB189, DUB191.

3.5.1 Gravity data

3.5.1.1 Downhole gravity data

The downhole gravity data were acquired by the Geological Survey of Canada along five drill-holes (DUB202, DUB279, DUB280, DUB282, and DUB287), intersecting the Lalor VMS. Drillholes DUB202, DUB280, DUB282 and DUB287 intersect geological formations in the down-plunge extent of the Lalor sulphide ore lenses and drill hole DUB279 intersects the host rocks up-plunge from the known sulphide ore lenses. All five surveyed holes were located at a distance greater than 250 m away from the Lalor lenses. Figure 3.8 shows the location of these five boreholes on the geological map of Chisel Basin. The survey was conducted to improve the 3D gravity inversion using combined surface and borehole gravity data. The data were collected using an irregular spacing varying from 10 to 100 m, 10 m in the zone of interest up to 100 m in the near-surface zones (Schetselaar et al., 2015). Downhole measurements were carried out using the Scintrex Gravilog slim-hole gravity sensor (Nind et al., 2007). Figure 3.9 shows the instrument while taking measurements at a station. A total of 155 gravity measurements were acquired. For the purpose of quality control, 39 % of the readings were repeated that showed the average absolute error to be less than 6.5 $\mu\mathrm{Gals}$. Table 3.1 shows the specifications of the Scintrex GRAVILOG probe.

Abitibi Geophysics corrected the borehole gravimeter data for time-based drift, tidal, sensor temperature and sensor rotation (instrument related corrections) to obtain the observed gravity (G_{obs}). The density value of 2.86 g/cm^3 was used to calculate the Bouguer anomaly and the terrain correction (Schetselaar et al., 2015)(unpublished results: Borehole Gravity Survey, Lalor deposit project, ABITIBI Geophysics, 2014).

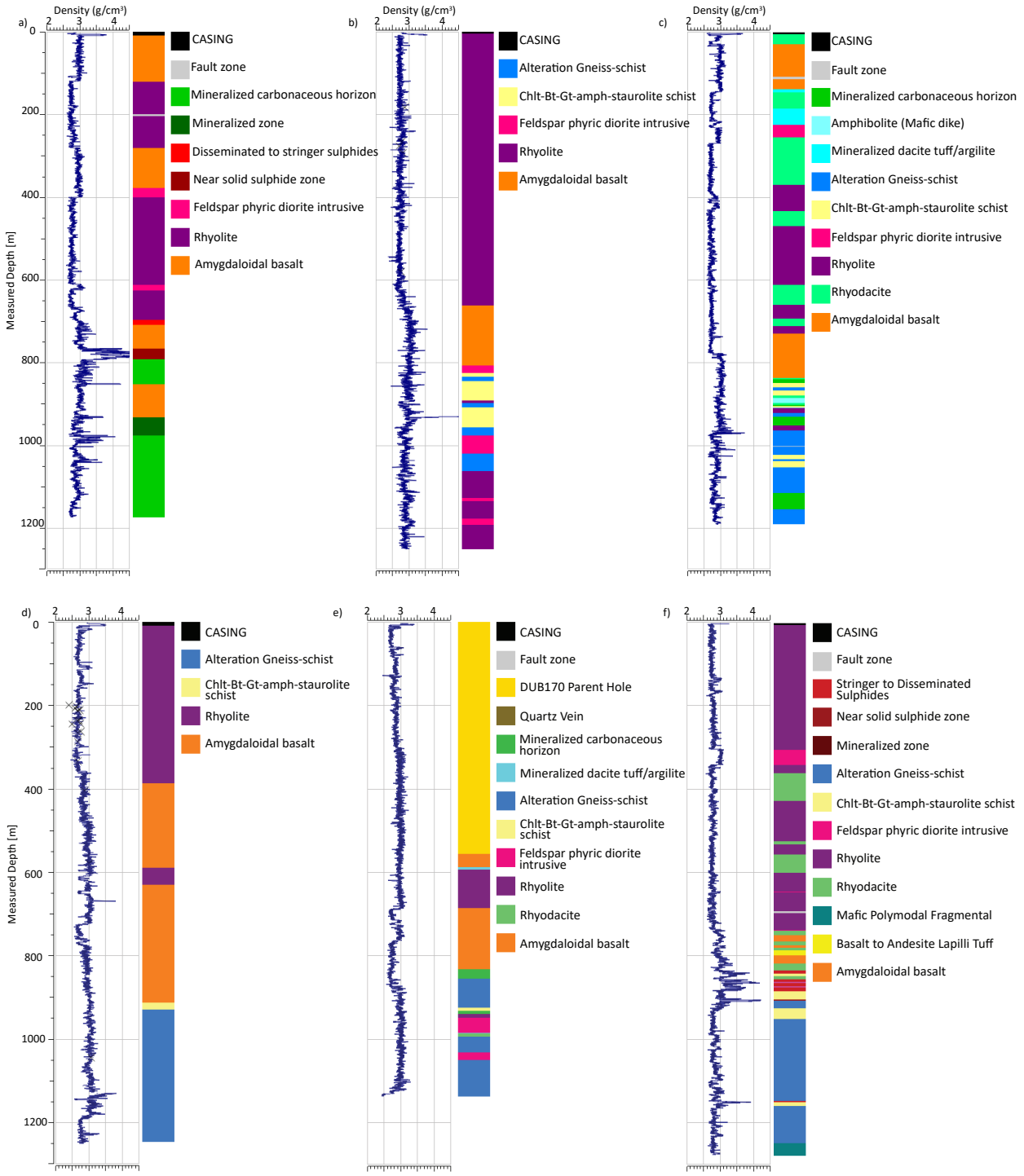

FIGURE 3.7 : Combined plots of density and lithofacies logs from boreholes a) DUB260, b) DUB253, c) DUB245, d) DUB202, e) DUB189, f) DUB191. The rock units are modified from unpublished results by Mira Geoscience (2014).

Figure 3.10 shows the Bouguer anomalies within each borehole. The borehole gravity data show the increase in density values generally correspond to mafic rocks locations. Overall density variations reflect changes in lithology. Mafic rocks intersected in DUB202 and DUB287 explain

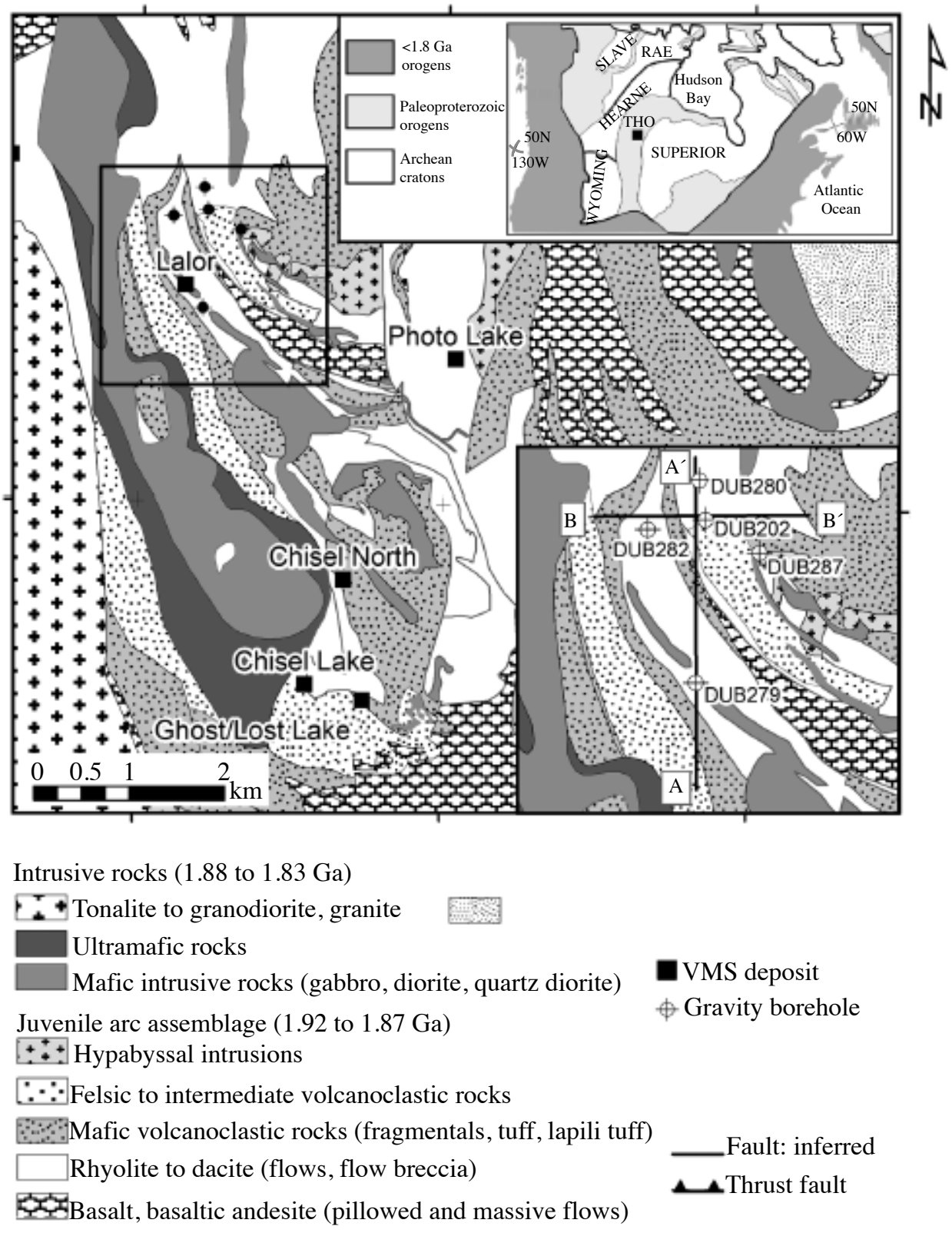

FIGURE 3.8 : Geological map of the Chisel Basin showing the location of the Lalor VMS deposit as well as the location of the five drillholes, Bailes et al. (2007); Schetselaar et al. (2015)

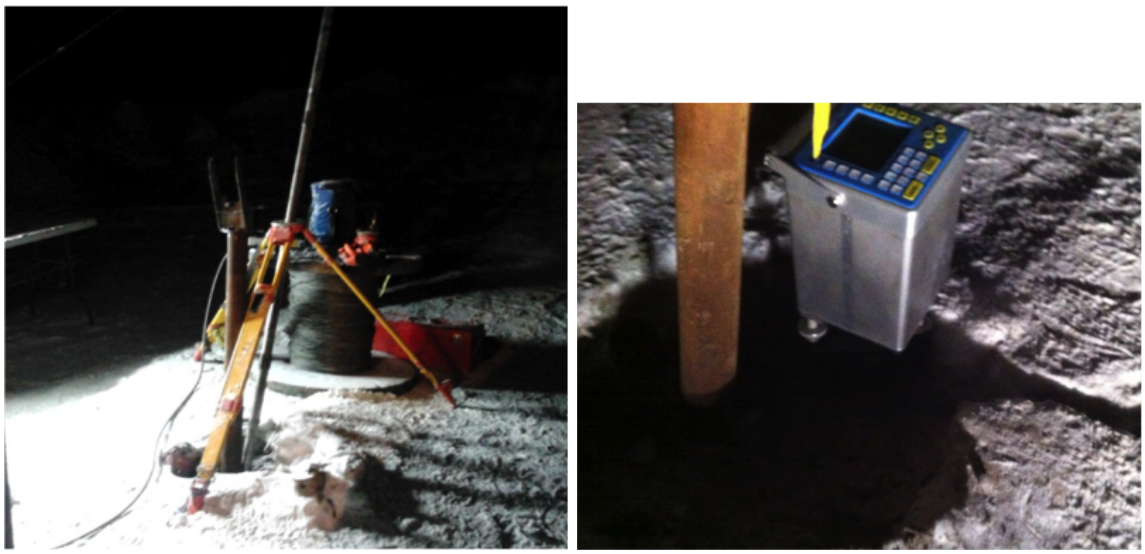

FIGURE 3.9 : Gravilog probe and the surface CG-5 gravimeter taking readings at the surface of the borehole

TABLE 3.1 : Specifications of the Scintrex Gravilog probe (Schetselaar et al., 2015).

Specifications	
Sensitivity	$< 5\mu\text{Gals}$ with a 1 minute reading time (1 μGals is 10^{-9} of the earth's gravity field)
Operating range	7000 $m\text{Gals}$
Probe diameter	48 mm
Probe length	Approximately 3 m
Operating depth	Approximately 2500 m
Hole diameter	BQ (60 mm) and NQ drill rods (57.2 mm)
Maximum hole deviation from the vertical	60°
Temperature range	$0^{\circ}C$ to $+70^{\circ}C$ (downhole section) $-40^{\circ}C$ to $+50^{\circ}C$ (uphole section excluding PC)
Vertical position determination in borehole	$\pm$ 5 cm (depth and trajectory are determined with a combination of pressure sensor, winch encoder, and fluxgate magnetometer)

the high 3 $m\text{Gals}$ anomalies observed in these boreholes. In DUB279 the anomalous response between the depths of 800 m to 900 m indicates a higher volume of sulphide minerals than the weak mineralization intersected in the hole (Schetselaar et al., 2015; Newton et al., 2017).

It should be mentioned that the residual borehole gravity response is, in most cases a cross-over anomaly over a VMS deposit. The positive gravitational anomaly is observed when the GRAVILOG sensor is above the deposit. This is due to the cumulative downward force on the sensor resulting from both the earth's gravitational pull and the attraction of the deposit being in the same direction as that of the earth's field. On the other hand when the GRAVILOG sensor is below the deposit the gravitational attraction of the deposit on the sensor is upward while the gravitational pull from the

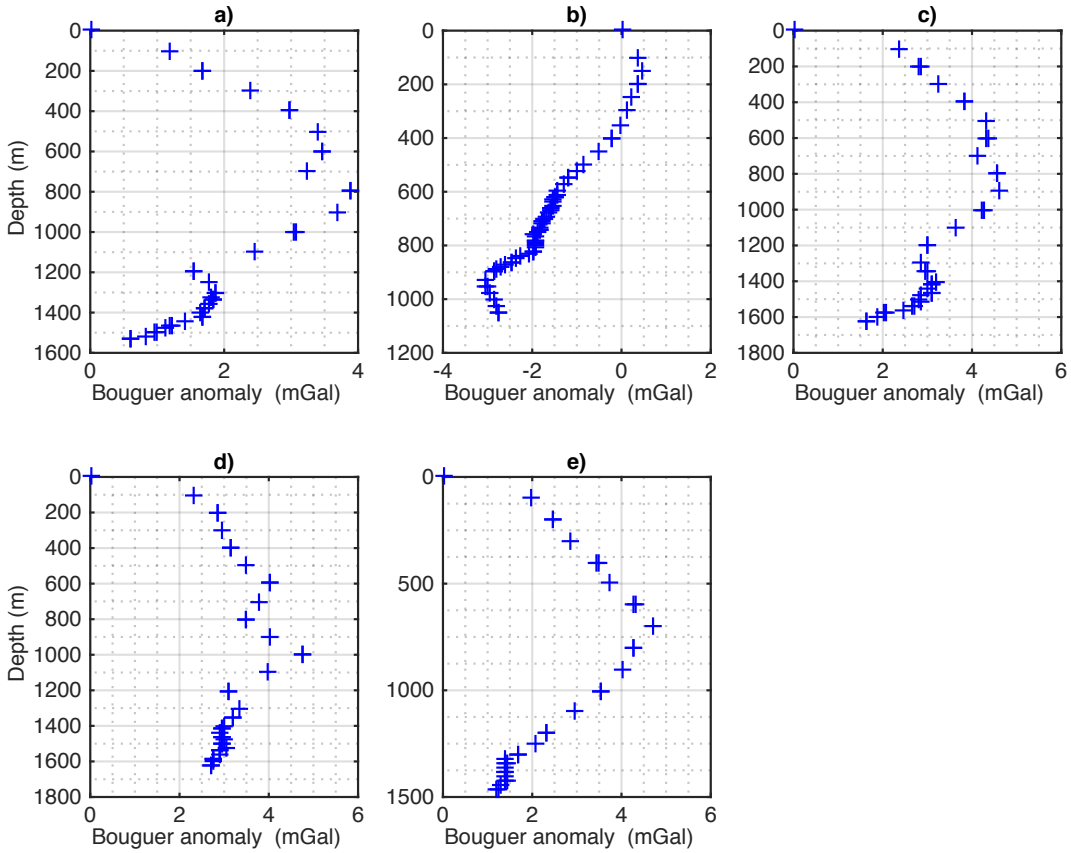

FIGURE 3.10 : Bouguer anomalies from boreholes a) DUB202 b) DUB279 c) DUB280 d) DUB282 and e) DUB287 Schetselaar et al. (2015).

earth's field is downward. This opposition in the direction of forces results in a negative peak in the residual anomaly value (Wasylechko et al., 2014).

3.5.1.2 Surface gravity data

The surface gravity data were acquired, processed and distributed by Hudbay Minerals. Only few information is available about these data. The raw data were interpolated on a grid spacing of 72.7 m × 65.2 m. The raw gravity data were corrected for temporal drift, latitude, free air, Bouguer slab, and terrain. The regional anomaly is obtained by upward continuation. Removing the regional trend from the Bouguer anomaly results in the residual anomaly (Figure 3.11).

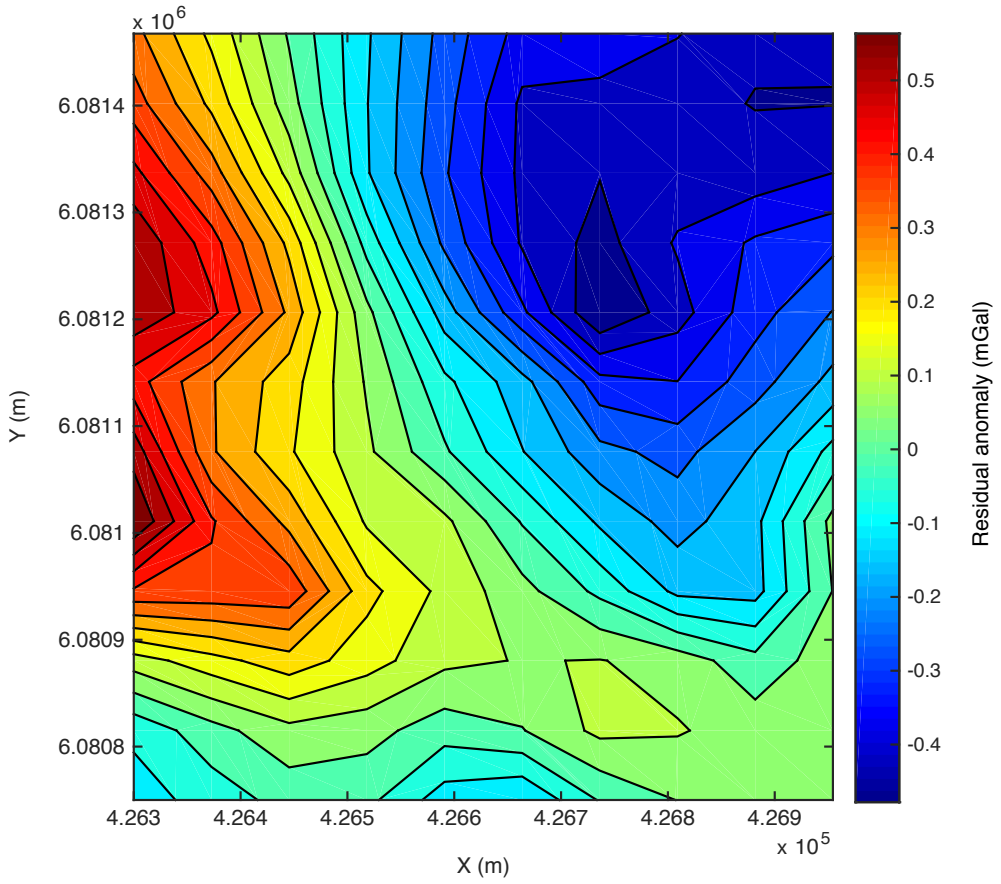

FIGURE 3.11 : Residual anomaly map of the Lalor deposit

3.5.2 DC resistivity data

In 2009, 2D DC resistivity and IP imaging were carried out along 3 parallel profiles of 4.6 Km above Lalor deposit (Figure 3.12). The data were acquired using a pole-dipole array configuration with 200 m electrode spacing and 100 m for a repeat of the central line (L184N) while the infinity electrode was placed approximately at 5 km from the survey area. The acquisition system used to collect the DC and IP data was the Titan 24, which is a 24-bit multi-channel system with a pole-dipole array configuration. The system allows recording of the full-waveform time series of potential data (Sharpe et al., 2014). Figure 3.13 shows the acquisition system layout. The Titan-24 and electrode configuration permitted shallow to mid-depth (<1000 m) penetration. The design of the system allows for discriminating between massive and disseminated mineralization and makes it possible to map geological contacts and deep conductors potentially representing alteration and mineralization zones at depth. In DCIP survey measurement errors are greater at depth

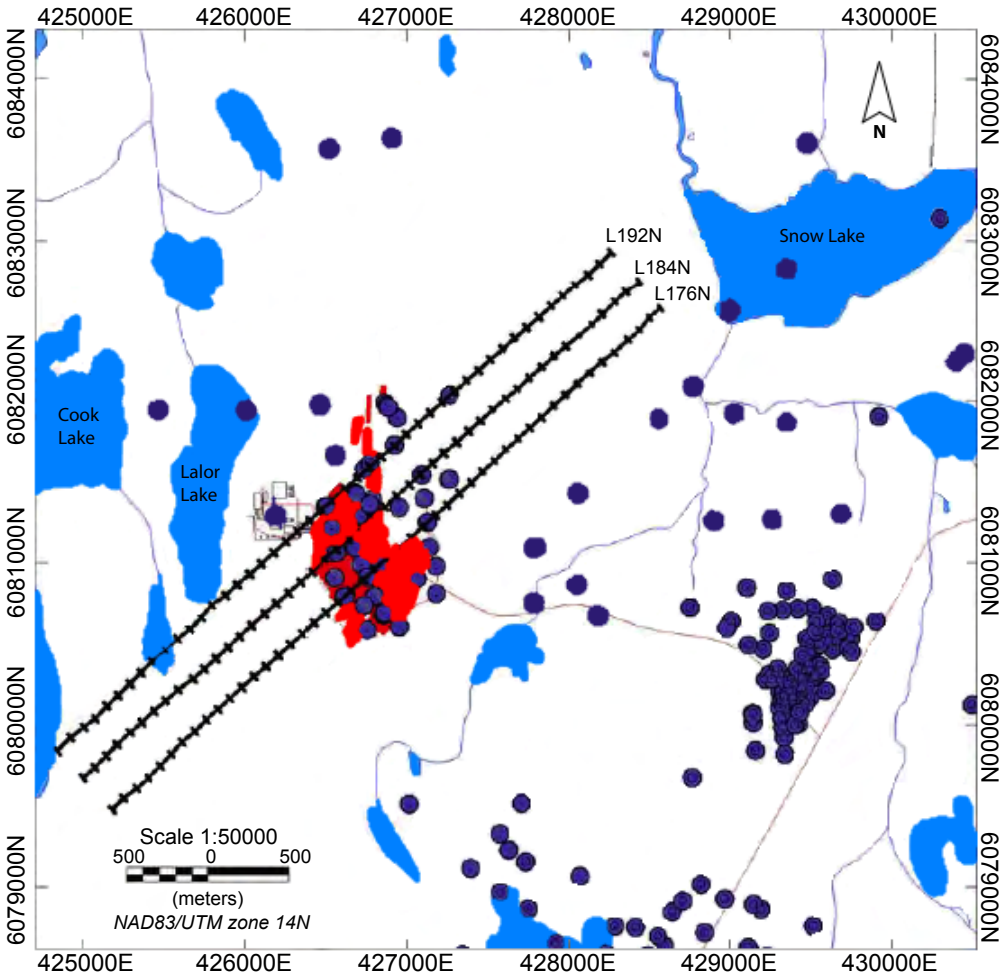

FIGURE 3.12 : Titan 24 2009 survey map depicts DC-IP Lines locations over Lalor deposit. The deposit and the drillings are shown in red and in purple dots respectively (Sharpe et al., 2014)

due to decreasing signal levels that sometimes cause negative phase values for low-signals. In order to improve contact resistance at transmit and receive locations, saline solution was used (unpublished: logistics report by Quantec Geoscience Ltd). Tables 3.2 and 3.3 show the parameters and instrumentation specifics used in the DCIP survey carried out by Quantec Geoscience.

In the previous sections, we presented the data used at Lalor for the present study. In the next sections, we detail the different steps of the proposed workflow.

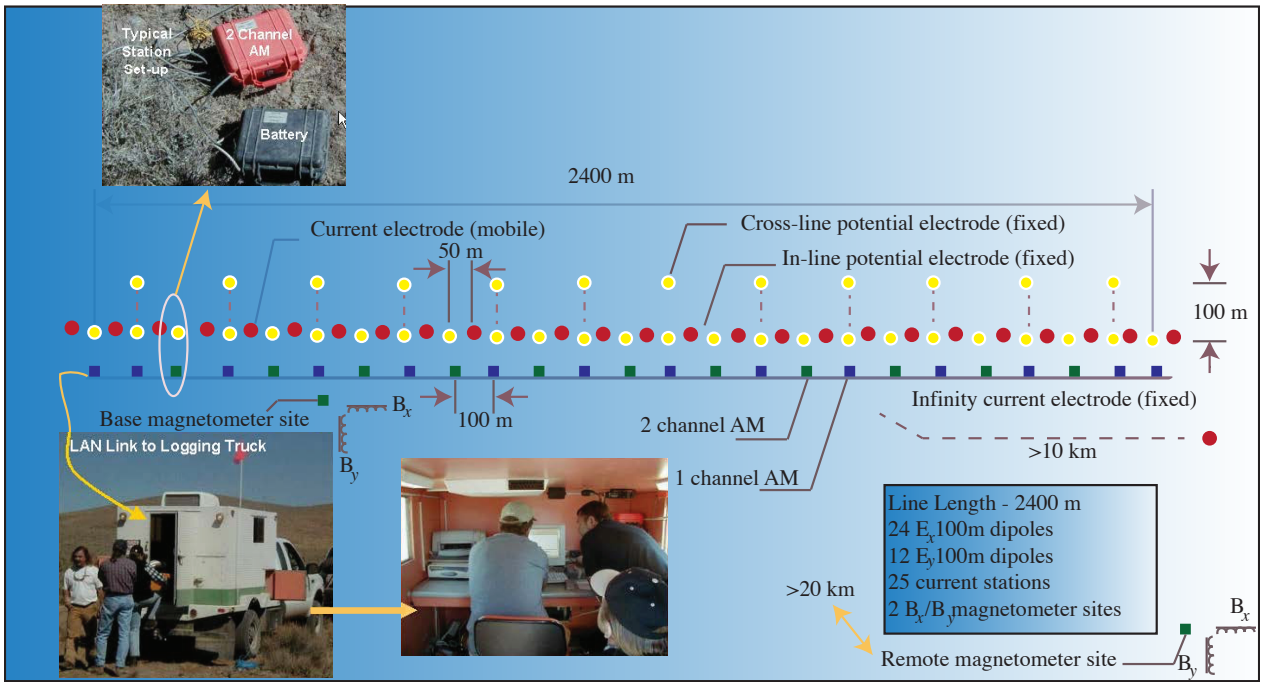

FIGURE 3.13 : Titan 24 acquisition system layout (Sharpe et al., 2014)

TABLE 3.2 : Parameters of the DCIP survey.

Specifications	
Transmitter waveform	30/256 Hz square waves at 100% duty cycle
Transmitter output current	Minimum 0.11 amperes to maximum 4.02 amperes
Receiver sampling speed	240 samples/second
Time-series stacking	20 cycles (full-waveform)
Read time	Approximately 3.0 minutes per event
Final Data Output	1) Normalized voltage (volts/ampere) 2) Voltage error (millivolts/ampere) 3) Phase (milliradians) 4) Phase error (milliradians) 5) Apparent resistivity (ωm)

TABLE 3.3 : Instrumentation specifications used in the DCIP survey (logistics report from Quantec Geoscience).

Specifications	
Receiver System	
Transmitter	2 GDD $(5kW)$ in series with frequency/waveform control, using CPU and Current Monitor (CM)
Power Supply	Honda $6500W$ generator
Receiver Electrodes	Ground contacts using stainless steel rods
Transmit Electrodes	4 $\times$ 1.2 cm diameter 1 m long stainless steel rods

3.6 Simulation of geological units with MPS

A set of 100 realizations were first computed from the geology using the 3D modified geological model originally built by Caté et al. (2015) and the geological units identified on drill cores in a volume of 974 m × 1929 m × 1663 m with a cell-size of 19.8 m × 39.4 m × 33.9 m along the x, y, and z-axis, respectively. The geological model used as the training image contains nine lithological units with different densities. As mentioned previously, MPS preserves all known structural constraints of these lithologies. The objective was to simulate the geological models in such a way that the statistics and the patterns of the models were similar to those of the training image and conformed to drillhole geological unit data. Figure 3.14 shows the workflow of MPS algorithm.

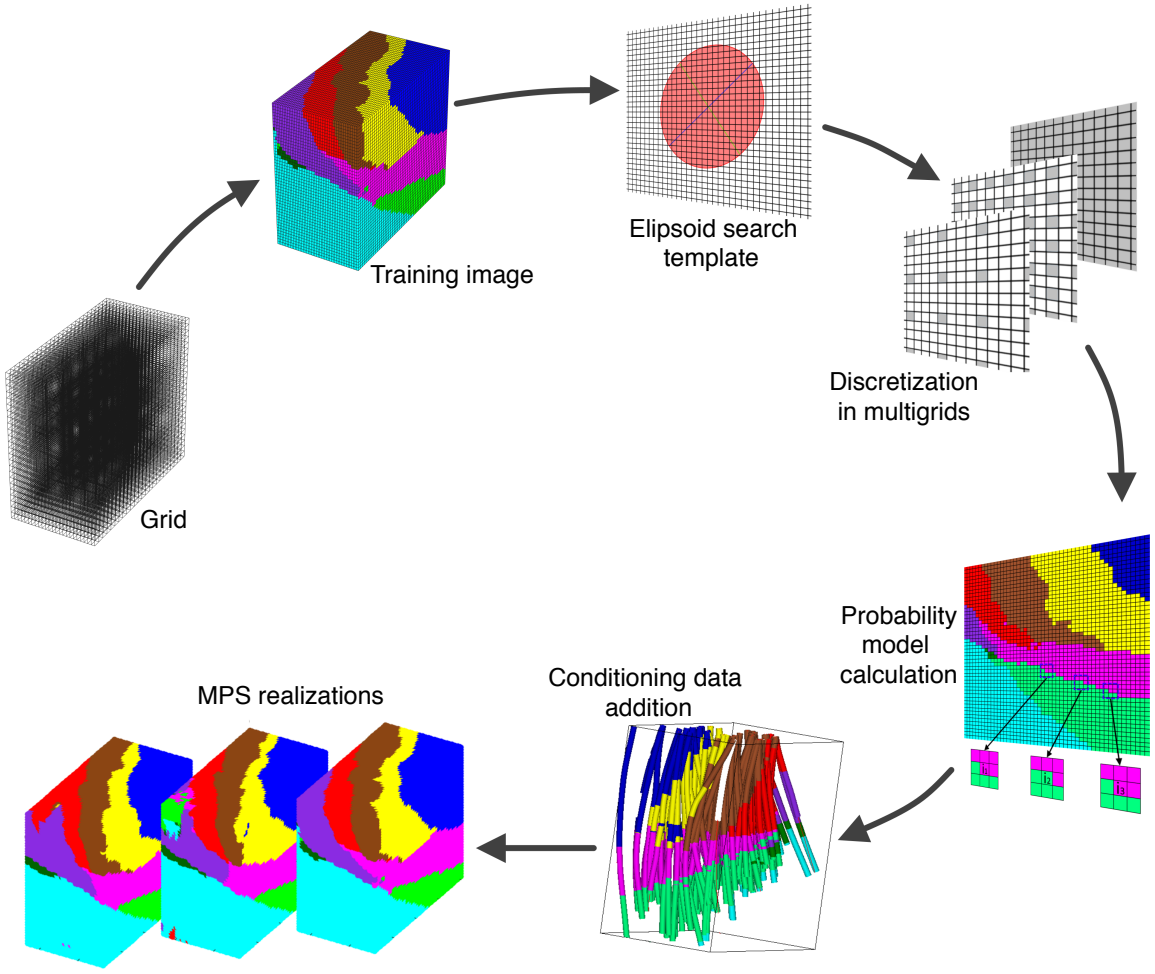

FIGURE 3.14 : MPS workflow.

The first step of the simulation is the selection of the grid and of the training image (TI). Then, we choose how to scale and orient the search template in case the TI and the grid features do not have the same rotation and scale. Next, we define the search template by specifying three axes of an ellipsoid to apply the probability model. The size of the search template defines the number of neighbouring cells to be simulated, which are used to calculate the conditional probability during the simulation. After the definition of TI multi-grid levels, the simulation grid and the TI are discretized. The multi-grid definition allows the algorithm to first preserve the larger scale features and then focus on smaller scale spatial variability. An optional step in the MPS workflow is to specify trends such as channels by using an auxiliary property if they exist in the training image. An other optional step includes defining additional facies proportions and how much weight should be assigned to them in the simulation process. Figure 3.15 shows a selection of these equiprobable 3D realizations for the initial 3D training image shown in Figure 3.4. The grid used here is the same as the geological model, and the same training image is used for all the units. The histograms of a selection of realizations generated by MPS are shown in Figure 3.16.

3.7 Density realizations using CSGS

In the next step of our workflow, each geological unit is populated by density values with respect to petrophysical relationships, and to the geological model of the deposit. To this end, a conventional conditional sequential Gaussian simulation (CSGS) (Deutsch et al., 1998; Doyen, 2007) method is used to compute the stochastic realizations within each geological unit in the model with their own semivariogram and mean. We computed and modelled the experimental variograms within each unit using density logs.

For each geological unit of the 100 geological models that were simulated at the MPS step, five different and equiprobable density distributions are calculated, thus leading to 500 3D density models. The spatial variability of simulated densities is maintained by the geological models obtained by MPS, whereas their spatial correlation, means and standard deviations are constrained from well-log data and modelled variograms. It should be mentioned that before using the conditioning borehole density values for the simulation, densities are classified based on the nine existing geological units and then normalized. Figure 3.17 shows the histograms of density values within each unit before normalization.

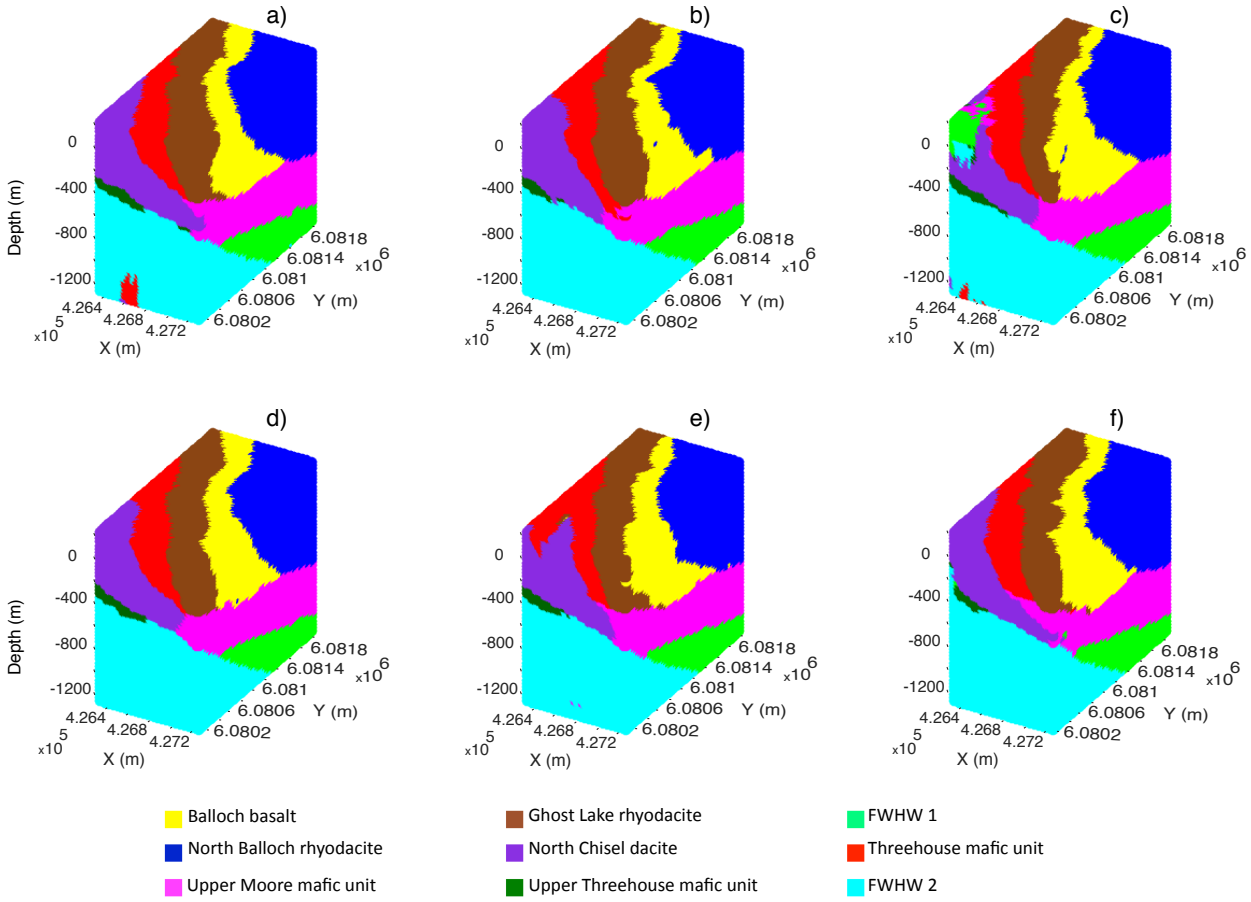

FIGURE 3.15 : Equiprobable simulated 3D realizations from the geological model using MPS method.

3.7.1 Normal score transform of density data

Since the density distributions of raw density data do not follow a normal distribution (Gaussian) and because we used CSGS to compute realizations of the density model, the distribution of the raw data were first normalized. This normalization involves the following steps as explained in Goovaerts (1997):

- 1- Normal scores of density data are calculated using a normal score transform and a table linking raw and normal scored histogram is stored.
- 2- Experimental and theoretical variograms are computed in the normal space
- 3- The Gaussian conditional cumulative distribution function (cdf) at un-sampled locations are computed and a value is randomly picked from the distribution.
- 4- The simulated data in the normal space are back transformed to the original space using the table of step 1.

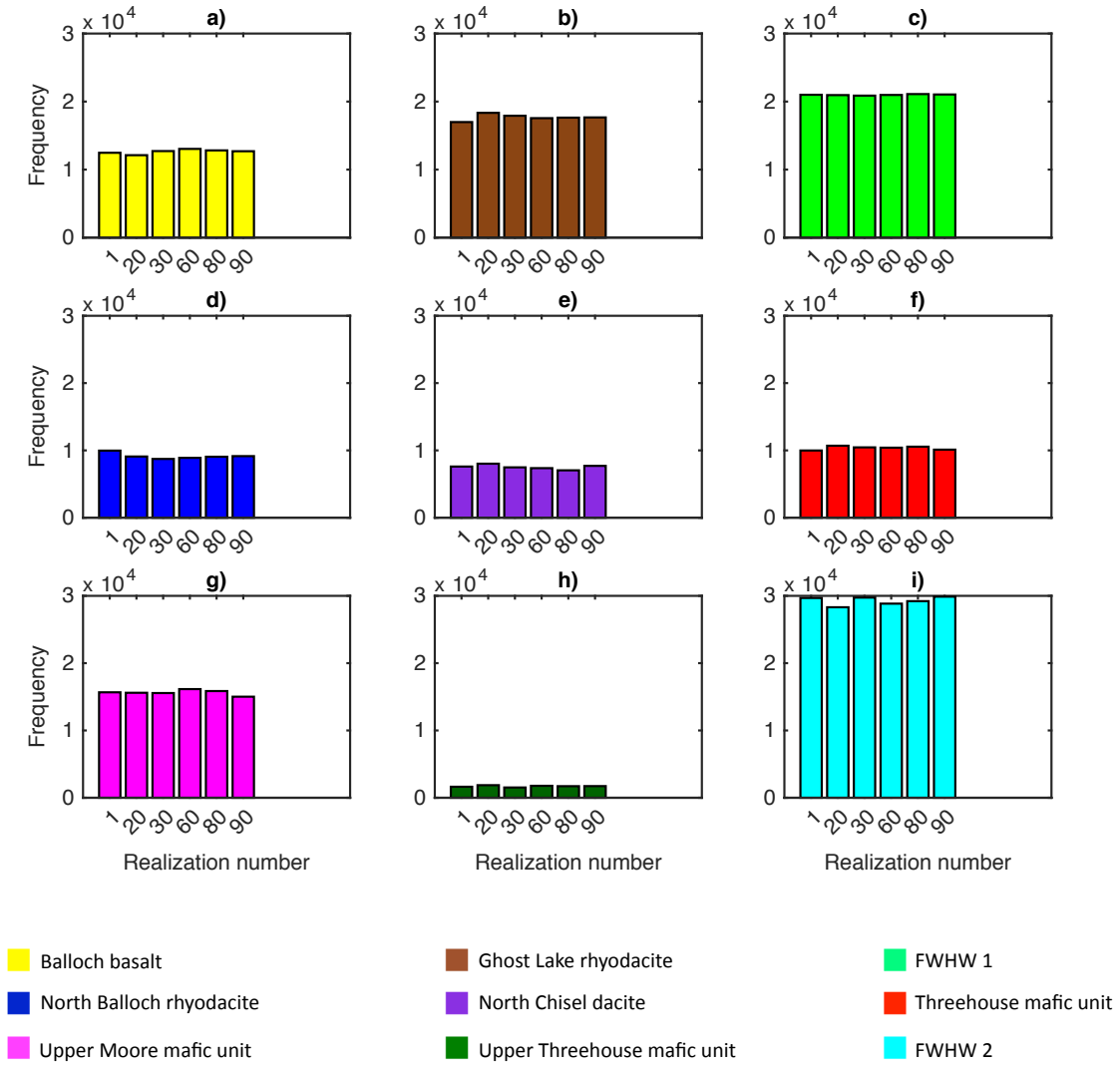

FIGURE 3.16 : Histogram of six different realizations generated using MPS algorithm.

There are several models for the interpolation and extrapolation of cdf lower and upper tails (Goovaerts, 1997). Here, we have used a power cdf model for extrapolation of lower and upper tails of density data distribution (equation 3.1). It should be mentioned that this normalization is done within each geological unit.

$$[F(z)]_{pow} = F^*(z_{k-1}) + [\frac{z - z_{k-1}}{z_k - z_{k-1}}]^{\omega}.[F^*(z_k) - F^*(z_{k-1})] \tag{3.1}$$

where $z \in (z_{k-1}, z_k]$ and $[F(z)]$ is the cumulative frequency distribution function. The power ω varies for different models. $\omega = 1$ corresponds to a uniform distribution with the linear model to interpolate cdf values within the classes of threshold values $z \in (z_{k-1}, z_k]$. For the negatively skewed lower tail,

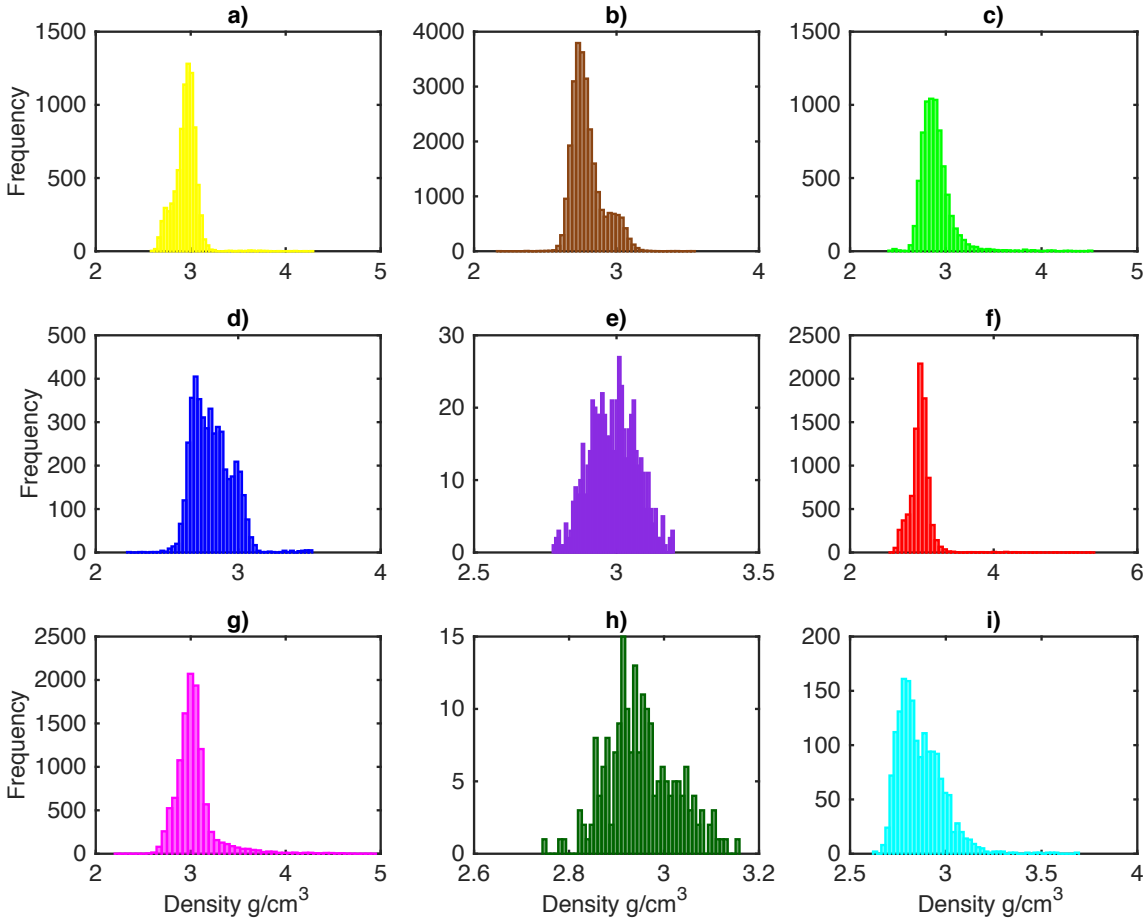

FIGURE 3.17 : Histogram of density values in a) Balloch basalt, b) Ghost Lake rhyodacite, c) FWHW1, d) North Balloch rhyodacite, e) North Chisel dacite, f) Threehouse mafic unit, g) Upper Moore mafic unit, h) Upper Threehouse mafic unit, i) FWHW2.

ω is bigger than 1 and for the positively skewed upper tail, ω is less than 1. In our case we have set the ω for the lower tail and upper tail distribution 2 and 0.5, respectively. Then the experimental variograms are modelled. Figure 3.18 shows the fit of experimental variograms by theoretical models in four regions of the study area including the FWHW1 and the Upper Moore mafic units.

The CSGS algorithm is computed separately for each geological unit to effectively reproduce the corresponding histogram and spatial distribution of the density within each unit. During the simulation, the realizations in each of the regions are conditioned by the corresponding logged density, which were previously classified. Figure 3.19 shows six 3D density realizations of the populated models generated at CSGS step and Figure 3.20 shows the histograms of a selection of different realizations generated through the CSGS step. The 500 density realizations are all at high resolution (resolution of the logs) but none fits perfectly the raw gravity data as they are

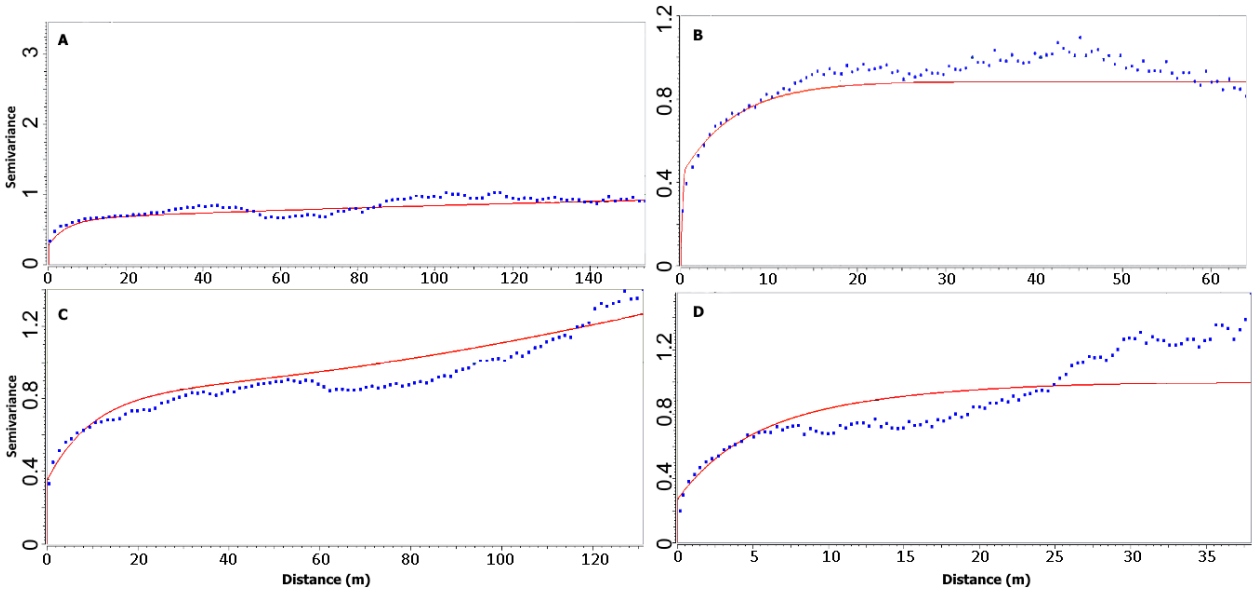

FIGURE 3.18 : Vertical variogram models shown with red curves built for geological units A) Balloch basalt, B) FWHW1, C) Upper Moore mafic unit, D) FWHW2.

stochastic realizations. As presented in the next section, to deal with this problem an optimization step is applied on the realizations to combine the 500 realizations with the objective to minimize the difference between measured Bouguer anomaly and the one computed on the combined realizations.

3.8 Model combination using gradual deformation method

In our study, we used a modified version of the multidimensional gradual deformation method called gradual conditioning. As Ying et al. (2000) have shown in gradual conditioning the GDM can be directly applied to realizations conditioned to observed data resulting in an output realization conditioned to the same data set. In this case, the gradual conditioning density y(r) is built from combining three randomly selected conditioned density realizations using equation 3.2 to ensure that the combined model y(r) is also conditional to the measured densities along boreholes. In our case all these realizations are already conditioned being generated in the CSGS step. The weights applied to realizations are iteratively optimized using equation 3.3 as proposed by Hu (2002).

$$y(r) = \alpha_1 y_1 + \alpha_2 y_2 + \alpha_3 y_3 \tag{3.2}$$

$$\alpha_1 = \frac{1}{3} + \frac{2}{3}\cos r$$
$$\alpha_2 = \frac{1}{3} + \frac{2}{3}\sin(\frac{-\pi}{6} + r) \tag{3.3}$$
$$\alpha_3 = \frac{1}{3} + \frac{2}{3}\sin(\frac{-\pi}{6} - r)$$

where r is between [-π , π]. It should be mentioned that the constraint on the weights (α_1,α_2,α_3) still requires that the sum and the sum of the square of the weights be equal to one to prevent bias and preserve the variance. Figure 3.21 shows the gradual deformation method workflow applied in the present study.

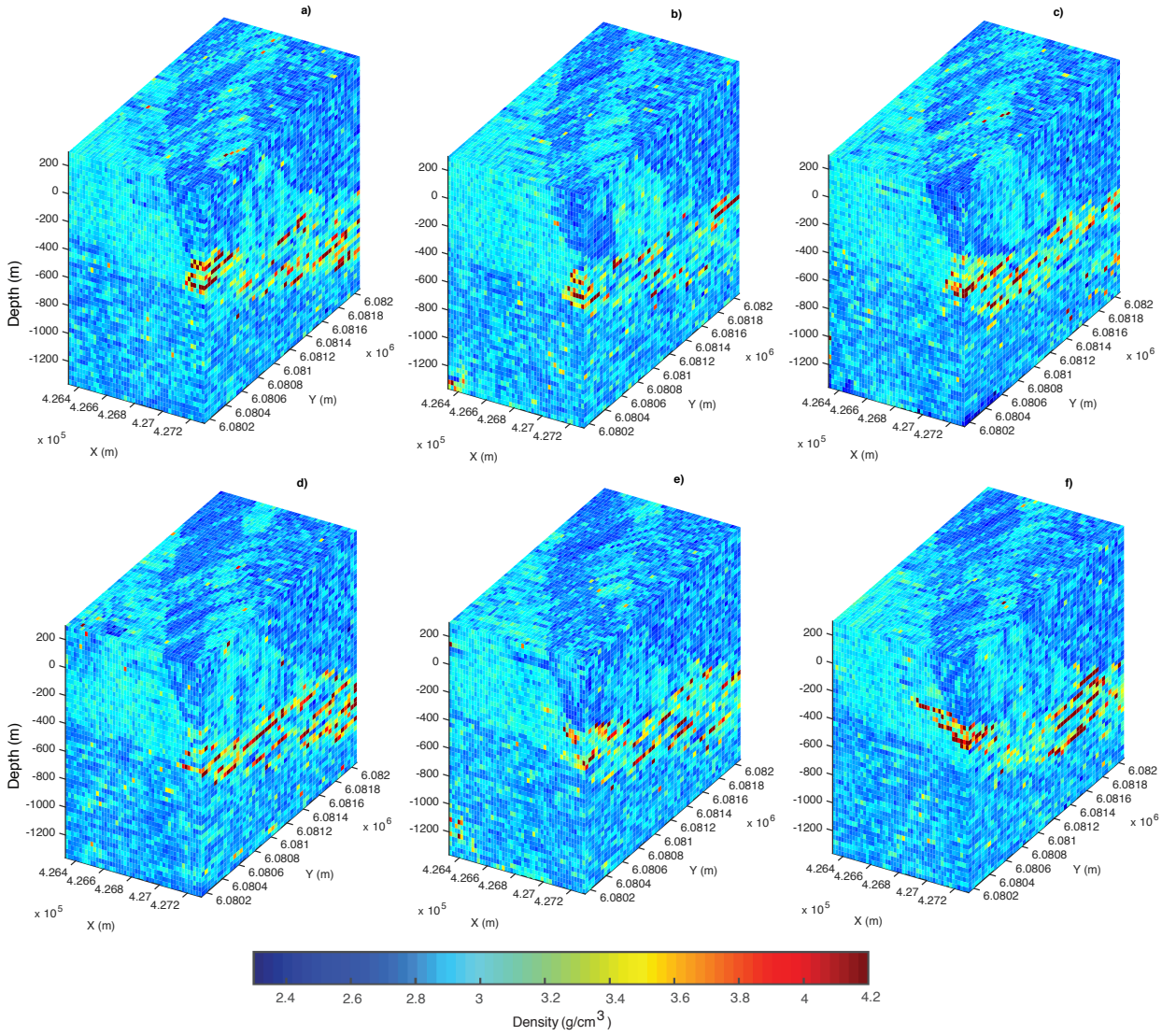

FIGURE 3.19 : 3D density realizations for the 1^{st}, 80^{th}, 120^{th}, 250^{th}, 380^{th} and 450^{th} iterations of the simulation.

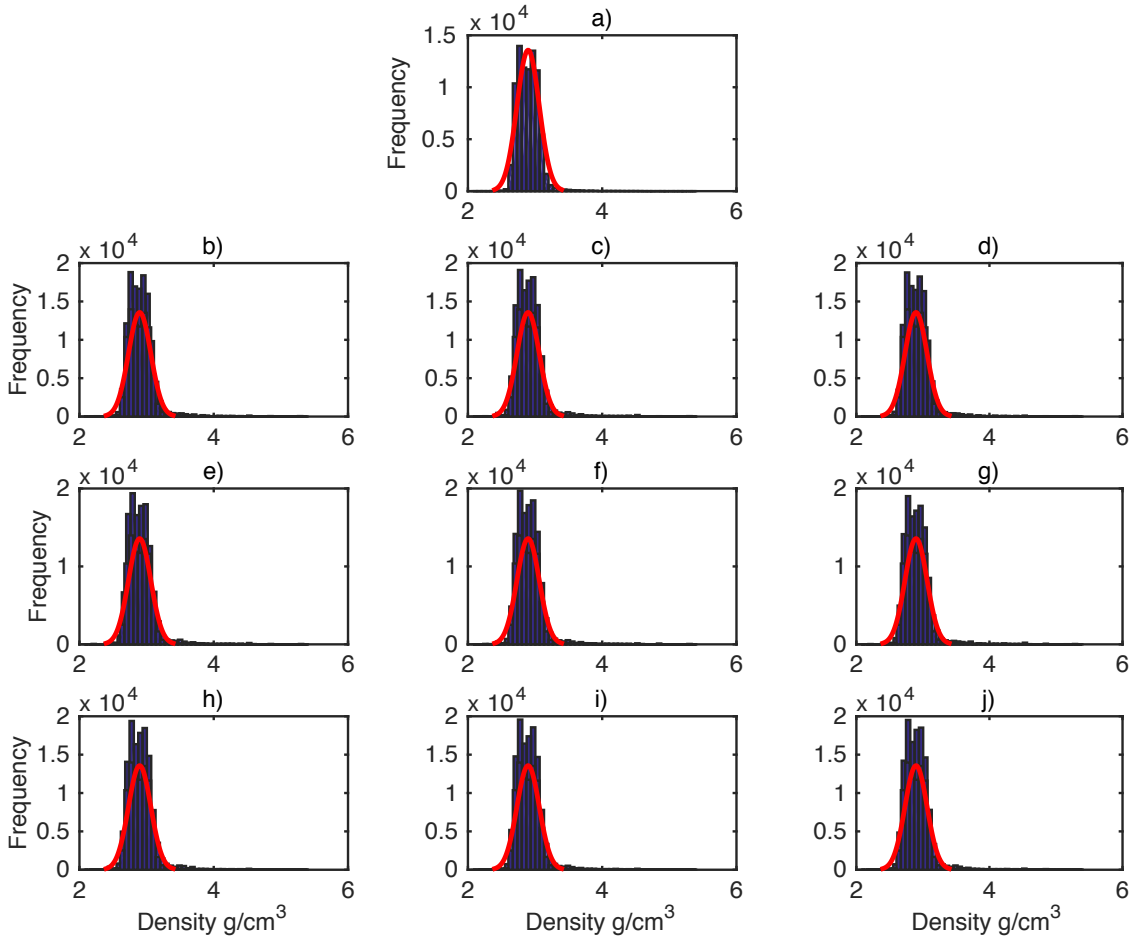

FIGURE 3.20 : Histograms of a) the borehole density data b) 30^{th}, c) 60^{th}, d) 80^{th}, e) 90^{th}, f) 120^{th}, g) 280^{th}, h) 320^{th}, i) 370^{th}, j) 420^{th} realizations of simulated densities from CSGS step. The red curve represents the normal density function fitted to the borehole data.

3.8.1 Gravimetry forward modelling

In order to apply the gradual conditioning, we need to compute a forward model of the gravity field g due to the density (ρ) distribution in the subsurface of the realizations in order to compare them with the measured residual anomaly. The 3D subsurface volume of the ground is discretized into a grid with a cell-size of 19.8 m × 39.4 m × 33.9 m along the x, y, and z-axis, respectively. The 3D domain is therefore divided into 50×50×50 = 125000 cubic prisms. When there are n gravity observations and m rectangular prisms the matrix form of their relationship is described as:

$$g_{n\times 1} = G_{n\times m}\rho_{m\times 1} \tag{3.4}$$

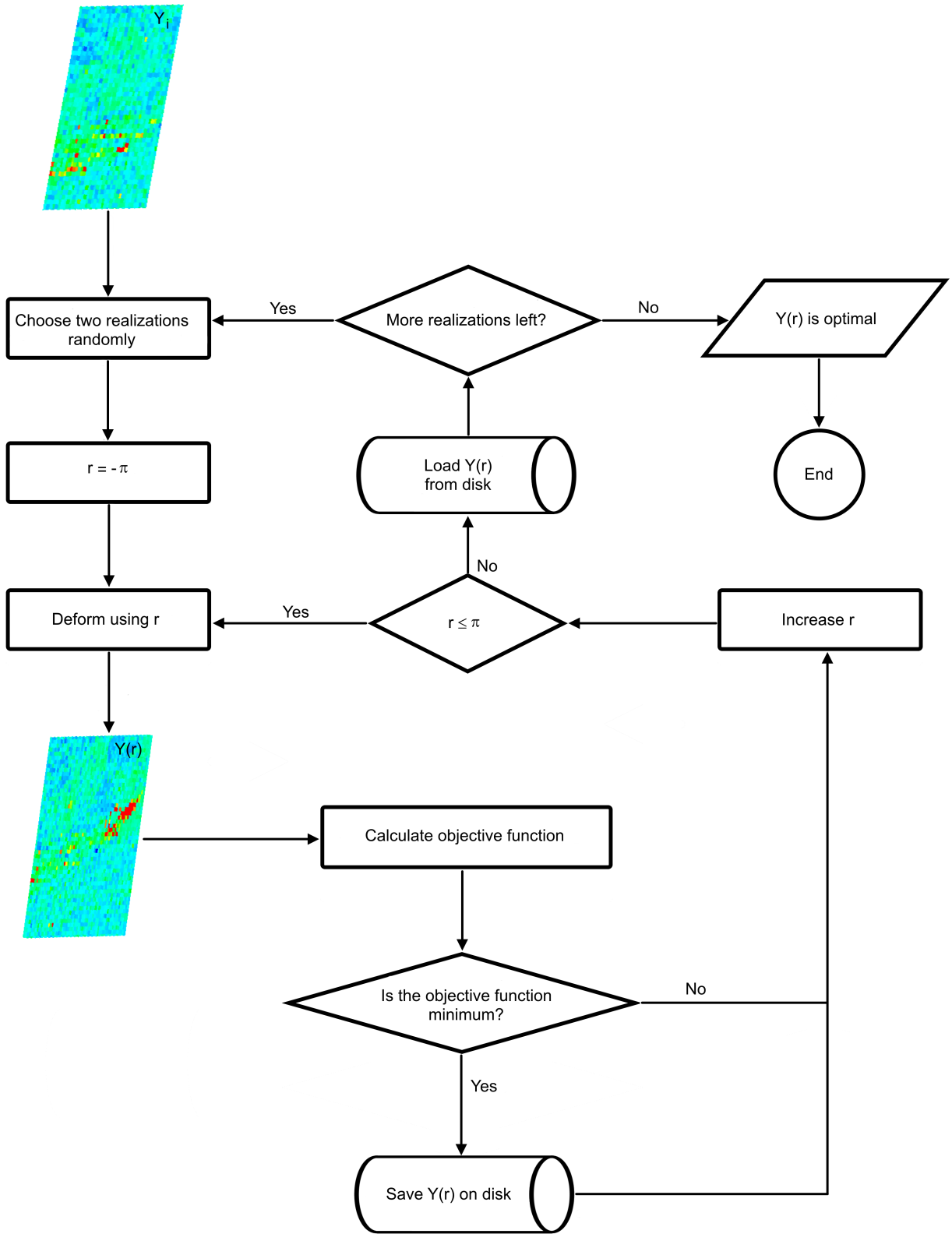

FIGURE 3.21 : Workflow of the gradual deformation step. y_i is the ith petrophysical realization acquired from conditional sequential Gaussian simulation (CSGS), randomly selected for gradual deformation, r is the deformation parameter and $y(r)$ is the deformed density realization from combining three realizations.

where G is the matrix of the geometric terms. The G matrix is computed using the Haáz (1953) formula and each of its rows show the effect of all prisms on one observation point (Shamsipour et al., 2010).

3.8.1.1 Borehole gravity data incorporation

The volume of the target plays an important role on the anomalous signals in a gravity survey. In the case of Lalor deposit the surface gravity data can only capture the mineralization at a regional scale. This is due to the thickness of the ore lenses which is only tens of meters and also that they are buried at more than 600 m deep (Yang et al., 2018). As described in Shamsipour et al. (2011b), in order to retrieve a more accurate density distribution, borehole gravity data are incorporated in the forward modeling system. Equation 3.5 shows how these data are incorporated in a forward modelling system.

$$\begin{bmatrix} g \\ g_{bh} \end{bmatrix}_{(n+n_{bh})\times 1} = \begin{bmatrix} G \\ G_{bh} \end{bmatrix}_{(n+n_{bh})\times m} \rho_{m\times 1} \tag{3.5}$$

where g_{bh} is the gravity measurements along the boreholes and n_{bh} are the number of prisms with known borehole gravities. The geometric term corresponding to the borehole gravities is shown by G_{bh}. This incorporation helps the algorithm to converge to a more reliable density distribution for Lalor data, especially since the borehole gravity data on Lalor are shown to be effective for capturing mineralization (Schetselaar et al., 2015). However, this is not directly possible to implement with Lalor gravity data. The surface Bouguer anomaly and the borehole Bouguer anomaly show that there is an incompatibility between the data sets. This is due to the corrections applied in the calculation of the Bouguer anomaly from the raw data. Therefore in the following sections separate stochastic assimilations are carried out for surface and borehole gravity data in order to improve the density models.

3.8.2 Objective function

In contrary to conventional deterministic or stochastic inversion, the gradual deformation allows for multiple types of norms as the objective function. Here, we first use the L2-norm (Equation 3.6) sensitive to extreme data values and L1-norm (Equation 3.7) sensitive to the median of the data. The order of the norm is the order of the power of the sum of the differences between observed and

computed data. Indeed, if we have N data locations, the misfit indicators between the measured d_{obs} and computed data $G(m)$ for a given set of parameters m are given by:

$$\|G(m) - d\|_2 = \sqrt{\sum_{i=1}^{N} (G(m)_i - d_{obs})^2} \tag{3.6}$$

$$\|G(m) - d\|_1 = \sum_{i=1}^{N} \mid G(m)_i - d_{obs} \mid \tag{3.7}$$

3.9 Borehole gravity modelling results

The L1-norm function is less sensitive to data points that exhibit large variability with respect to the measured data. The L1-norm function in the gradual deformation optimization of all the simulated density models converges faster than the L2-norm function. Figure 3.22 shows the evolution of the L1-norm and L2-norm objective functions for borehole gravity data modelling.

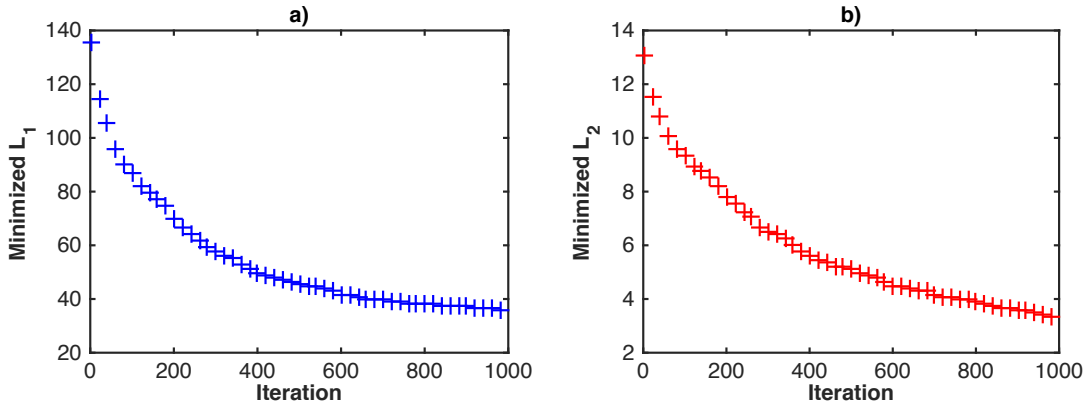

FIGURE 3.22 : Comparison of the decrease in the objective function over the iterations for a) L1-norm and b) L2-norm, in borehole gravity modelling.

As shown in Figure 3.23 the RMS error of L2-norm at convergence is less than the error calculated for the L1-norm. Figure 3.24 shows the quantile-quantile (Q-Q) plot for the observed and calculated gravity data from L2-norm objective function for different iterations in GDM. As can be seen for the last iteration of GDM the plot produces an approximately straight line, suggesting that the two sets of residual gravity data (observed and simulated) have the same distribution.

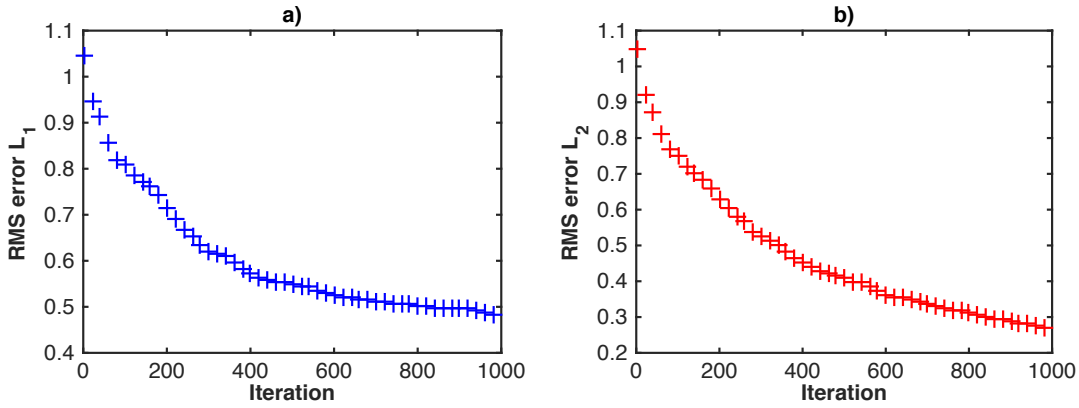

FIGURE 3.23 : Comparison of the RMS error for objective functions: a) L1-norm and b) L2-norm, in borehole gravity modelling.

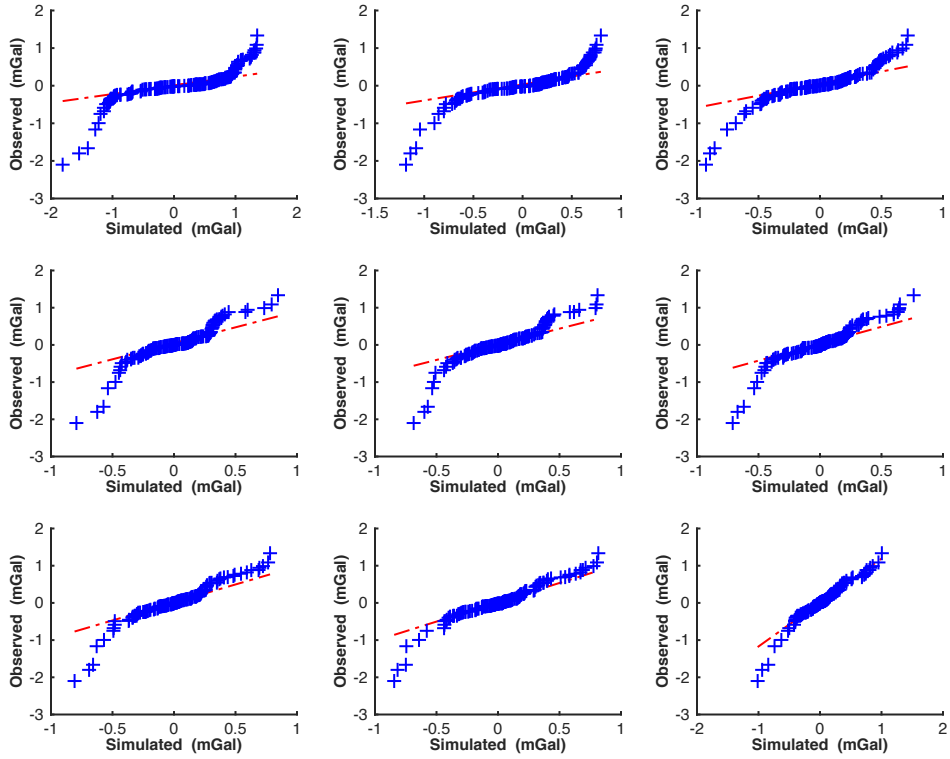

FIGURE 3.24 : Observed gravity data versus calculated gravity data from L2-norm objective function

Figure 3.25 shows a section of calculated gravity model in depth for values higher than 0.5 $m\mathrm{Gals}$ at different iterations using L2-norm objective function.

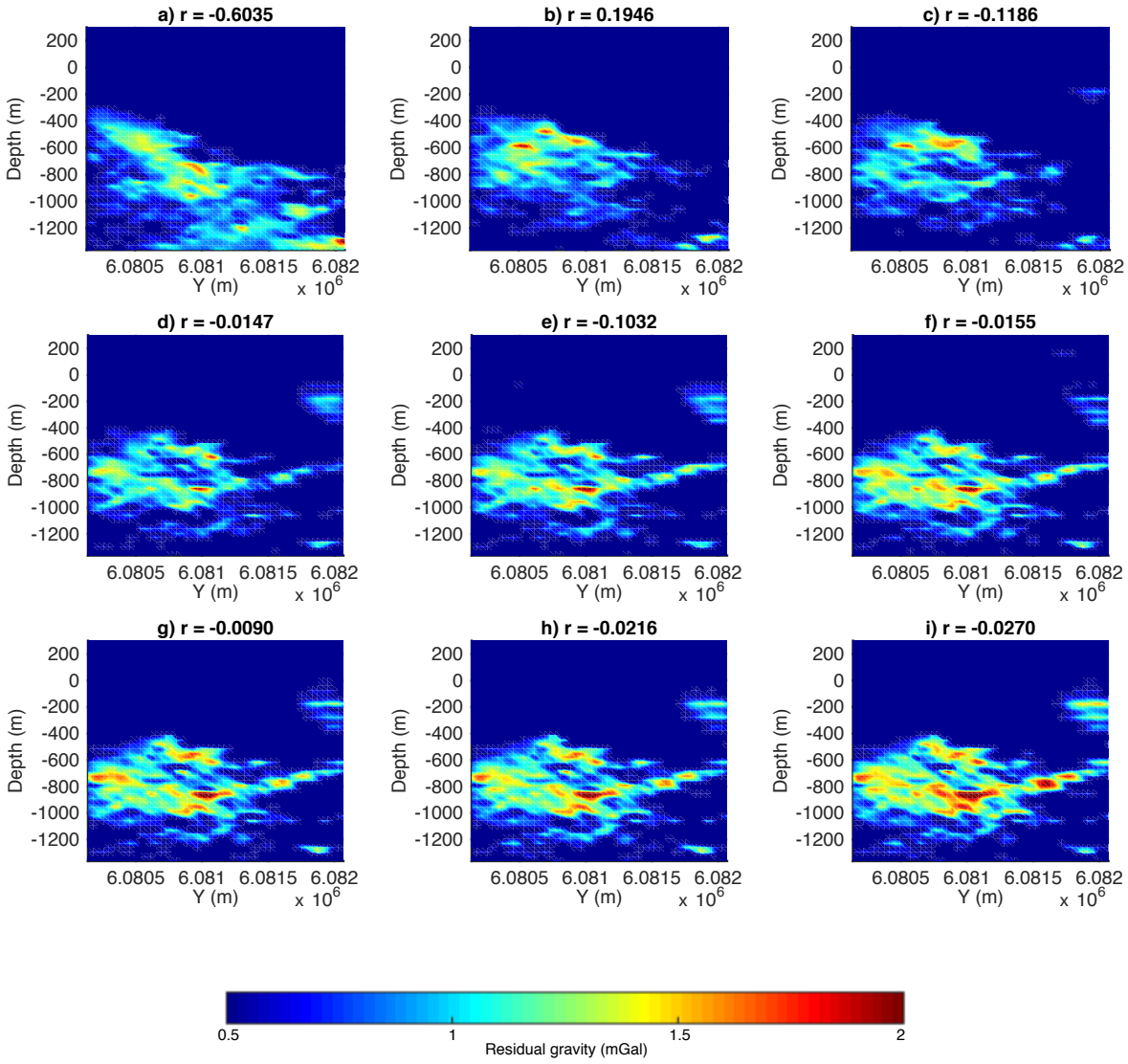

FIGURE 3.25 : Vertical section at $x = 4.267 \times 10^5$ of 3D residual gravity anomaly models from the series generated using GDM optimization for iterations number a) 1 b) 100 c) 200 d) 400 e) 500 f) 600 g) 700 h) 800 and i) 1000.

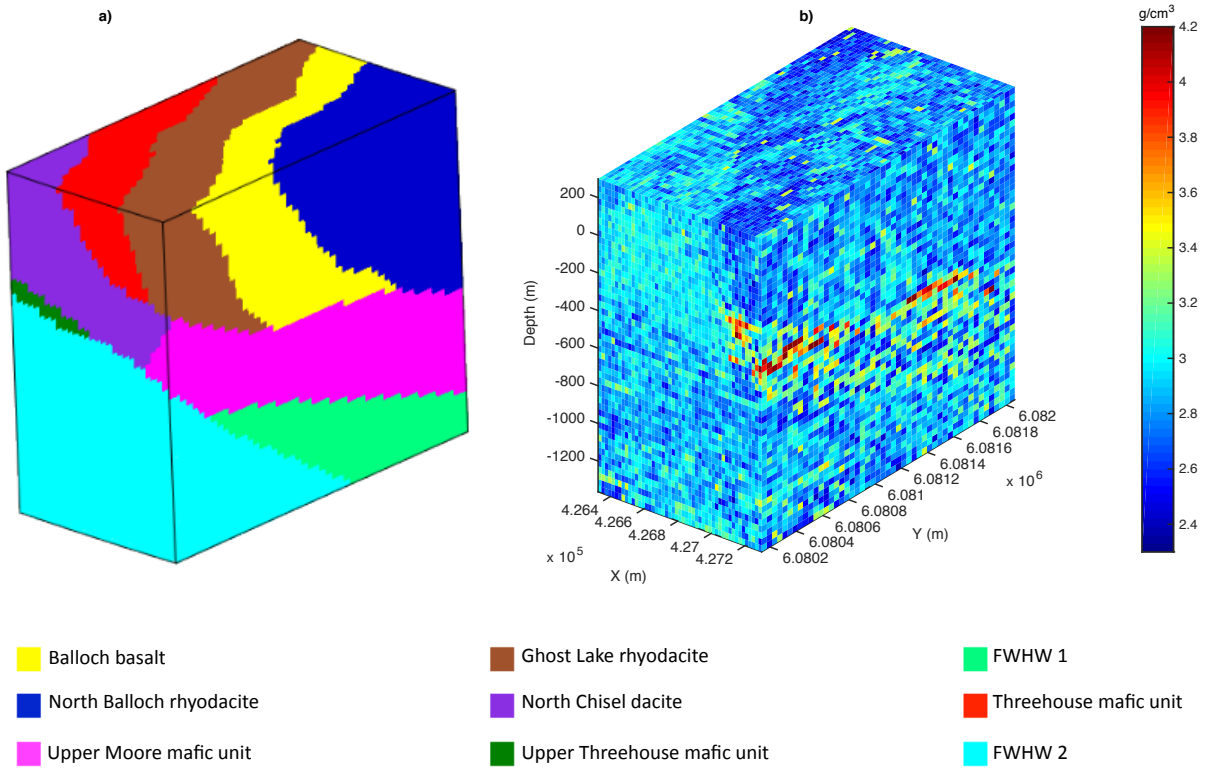

FIGURE 3.26 : a) 3D geological model, b) 3D optimized density model using stochastic inversion for L2-norm.

The density model obtained using the L2-norm function is illustrated in 3.26b. As can be seen, there is a clear correspondence between the lithological units in the geological model (Figure 3.26a) and the density contrasts in the density model (Figure 3.26b), specifically the high-density zone corresponds to the Upper Moore mafic unit. The high-density zone is less continuous compared to the simulated realizations, which are more in accordance with the geology of the mineralized lenses at Lalor (Schetselaar et al., 2015). The structural details in the final image are controlled by the noise in the data as modelled with the nugget effect in the variogram. The cell size in the model and the resolution of the data contribute to the resolution of the final model. Figure 3.27 shows the histogram of the optimized density model.

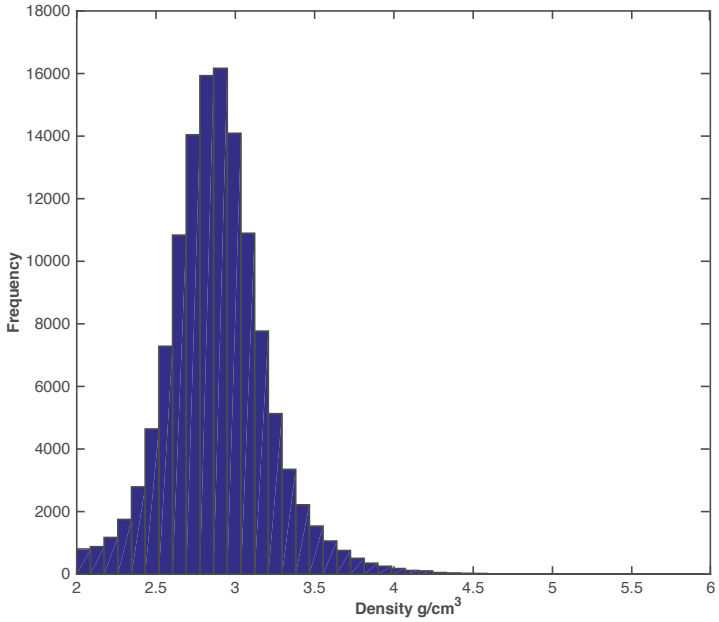

FIGURE 3.27 : Histogram of the 3D optimized density model

3.10 Surface gravity modelling results

Figure 3.28 shows the evolution of the L1-norm and L2-norm objective functions for surface gravity data modelling. The behaviour of the objective functions during the gradual deformation exhibit that the largest changes in the value of these functions occur during the first iterations. This is due to the nature of the GDM that the first iterations are used to impose the global structure of the optimal model from the points of misfits in the combined realizations (Yrro, 2018). Similar to borehole gravity modelling, the L1-norm function in the gradual deformation of all the simulated models converges faster than the the L2-norm function. The RMS error, however, is less for the L2-norm function than the L1-norm at their convergence (Figure 3.29).

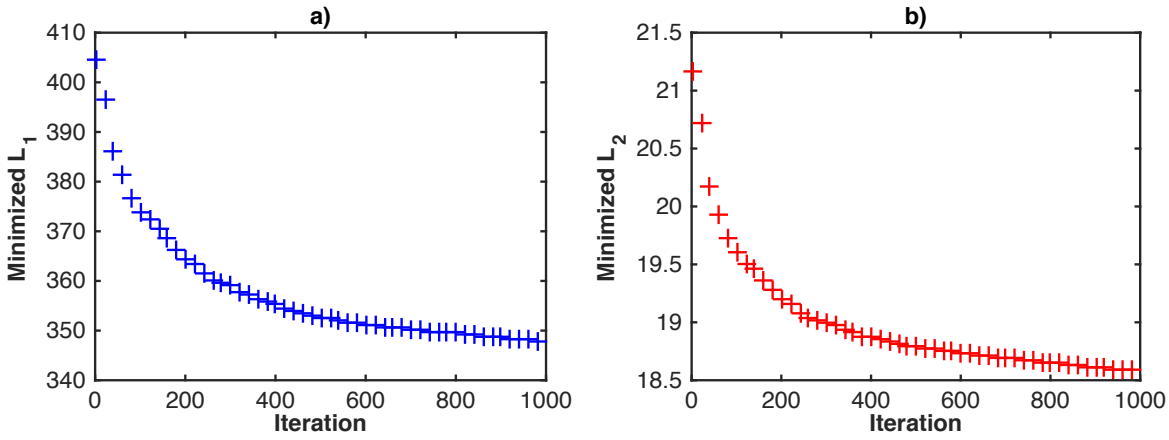

FIGURE 3.28 : Comparison of the decrease in the objective function for surface gravity modeling over the iterations for a) L1-norm and b) L2-norm.

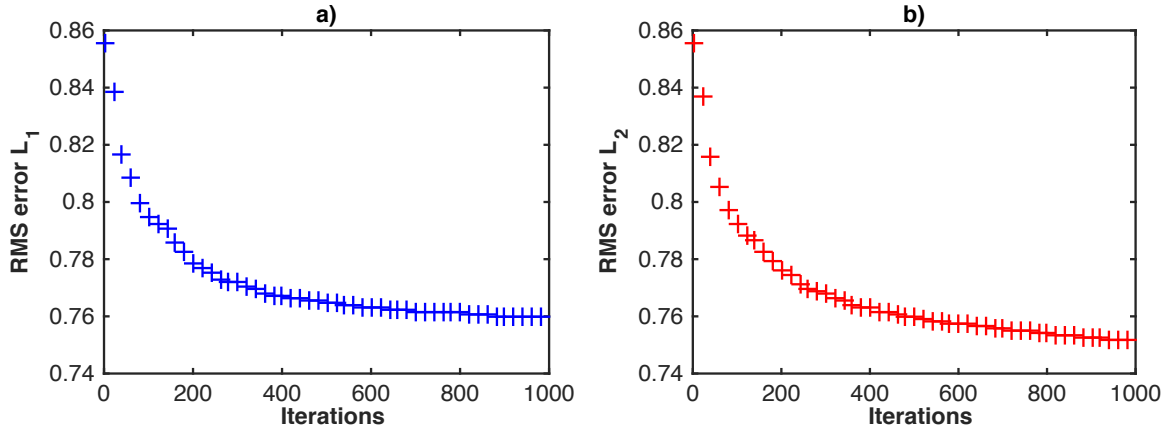

FIGURE 3.29 : Comparison of the RMS error for objective functions: a) L1-norm and b) L2-norm, in surface gravity modelling.

3.11 Conductivity modelling using Bayesian sequential simulation

The relation between density and resistivity is not linear. This non-linearity between variables prevents the use of any conventional cosimulation algorithm. However, Dubreuil-Boisclair (2013) developed a Bayesian sequential simulation (BSS) algorithm in Matlab. This algorithm allows simulating non-Gaussian and non-linear random variables by using an empirical kernel instead of a cross-variogram. The implementation of the method comprises 6 steps (Dubreuil-Boisclair, 2013):

— 1- A random path is defined to visit each cell of the grid once. This path is unique for each realization.

— 2- The cell chosen in the simulation process goes through a simple kriging step to obtain the prior distribution which is the pdf for the primary variable (conductivity) conditional to the previously simulated values and to the measured data in a given neighbourhood. Here we assume that the conductivity data follow a log-normal distribution since we do not have knowledge of their original distribution. This allows estimating the conditional mean and variance of conductivities from conductivity measurements (Chiles et al., 2009). Since the density and conductivity data both exhibit a bi-modal distribution, we used mixture models to determine the level of membership of the cells under simulation to these distinct populations. These populations can be thought of as families. In this case, two families can be established: 1- high-density high-conductivity values and 2- low-density low-conductivity values are depicted in Figure 3.30. Here, the marginal distribution of the conductivity data are calculated using the Gaussian Mixture Models (GMM) (McLachlan et al., 1988). In order to obtain the probability of a cell belonging to a family, the ratio of the area under the curve of the Gaussian distribution corresponding to that family is normalized to the total area under the curve. To obtain the prior distribution of conductivity data, the variogram and the mean of the chosen family are used for simple kriging of the measured and all the previously simulated conductivity data (Dubreuil-Boisclair, 2013). Family 1 has a mean conductivity value of 0.0233 S/m and a standard deviation of 0.3283. Family 2 has a mean conductivity of 4.014×10^{-4} S/m and a standard deviation of 0.6416.

— 3- In this step the statistical petrophysical relationship between density and conductivity is inferred and the joint probability density function (pdf) is estimated using kernel density estimators, which have been developed by Rosenblatt (1956) and Parzen (1962). The likelihood function is calculated from the collocated borehole density and conductivity data measured along the boreholes. A Gaussian kernel was used with bandwidths of 0.35 S/m and 0.2 g/cm^3 for the conductivity in logarithmic space and density, respectively. Figure 3.30 shows the joint pdf of the data. Well-log data measured at the scale of 20 cm intervals are shown with white crosses.

— 4- The posterior probability distribution is computed by updating the prior with the likelihood based on Bayes rule. The spatial relationships of conductivity and density values themselves conditioned to borehole densities and lithological logs are accounted for in the posterior distribution.

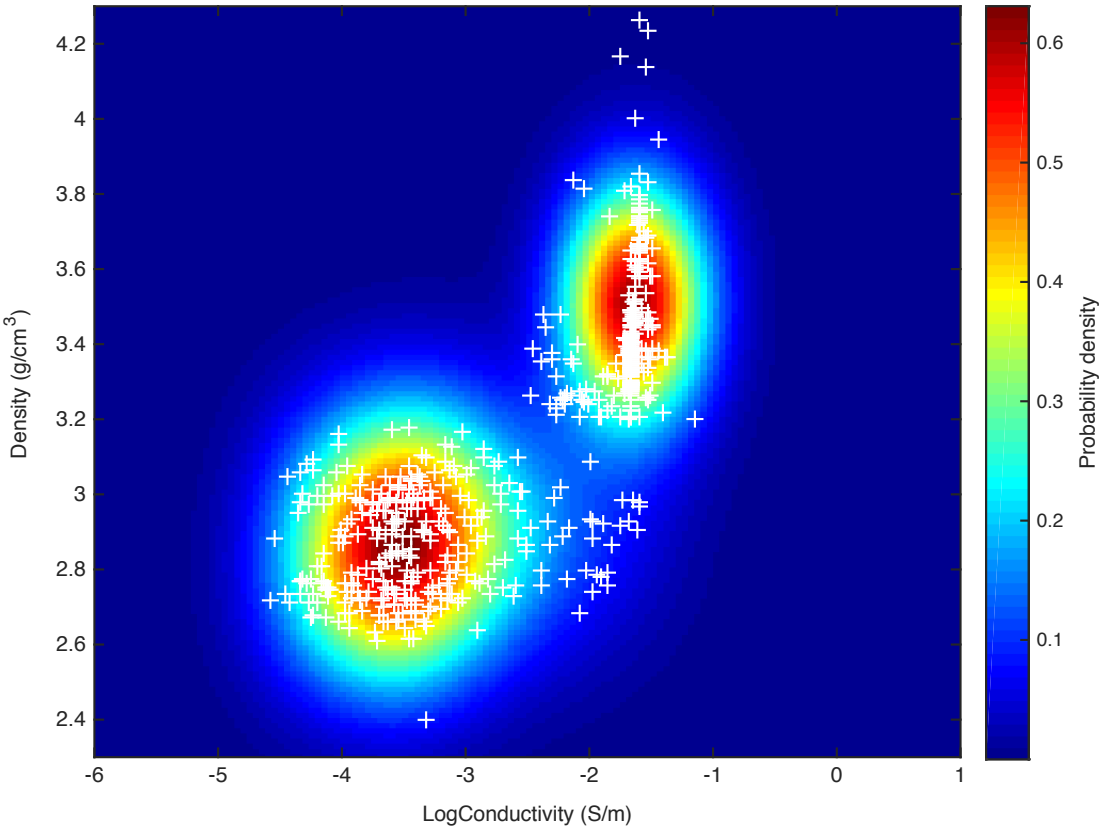

FIGURE 3.30 : The joint probability density between density and conductivity data. The white crosses represent the data.

— 5- This step includes randomly drawing a conductivity value from the posterior distribution and assigning it to the visited cell. This simulated conductivity value is taken as a measured value for the next iterations of the simulation.

— 6- Steps 1 to 5 are repeated as long as all the grid nodes have been visited once.

The advantage of BSS is that the statistical relation between our data can be of any nature such as in our case a non-linear relationship. A selection of 3D conductivity realizations from the 100 realizations generated using BSS is shown in Figure 3.31.

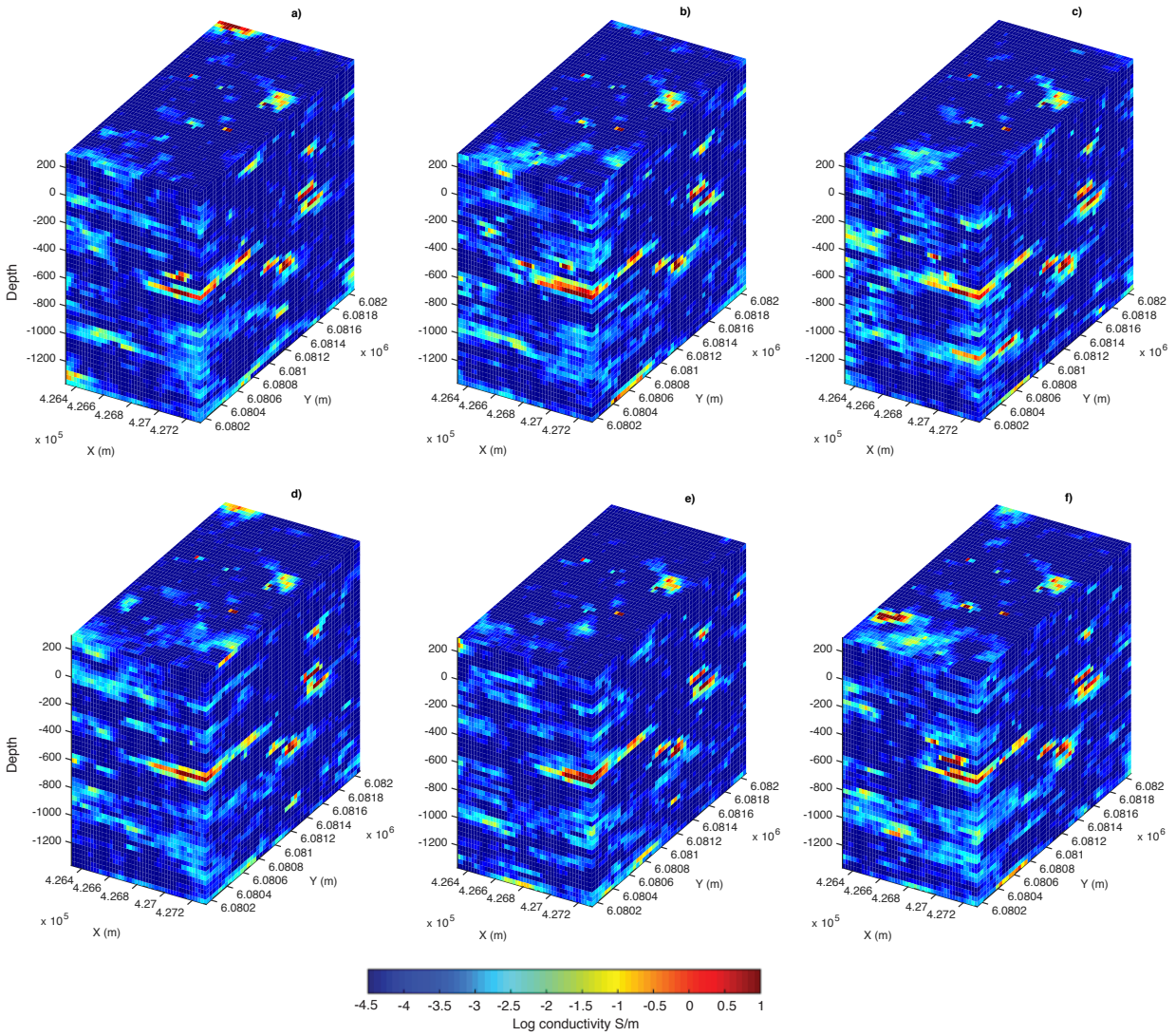

FIGURE 3.31 : 3D conductivity models from the a) 1^{st} **b)** 20^{th} **c)** 30^{th} **d)** 60^{th} **e)** 80^{th} **f)** 100^{th} **realization generated by BSS algorithm.**

3.12 Conductivity model combination

In this step, the same GDM algorithm applied in gravimetry modelling is used in conductivity model combination. Here, the gradually conditioned conductivity model $y(r)$ is built from combining three randomly selected conditioned conductivity realizations built with BSS algorithm. The combination is done using equation 3.2. Since the conductivity realizations are generated from conductivity logs, the combined model y(r) is also conditional to the measured conductivities along boreholes. The weights applied to conductivity realizations are iteratively optimized using equation 3.3. In

order to iteratively improve the conductivity model, the response calculated from the simulations is compared with the measured electric potentials using the L2-norm objective function (Equation 3.6).

3.12.1 DC forward modelling

In order to calculate the DC potentials caused by an electrical conductivity distribution in the subsurface, forward modelling is undertaken. The potential measured when the current is turned on of a given conductivity model is computed as:

$$\phi_\sigma = F_{dc}[\sigma] \tag{3.8}$$

where σ is the electrical conductivity and ϕ_σ is the potential that is measured in the absence of chargeability effects. The forward mapping operator F_{dc} in a a pole-pole survey is defined by equation 3.9.

$$\nabla.[\sigma \nabla \phi_\sigma] = -I\delta(r - r_s) \tag{3.9}$$

where I is the strength of the input current in Amperes, and r_s is the location of the current source. In order to model the potentials from pole-dipole or dipole-dipole surveys when we are computing equation 3.9 the principle of superposition is used. For DC data the modelling is carried out on a mesh grid of rectangular cells, each of which has a constant value of conductivity. The electrode locations can be anywhere within the model volume. The grid has the same dimensions as in gravimetry modelling. The DC equations are solved using finite volume method (Dey et al., 1979). Figure 3.32 shows the simulated conductivity models from different optimization iterations in GDM algorithm. Figure 3.33 shows the optimized simulated conductivity model after 100 iterations in GDM algorithm. The structural details in the this final model are controlled by the noise in the data as modelled with the nugget effect in the variogram. The other contributing factor in the resolution of the final model is the cell size in comparison to the thickness of ore lenses as well as the resolution of the data. Figure 3.34 shows the geological, density and conductivity models over the same section.

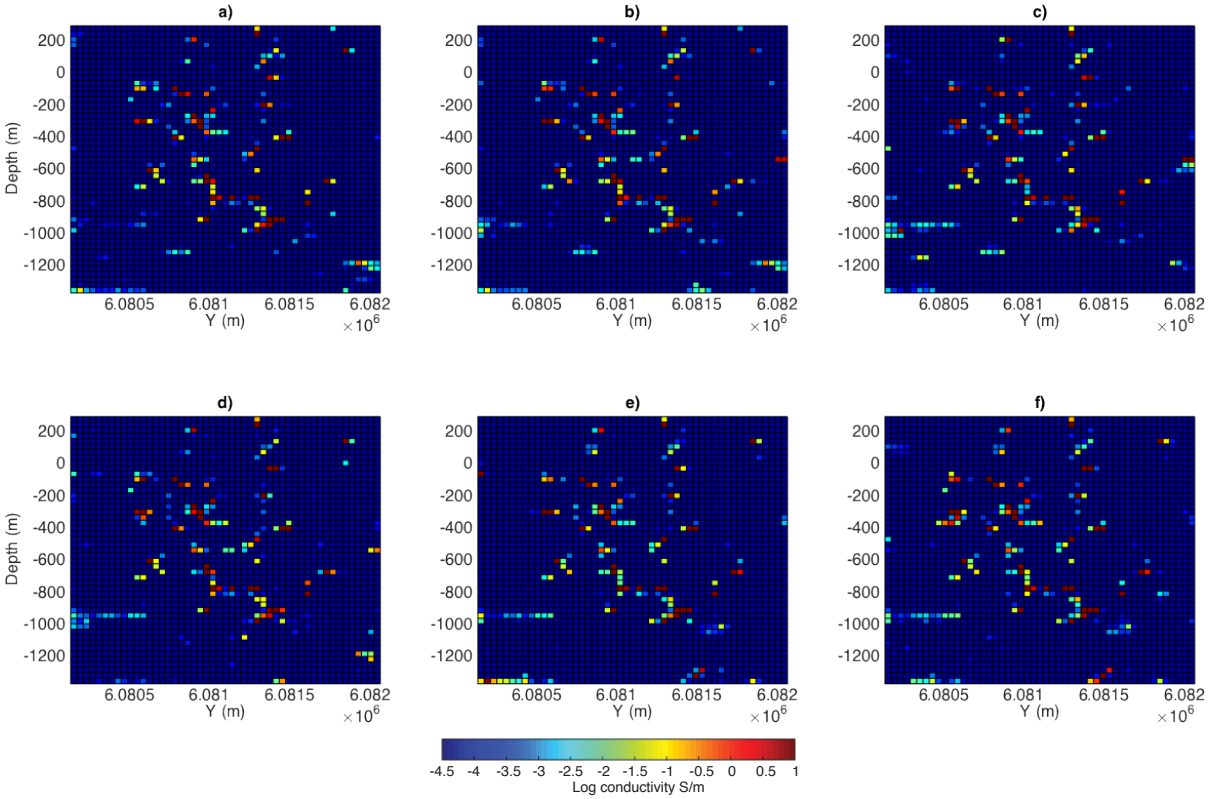

FIGURE 3.32 : Vertical section at $x = 4.267 \times 10^5$ of 3D conductivity models from the series generated using GDM optimization for iterations number a) 1 b) 20 c) 30 d) 50 e) 80 f) 100.

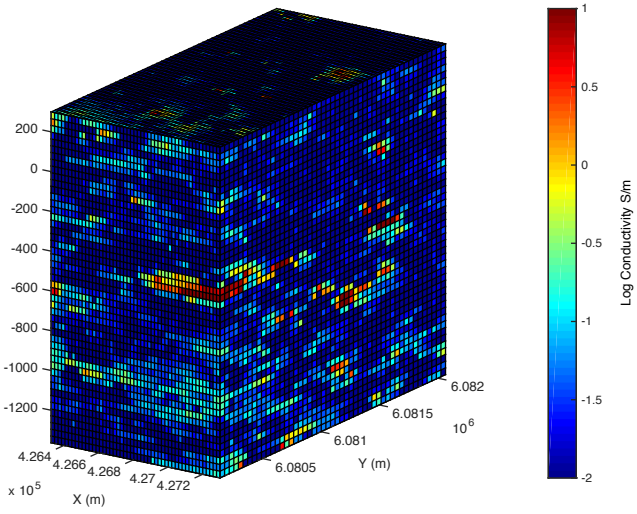

FIGURE 3.33 : Optimized conductivity model after 100 iterations

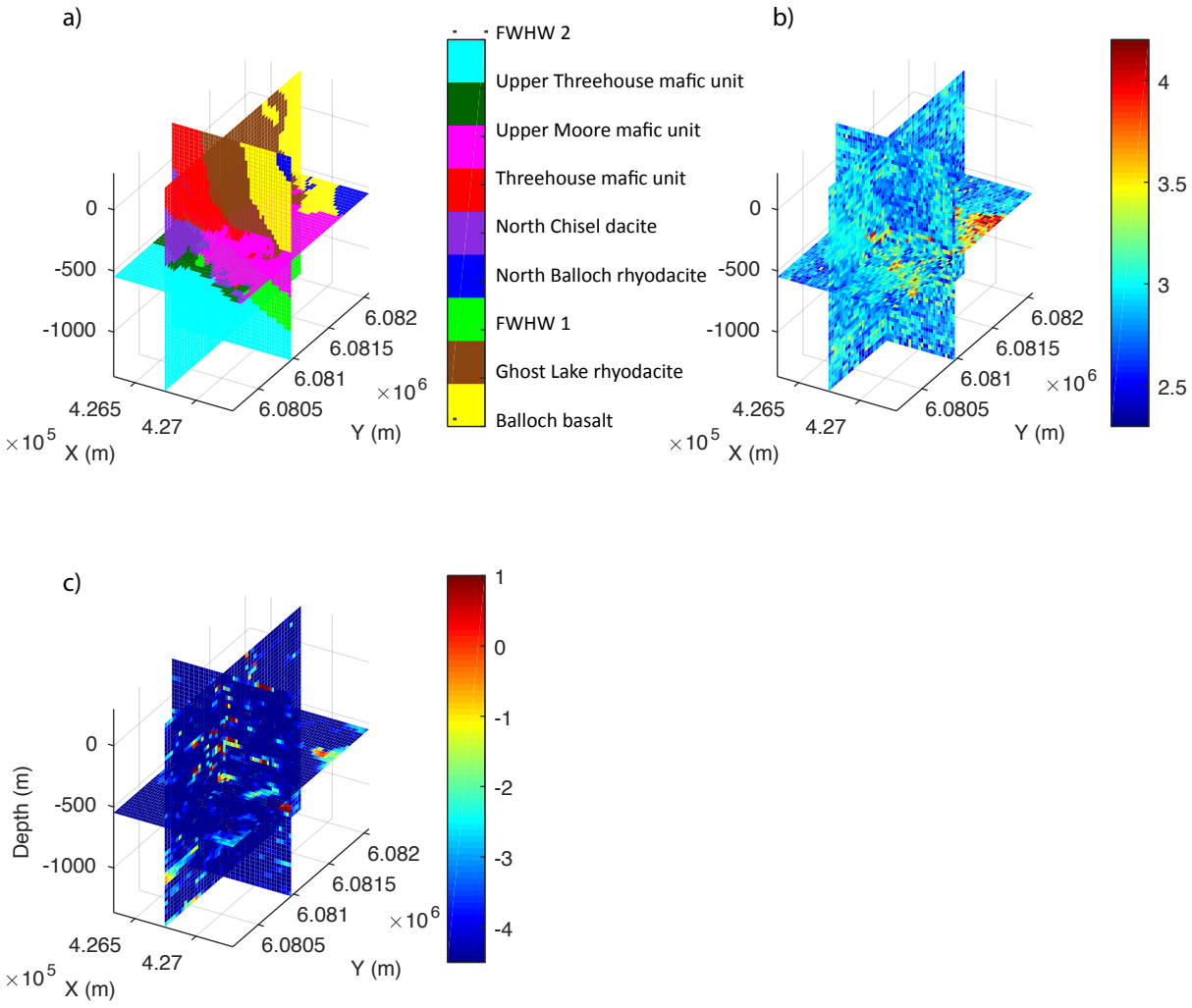

FIGURE 3.34 : a) Geological model, b) Optimized density model and c) Optimized conductivity model

4 DISCUSSION

This section reviews this research project by looking at its innovative aspects and then critically examining some of its methodological aspects. Despite the great effort put in building the geological model, there are still inconsistencies between the provided geological model and the geophysical models, notably, in terms of physical properties. Indeed, geological units that have been classified in the same category show different geophysical responses. This has an impact on the results of the proposed methodology since geological units cannot be unambiguously assigned to a geophysical response.

The stochastic assimilation of gravimetry data has shown a significant improvement in terms of residual model and in terms of geological realism in comparison with the least-squares inversion. This sole point demonstrates the advantage and applicability of the proposed methodology to build better geo-models. It also allows for validation of the a priori geological model. One of the main advantages of the method is to build a unified numerical twin of the deposit. This means, re-uniting all the available data in a numerical model such that inconsistencies in the geological model can be detected. By populating this geological model with measured physical properties and computing the forward model it is possible to compare the expected value from the model with the measured data. This process allows us to see if there are major gaps in the underlying geological model. The stochastic assimilation methodology only allows for improvements in the starting model as the model keeps its general shape. The CSGS algorithm computed on each region allows us to reproduce the histograms and density models that are in accordance with the geological model. The classification of density values for each region is based on the boreholes passing through the regions and geological interpretation of value thresholds for each region.

Unfortunately the logged data for resistivity were of poor quality and made it more difficult to obtain reliable results. This may be related to a tool calibration problem in the field or in using the wrong type of tool for the resistivities encountered in the borehole. We still used the data that were available and followed our methodology to see what could be done. We can clearly see in the results that objective function decreases with this addition of new data. This indicates that even if the data is of questionable quality, the numerical model is improved from its original form that only included the density information. We can conclude that the model benefits from the integration

of high-resolution data even if it may be sparsely sampled in space. The Bayesian algorithm has the advantage of being able to incorporate strongly non-linear relationships between variables into simulation (Doyen, 2007). The joint probability density in this algorithm that is estimated using a non-parametric method is extremely flexible making it possible to calculate a probability density for any sorts of relations non-linear or multi-modal (Dubreuil-Boisclair, 2013). This was demonstrated in these results. It should be mentioned that due to the complex nature of the relationship between the density and conductivity data and lack of quality resistivity logs, the joint probability density model plays a critical role in the final conductivity model. Although the final conductivity model exhibits more discontinuities and compared to the density model shows less correspondence to the geological model, there is still a consistency between where the high conductivity and the high density values are retrieved in the final optimized conductivity and density models. It was shown that the optimized density model showed discontinuities in comparison with the initial geological model. The resolution of this model is controlled by the noise in the data and size of the grid cells. Since this density model is next used as the initial model in the Bayesian sequential simulation algorithm the level of discontinuities is yet increased.

The final 3D numerical model integrates, the geological conceptual model, the geological lithology information at the borehole, surface and downhole gravity surveys and surface and log resistivity data. The stochastic approach accounts for different sources of uncertainty including the uncertainty inherent to the geological model, the petrophysical relationship inferred from borehole from collocated data and the geophysical measurements. The simulation steps within the workflow consider these uncertainties through generation of multiple equiprobable realizations. In BSS step the uncertainty is accounted for in posterior distribution.

The GDM step consists of development of a set of codes for forward-modeling and combination of realizations for an optimization process.

In short the model developed here allows:

— to have a tangible tool that permits to reunite geological and geophysical knowledge. It eventually allows to identify zones where the geology and geophysics might not be consistent. It is then a valuable tool to start a discussion between experts with different backgrounds working on the same object which is the deposit.

— the assimilation of different geophysical data probing very different physical properties of a deposit to diminish the uncertainty on the final petrophysical model.

— performing a multiple scale data integration, permitting to assimilate each data at its own spatial resolution.

Future studies could be carried out to explore a modified version of the methodology used in the present study in order to change the sequence of forward modelling steps for different geophysical data. In the present study the logic of the sequence in the workflow is based on going from low-resolution to high-resolution data. The possibility of computing the forward modelling steps in parallel and integration of these data could also be examined in future work. The application of the method could also be tested on a deposit for which data acquisition has continued after building the geological model and the data are available to validate the anomalous zones detected by the geophysical models.

5 CONCLUSION

Understanding the relationships between geology, rock physical properties and geophysical responses is very important for integrating geological and geophysical data in order to improve resources management and recovery. The purpose of this work was to study geological and geophysical data integration with the objective of building geologically plausible geophysical models. To this end, we proposed a new approach consisting of using a priori geological model as a training image for multiple-point simulations of geological units. We then applied conditional sequential Gaussian simulation to simulate multiple equiprobable scenarios of the physical properties based on geological and geophysical logs. Surface and borehole raw measurements were then used to combine the different realizations leading to an optimal 3D petrophysical geo-model. The proposed data integration method has the advantage of avoiding any matrix inversion and over-smoothing effects as is normally the case with conventional least-squares inversion methods. By the assimilation of all the available data (geology, borehole logs, surface geophysical data), the model obtained from stochastic inversion explicitly represents the complex geology of the deposit and the spatial variation of the density contrasts caused by the orebody. This meets the main objective of the thesis.

The geophysical data were integrated following a coarse to fine resolution scheme: integrating the data with the lowest resolution first in order to get the long wavelengths structures and then adding the finer resolution data in order to increase the resolution content within the model. This is the reason why we first modelled the geology, then we added the gravimetry to finish with the resistivity data.

We decided to use gradual deformation scheme in order to optimize the misfit between measured and computed data. This choice leads to one best model per norm. We might have decided to utilize other types of assimilation techniques such as ensemble methods that permits to carry an ensemble of stochastic models up to the end of the assimilation. We could also have chosen to use heuristic methods such as simulated annealing or emerging technique such as deep neural networks. In our case, we wanted to develop a workflow applicable to real data that is quick and reliable. Gradual deformation possess those two qualities.

The fundamental piece of information for the success of our methodology is to have collocated geological and physical data. This has been a game changer in the oil industry in the 70s and

could also be for the mining industry. Indeed, many research groups, private or public, spend time to establish petrophysical relations between physical properties and key reservoir parameters. However, during the time allowed for this thesis, we just explored the surface of the petrophysical relations. We claim here that much more effort must be put in the understanding of petrophysical relations in order to improve the geological model of the deposit under study. Also, electrical geophysical loggings were not of very high quality which has prevented a more meaningful use of these data.

REFERENCES

Alabert FG (1987) *Stochastic imaging of spatial distributions using hard and soft information. Ms. Sc*. Thèse de doctorat, Stanford University.

Armstrong M (1998) *Basic linear geostatistics*. Springer Science & Business Media.

Arpat GB, Caers J (2007) Conditional simulation with patterns. *Mathematical Geology*, 39(2):177–203.

Asli M, Marcotte D, Chouteau M (2000) Direct inversion of gravity data by cokriging. *Geostatistics 2000 Cape Town*, pages 64–73.

Aster RC, Borchers B, Thurber CH (2018) *Parameter estimation and inverse problems*. Elsevier.

Bailes AH (2013) Logging notes for the 17 Lalor drill holes (unpublished report).

Bailes AH, Galley AG (2007) *Geology of the Chisel-Anderson lakes area, Snow Lake, Manitoba (NTS areas 63K16SW and west half of 63J13SE)*. Manitoba Science, Technology, Energy and Mines, Manitoba Geological Survey.

Bayes T (1763) Lii. an essay towards solving a problem in the doctrine of chances. by the late rev. mr. bayes, frs communicated by mr. price, in a letter to john canton, amfr s. *Philosophical transactions of the Royal Society of London*, (53):370–418.

Bellefleur G, Schetselaar E, Craven JE (2015a) *Targeted geoscience initiative 4: A synthesis of the methodology project at the Lalor VMS deposit, Manitoba*. Natural Resources Canada,Open File 7863, 50 pages.

Bellefleur G, Schetselaar E, White D, Miah K, Dueck P (2015b) 3d seismic imaging of the lalor volcanogenic massive sulphide deposit, manitoba, canada. *Geophysical Prospecting*, 63(4):813–832.

Beyer L (1987) Porosity of unconsolidated sand, diatomite, and fractured shale reservoirs, south belridge and west cat canyon oil fields, california: Section iv. exploration methods.

Bing Z, Greenhalgh S (2001) Finite element three dimensional direct current resistivity modelling: accuracy and efficiency considerations. *Geophysical Journal International*, 145(3):679–688.

Bishop J, Lewis R (1992) Geophysical signatures of australian volcanic-hosted massive sulfide deposits. *Economic Geology*, 87(3):913–930.

Blais RA, Carlier PA (1968) Applications of geostatistics in ore evaluation. *CIM spec*, 9:41–68.

Blakely RJ (1996) *Potential theory in gravity and magnetic applications*. Cambridge university press.

Blakley IT, Geo P (2008) Technical report on the lalor lake deposit, snow lake, manitoba, canada.

Bosch M, Meza R, Jiménez R, Hönig A (2006) Joint gravity and magnetic inversion in 3d using Monte Carlo methods. *Geophysics*, 71(4):G153–G156.

Bosch M, Mukerji T, Gonzalez EF (2010) Seismic inversion for reservoir properties combining statistical rock physics and geostatistics: A review. *Geophysics*, 75(5):75A165–75A176.

Bouchedda A, Tirdad S, Gloaguen E, Giroux B (2016) Small scale conductivity estimation using dc resitivity and well logs data-lalor case study. *78th EAGE Conference and Exhibition 2016*.

Bowman A, Foster P (1993) Density based exploration of bivariate data. *Statistics and computing*, 3(4):171–177.

Brent RP (1973) *Algorithms for Minimization without Derivatives, chap. 4*.

Burmeister B (1988) From resource to reality: a critical review of the achievements of new australian gold mining projects during the period january 1983 to september 1987. *Macquarie University*.

Caers J (2007) Comparing the gradual deformation with the probability perturbation method for solving inverse problems. *Mathematical Geology*, 39(1):27–52.

Caers J, Hoffman T (2006) The probability perturbation method: a new look at bayesian inverse modeling. *Mathematical geology*, 38(1):81–100.

Caers J, Journel AG (1998) Stochastic reservoir simulation using neural networks trained on outcrop data. *SPE Annual Technical Conference and Exhibition*, Society of Petroleum Engineers.

Caers J, Zhang T (2004) Multiple-point geostatistics: a quantitative vehicle for integrating geologic analogs into multiple reservoir models. in integration of outcrop and modern analogs in reservoir modeling. *AAPG Memoir 80*, pages 383–394.

Carter R, Schwartz T, West S, Hoover K (2012) Pre-feasibility study technical report, on the lalor deposit, snow lake, manitoba, canada.

Caté A (2016) *Geology of the Paleoproterozoic Zn-Cu-Au Lalor volcanogenic massive sulphide deposit and its gold-rich lenses, Snow Lake, Manitoba./Géologie du gisement de sulfures massifs volcanogène Paléoprotérozoïque à Zn-Cu-Au de Lalor et de ses lentilles riches en or, Snow Lake, Manitoba.* Thèse de doctorat, Université du Québec, Institut national de la recherche scientifique.

Caté A, Mercier-Langevin P, Ross P, Duff S, Hannington M, Dubé B, Gagné S (2013) Preliminary observations on the geological environment of the paleoproterozoic auriferous volcanogenic massive sulfide deposit of lalor, snow lake, manitoba. *Geological Survey of Canada, Open File 7372*, 13 pages. DOI:10.4095/292516.

Caté A, Mercier-Langevin P, Ross PS, Duff S, Hannington MD, Dubé B, Gagné S (2015) Geology and au enrichment processes at the paleoproterozoic lalor auriferous volcanogenic massive sulphide deposit, snow lake, manitoba. *Geological Survey of Canada*.

Caté A, Perozzi L, Gloaguen E, Blouin M (2017) Machine learning as a tool for geologists. *The Leading Edge*, 36(3):215–219.

Caté A, Schetselaar E, Mercier-Langevin P, Ross PS (2018) Classification of lithostratigraphic and alteration units from drillhole lithogeochemical data using machine learning: A case study from the lalor volcanogenic massive sulphide deposit, snow lake, manitoba, canada. *Journal of Geochemical Exploration*, 188:216–228.

Chasseriau P, Chouteau M (2003) 3d gravity inversion using a model of parameter covariance. *Journal of applied geophysics*, 52(1):59–74.

Chatterjee S, Dimitrakopoulos R, Mustapha H (2009) Three-dimensional wavelet based conditional co-simulation using training image. *COSMO Res Rep*, 3(2):143–181.

Cheraghi S, Craven JA, Bellefleur G (2015) Feasibility of virtual source reflection seismology using interferometry for mineral exploration: A test study in the lalor lake volcanogenic massive sulphide mining area, manitoba, canada. *Geophysical Prospecting*, 63(4):833–848.

Chiles JP, Delfiner P (2009) *Geostatistics: modeling spatial uncertainty*. volume 497. John Wiley & Sons.

Chugunova TL, Hu LY (2008) Multiple-point simulations constrained by continuous auxiliary data. *Mathematical geosciences*, 40(2):133–146.

Claprood M, Gloaguen E, Giroux B, Duchesne M, Malo M (2013) Modelling the porosity of the saint-flavien gas reservoir by geostatistical methods. Report No. INRSCO2-2013-V2. 13, presented to the Ministère du Développement durable, de l'Environnement et des Parcs du Québec (in French).

Clow G (1991) Why gold mines fail. *Northern miner magazine*, 6(2):31–34.

Crossley D, Hinderer J, Riccardi U (2013) The measurement of surface gravity. *Reports on Progress in physics*, 76(4):046101.

Daly C (2005) Higher Order Models using Entropy, Markov Random Fields and Sequential Simulation. *Geostatistics Banff 2004*. Leuangthong O, Deutsch CV (éditeurs), Springer Netherlands, numéro 14 de Quantitative Geology and Geostatistics, pages 215–224.

David M (1969). The notion of extension variance and its application to the grade estimation of stratiform deposits. *A decade of digital computing in the mineral industry: Am. Inst. Mining Metallurgical and Petroleum Eng*.

David M (1977). Geostatistical ore reserve estimation: Elsevier sci. *Publ Co, New York*.

David M (1988). *Development in Geomathematics 6, handbook of Applied Advanced Geostatistical Ore reserve estimation*.

David M (2012). *Geostatistical ore reserve estimation*. Elsevier.

Deheuvels P (1977). Estimation non paramétrique de la densité par histogrammes généralisés. *Revue de Statistique Appliquée*, 25(3):5–42.

Dekkers A, Aarts E (1991). Global optimization and simulated annealing. *Mathematical programming*, 50(1-3):367–393.

Deutsch CV (2002). Geostatistical reservoir modeling. *Applied Geostatistics Series, G., JA, Ed., Oxford University Press, New York, USA*.

Deutsch CV, Journel AG, others (1998). Geostatistical software library and user's guide. *Oxford University Press, New York*.

Dey A, Morrison HF (1979). Resistivity modeling for arbitrarily shaped three-dimensional structures. *Geophysics*, 44(4):753–780.

Dimitrakopoulos R (1990). Conditional simulation of intrinsic random functions of orderk. *Mathematical Geology*, 22(3):361–380.

Dimitrakopoulos R (1994). *Geostatistics for the next century*. Kluwer.

Dimitrakopoulos R (1998). Conditional simulation algorithms for modelling orebody uncertainty in open pit optimisation. *International journal of surface mining, reclamation and environment*, 12(4):173–179.

Dimitrakopoulos R, Farrelly C, Godoy M (2002). Moving forward from traditional optimization: grade uncertainty and risk effects in open-pit design. *Mining Technology*, 111(1):82–88.

Dimitrakopoulos R, Martinez L, Ramazan S (2007). A maximum upside/minimum downside approach to the traditional optimization of open pit mine design. *Journal of Mining Science*, 43(1):73–82.

Dominy S, Annels A, Noppe M (2002). Errors and uncertainty in ore reserve estimates—operator beware. *Proceedings, Underground Operators Conference*, pages 121–126.

dos Santos GJ, Ribeiro DT, Pereira CA (2014). Methodology for selection of samples from borehole probe for technological characterization of iron ore. *Rem: Revista Escola de Minas*, 67(3):271–277.

Doyen P (2007). *Seismic reservoir characterization: An earth modelling perspective*. volume 2. EAGE publications Houten.

Doyen PM, Den Boer LD (1996). *Bayesian sequential Gaussian simulation of lithology with non-linear data*. US Patent 5,539,704.

Dubreuil-Boisclair C (2013). *Modélisation stochastique du réservoir d'hydrates de gaz de Mallik*. Thèse de doctorat, Université du Québec, Institut national de la recherche scientifique.

Dubreuil-Boisclair C, Gloaguen E, Bellefleur G, Marcotte D (2012). Non-Gaussian gas hydrate grade simulation at the Mallik site, Mackenzie Delta, Canada. *Marine and Petroleum Geology*, 35(1):20–27. DOI:10.1016/j.marpetgeo.2012.02.020.

Dubreuil-Boisclair C, Gloaguen E, Marcotte D, Giroux B (2011). Heterogeneous aquifer characterization from ground-penetrating radar tomography and borehole hydrogeophysical data using nonlinear bayesian simulations. *Geophysics*, 76(4):J13–J25.

Dubrule O (2003). *Geostatistics for seismic data integration in earth models*. Society of Exploration Geophysicists and European Association of Geoscientists and Engineers.

Duff S (2016). *Ore Types of the Auriferous Lalor VMS Deposit, Snow Lake, Manitoba: Implications for Genesis and Post Depositional Processes*. Thèse de doctorat, Université d'Ottawa/University of Ottawa.

Duff S, Hannington M, Caté A, Mercier-Langevin P, Kjarsgaard I (2015). Major ore types of the paleoproterozoic lalor auriferous volcanogenic massive sulphide deposit, snow lake, manitoba. *Targeted geoscience initiative*, 4:147–170.

Eidsvik J, Avseth P, Omre H, Mukerji T, Mavko G (2004). Stochastic reservoir characterization using prestack seismic data. *Geophysics*, 69(4):978–993.

Epanechnikov VA (1969). Non-parametric estimation of a multivariate probability density. *Theory of Probability & Its Applications*, 14(1):153–158.

Evensen G (2003). The ensemble kalman filter: Theoretical formulation and practical implementation. *Ocean dynamics*, 53(4):343–367.

Feller W (2008). *An introduction to probability theory and its applications*. volume 2. John Wiley & Sons.

Feraille M, Roggero F, Manceau E, Hu L, Zabalza-Mezghani I, Reis LC et al. (2003). Application of advanced history matching techniques to an integrated field case study. *SPE Annual technical conference and exhibition*, Society of Petroleum Engineers.

Fletcher R (2013). *Practical methods of optimization*. John Wiley & Sons.

Forsythe GE, Malcolm MA, Moler CB (1977). *Computer methods for mathematical computations*. volume 259. Prentice-Hall Englewood Cliffs, NJ.

Fouguet C, Armstrong M, Dowd PA (1994). *Reminders on the Kriging. Geostatistical Simulations*. Eds. , M. and Dowd, PA, Kluwer Academic Publishers.

Fowler C, Stead D, Pandit B, Janser B, Nisbet E, Nover G (2005). A database of physical properties of rocks from the trans-hudson orogen, canada. *Canadian Journal of Earth Sciences*, 42(4):555–572.

Franklin JN (1970). Well-posed stochastic extensions of ill-posed linear problems. *Journal of Mathematical Analysis and Applications*, 31(3):682–716.

Fullagar PK, Pears GA, McMonnies B (2008). Constrained inversion of geologic surfaces—pushing the boundaries. *The Leading Edge*, 27(1):98–105.

Galley AG, Syme E, Bailes AH, Goodfellow W (2007). Metallogeny of the paleoproterozoic flin flon belt, manitoba and saskatchewan. *Geological Association of Canada, Mineral Deposits Division*, pages 509–531.

Gastaldi C, Roy D, Doyen P, Den Boer L (1998). Using bayesian simulations to predict reservoir thickness under tuning conditions. *The Leading Edge*, 17(4):539–539.

Gill PE, Murray W, Wright MH (1981). Practical optimization. *London: Academic Press, 1981*.

Giroux B, Gloaguen E, Chouteau M (2007). bh_tomo—a matlab borehole georadar 2d tomography package. *Computers & Geosciences*, 33(1):126–137.

Gloaguen E, Dimitrakopoulos R (2009). Two-dimensional Conditional Simulations Based on the Wavelet Decomposition of Training Images. *Mathematical Geosciences*, 41(6):679–701. DOI:10.1007/s11004-009-9235-3.

Gloaguen E, Marcotte D, Chouteau M, Perroud H (2005). Borehole radar velocity inversion using cokriging and cosimulation. *Journal of Applied Geophysics*, 57(4):242–259.

Gómez-Hernández JJ, Journel AG (1993). Joint sequential simulation of multigaussian fields. *Geostatistics Troia'92*, Springer, pages 85–94.

Goovaerts P (1997). *Geostatistics for natural resources evaluation*. Oxford university press.

Grana D, Mukerji T, Dvorkin J, Mavko G (2012). Stochastic inversion of facies from seismic data based on sequential simulations and probability perturbation method. *Geophysics*, 77(4):M53–M72.

Guardiano FB, Srivastava RM (1993). Multivariate geostatistics: beyond bivariate moments. *Geostatistics Troia'92*, Springer, pages 133–144.

Haas A, Dubrule O (1994). Geostatistical inversion-a sequential method of stochastic reservoir modelling constrained by seismic data. *First break*, 12(11):561–569.

Haáz I (1953). Relations between the potential of the attraction of the mass contained in a finite rectangular prism and its first and second derivatives. *Geophysical Transactions II*, 7:57–66.

Halton JH (1970). A retrospective and prospective survey of the Monte Carlo method. *Siam review*, 12(1):1–63.

Hansen TM, Journel AG, Tarantola A, Mosegaard K (2006). Linear inverse Gaussian theory and geostatistics. *Geophysics*, 71(6):R101–R111.

Hinton G, Srivastava N, Swersky K (2012). Overview of mini-batch gradient descent. *Neural Networks for Machine Learning*, 575.

Hinze WJ (1990). The role of gravity and magnetic methods in engineering and environmental studies. *Geotechnical an Environmental Geophysics: Volume I: Review and Tutorial*, Society of Exploration Geophysicists, pages 75–126.

Hoffman BT (2005). *Geologically consistent history matching while perturbing facies*. Thèse de doctorat.

Hu LY (2000). Gradual deformation and iterative calibration of gaussian-related stochastic models. *Mathematical Geology*, 32(1):87–108.

Hu LY (2002). Combination of dependent realizations within the gradual deformation method. *Mathematical Geology*, 34(8):953–963.

Hu LY, Blanc G, Noetinger B (2001). Gradual deformation and iterative calibration of sequential stochastic simulations. *Mathematical Geology*, 33(4):475–489.

Isaaks E, Srivastava R (1989). *An Introduction to Applied Geostatistics, New York: Oxford Univ*.

Isaaks EH (1992). The application of monte carlo methods to the analysis of spatially correlated data.

Jageler A et al. (1976). Improved hydrocarbon reservoir evaluation through use of borehole-gravimeter data. *Journal of Petroleum Technology*, 28(06):709–718.

Journel A (1992). Computer imaging in the minerals industry-beyond mere aesthetics. *APCOM'92 Computer Applications in the Minerals Industries 23rd International Symposium*.

Journel A, Zhang T (2006). The necessity of a multiple-point prior model. *Mathematical Geology*, 38(5):591–610.

Journel AG (1974). Geostatistics for conditional simulation of ore bodies. *Economic Geology*, 69(5):673–687.

Journel AG (1993). Geostatistics: Roadblocks and Challenges. *Geostatistics Tróia '92*. Soares A, éditeur, Springer Netherlands, numéro 5 de Quantitative Geology and Geostatistics, pages 213–224.

Journel AG (1994). Modeling uncertainty: some conceptual thoughts. *Geostatistics for the next century*, Springer, pages 30–43.

Journel AG, Huijbregts CJ (1978). *Mining geostatistics*. volume 600. Academic press London.

Kelkar M, Perez G, Chopra A (2002). *Applied geostatistics for reservoir characterization*. Society of petroleum engineers Richardson, TX.

Kirkpatrick S (1984). Optimization by simulated annealing: Quantitative studies. *Journal of statistical physics*, 34(5-6):975–986.

Klefstad G, Sendlein LV, Palmquist RC (1977). Limitations of the electrical resistivity method in landfill investigations. *Groundwater*, 15(5):418–427.

Knoll K (1989). And now the bad news. *Northern miner magazine*, 4(6):48–52.

Krige DG (1951). A statistical approach to some basic mine valuation problems on the witwatersrand. *Journal of the Southern African Institute of Mining and Metallurgy*, 52(6):119–139.

Kumral M, Dowd P (2001). Short-term scheduling for industrial minerals using multi-objective simulated annealing, apcom 2001, phoenix, arizona.

LaFehr T (1983). Rock density from borehole gravity surveys. *Geophysics*, 48(3):341–356.

Le Ravalec M, Hu LY, Noetinger B et al. (1999). Stochastic reservoir modeling constrained to dynamic data: local calibration and inference of the structural parameters. *SPE Annual Technical Conference and Exhibition*, Society of Petroleum Engineers.

Le Ravalec M, Mouche E (2012). Calibrating transmissivities from piezometric heads with the gradual deformation method: An application to the culebra dolomite unit at the waste isolation pilot plant (wipp), new mexico, usa. *Journal of hydrology*, 472:1–13.

Le Ravalec-Dupin M (2011). *Introduction a l'inversion géostatistique des écoulements en milieux poreux*.

Le Ravalec-Dupin M, Hu L (2007). Combining the pilot point and gradual deformation methods for calibrating permeability models to dynamic data. *Oil & Gas Science and Technology-Revue de l'IFP*, 62(2):169–180.

Lee Ty, Kravaris C, Seinfeld J (1986). History matching by spline approximation and regularization in single-phase areal reservoirs.

Leney GW (1966). Field studies in iron ore geophysics. *Mining geophysics*, 1:391.

Li X, Chouteau M (1998). Three-dimensional gravity modeling in all space. *Surveys in Geophysics*, 19(4):339–368.

Loke M, Chambers J, Rucker D, Kuras O, Wilkinson P (2013). Recent developments in the direct-current geoelectrical imaging method. *Journal of applied geophysics*, 95:135–156.

Maharaja A (2008). TiGenerator: Object-based training image generator. *Computers & Geosciences*, 34(12):1753–1761. DOI:10.1016/j.cageo.2007.08.012.

Maillot E, Sumner J (1966). Electrical properties of porphyry deposits at ajo, morenci, and bisbee, arizona. *Mining geophysics*, 1:273–287.

Makhlouf EM, Chen WH, Wasserman ML, Seinfeld JH et al. (1993). A general history matching algorithm for three-phase, three-dimensional petroleum reservoirs. *SPE Advanced Technology Series*, 1(02):83–92.

Mantica S, Cominelli A, Mantica G et al. (2001). Combining global and local optimization techniques for automatic history matching production and seismic data. *SPE Reservoir Simulation Symposium*, Society of Petroleum Engineers.

Mariethoz G, Renard P, Straubhaar J (2010). The Direct Sampling method to perform multiple-point geostatistical simulations. *Water Resources Research*, 46(11).

Matheron G (1963). Principles of geostatistics. *Economic geology*, 58(8):1246–1266.

McCulloh TH (1965). A confirmation by gravity measurements of an underground density profile based on core densities. *Geophysics*, 30(6):1108–1132.

McCulloh TH (1967). *The US Geological Survey: LaCoste and Romberg Precise Borehole Gravimeter System Test Results*. US Geological Survey.

McLachlan GJ, Basford KE (1988). *Mixture models: Inference and applications to clustering*. volume 84. M. Dekker New York.

Meju MA (1994). *Geophysical data analysis: understanding inverse problem theory and practice*. Society of Exploration Geophysicists.

Menke W (1984). Geophysical data analysis. discrete inverse theory. academic press, new york, 312 p.

Menke W (2018). *Geophysical data analysis: Discrete inverse theory*. Academic press.

Mercier-Langevin P, Hannington MD, Dubé B, Bécu V (2011). The gold content of volcanogenic massive sulfide deposits. *Mineralium Deposita*, 46(5-6):509–539.

Monjezi M, Kashani MR, Ataei M (2013). A comparative study between sequential gaussian simulation and kriging method grade modeling in open-pit mining. *Arabian Journal of Geosciences*, 6(1):123–128.

Morgan LA (2012). Geophysical characteristics of volcanogenic massive sulfide deposits. *Volcanogenic Massive Sulfide Occurrence Model. US Geological Survey, Reston, VA*, 115:131.

Mosegaard K, Tarantola A (1995). Monte Carlo sampling of solutions to inverse problems. *Journal of Geophysical Research: Solid Earth*, 100(B7):12431–12447.

Mustapha H, Dimitrakopoulos R (2010). High-order Stochastic Simulation of Complex Spatially Distributed Natural Phenomena. *Mathematical Geosciences*, 42(5):457–485. DOI:10.1007/s11004-010-9291-8.

Newton O, Vowles A (2017). Geophysical overview of lalor vms deposit. *Exploration 17: Sixth Decennial International Conference on Mineral Exploration*, Decennial Minerals Exploration Conferences (DMEC).

Nind C, Seigel HO, Chouteau M, Giroux B (2007). Development of a borehole gravimeter for mining applications. *First Break*, 25(7).

Nind CJ, MacQueen JD, Wasylechko R et al. (2013). The borehole gravity meter: Development and results (russian). *SPE Arctic and Extreme Environments Technical Conference and Exhibition*, Society of Petroleum Engineers.

Nocedal J, Wright S (2006). *Numerical optimization*. Springer Science & Business Media.

Oliver DS, Chen Y (2011). Recent progress on reservoir history matching: a review. *Computational Geosciences*, 15(1):185–221.

Oliver DS, Reynolds AC, Liu N (2008). *Inverse theory for petroleum reservoir characterization and history matching*. Cambridge University Press.

Ouenes A, Doddi RS, Lin Y, Cunningham G, Saad N (1994). A new approach combining neural networks and simulated annealing for solving petroleum inverse problems. *ECMOR IV-4th European Conference on the Mathematics of Oil Recovery*.

Parker RL, Parker RL (1994). *Geophysical inverse theory*. Princeton university press.

Parzen E (1962). On estimation of a probability density function and mode. *The annals of mathematical statistics*, 33(3):1065–1076.

Paterson NR, Reeves CV (1985). Applications of gravity and magnetic surveys: The state-of-the-art in 1985. *Geophysics*, 50(12):2558–2594.

Perozzi L, Gloaguen E, Rondenay S, McDowell G (2012). Using stochastic crosshole seismic velocity tomography and bayesian simulation to estimate ni grades: Case study from voisey's bay, canada. *Journal of Applied Geophysics*, 78:85–93.

Popta JV, Heywood J, Adams S, Bostock D et al. (1990). Use of borehole gravimetry for reservoir characterisation and fluid saturation monitoring. *European Petroleum Conference*, Society of Petroleum Engineers.

Ramazan S, Dimitrakopoulos R (2018). Stochastic optimisation of long-term production scheduling for open pit mines with a new integer programming formulation. *Advances in Applied Strategic Mine Planning*, Springer, pages 139–153.

Ravenscroft P (1992). Risk analysis for mine scheduling by conditional simulation. *Transactions of the Institution of Mining and Metallurgy. Section A. Mining Industry*, 101.

Roggero F, Hu L et al. (1998). Gradual deformation of continuous geostatistical models for history matching. *SPE annual technical conference and exhibition*, Society of Petroleum Engineers.

Rosenblatt M (1956). Remarks on some nonparametric estimates of a density function. *The Annals of Mathematical Statistics*, pages 832–837.

Ross HP, Mackelprang CE, Wright PM (1990). Dipole-dipole electrical resistivity surveys at waste disposal study sites in northern utah. *Geotechnical and environmental geophysics*, 2:145–152.

Roy A (1972). Depth of investigation in wenner, three-electrode and dipole-dipole dc resistivity methods. *Geophysical Prospecting*, 20(2):329–340.

Ruggeri P (2014). *Quantitative integration of geophysical and hydraulic data: from the local towards the regional scale range*. Thèse de doctorat, Université de Lausanne, Faculté des géosciences et de l'environnement.

Ruggeri P, Irving J, Gloaguen E, Holliger K (2013). Regional–scale integration of multiresolution hydrological and geophysical data using a two-step bayesian sequential simulation approach. *Geophysical Journal International*, 194(1):289–303.

Scheidt C, Caers J (2008). Representing Spatial Uncertainty Using Distances and Kernels. *Mathematical Geosciences*, 41(4):397–419. DOI:10.1007/s11004-008-9186-0.

Schetselaar E, Bellefleur G, Craven J, Roots E, Cheraghi S, Shamsipour P, Caté A, Mercier-Langevin P, El Goumi N, Enkin R et al. (2018). Geologically driven 3d modelling of physical rock properties in support of interpreting the seismic response of the lalor volcanogenic massive sulphide deposit, snow lake, manitoba, canada. *Geological Society, London, Special Publications*, 453(1):57–79.

Schetselaar E, Shamsipour P (2015). Interpretation of borehole gravity data of the Lalor volcanogenic massive sulfide deposit, Snow Lake, Manitoba, Canada. *Interpretation*, 3(3):T145–T154. DOI:10.1190/INT-2014-0188.1.

Schetselaar E, Shamsipour P, Bellefleur G (2014). High resolution common earth modelling of the lalor vms deposit. *BC Geophysical Society Lalor Lake Symposium*.

Schwartz F, McClymont G (1977). Applications of surface resistivity methods. *Groundwater*, 15(3):197–202.

Sen MK, Stoffa PL (1991). Nonlinear one-dimensional seismic waveform inversion using simulated annealing. *Geophysics*, 56(10):1624–1638.

Shamsipour P, Chouteau M, Marcotte D (2011a). 3d stochastic inversion of magnetic data. *Journal of Applied Geophysics*, 73(4):336–347.

Shamsipour P, Marcotte D, Chouteau M (2012). 3d stochastic joint inversion of gravity and magnetic data. *Journal of Applied Geophysics*, 79:27–37.

Shamsipour P, Marcotte D, Chouteau M, Allard M (2011b). Stochastic inversion of a gravity field on multiple scale parameters using surface and borehole data. *Geophysical prospecting*, 59(6):998–1012.

Shamsipour P, Marcotte D, Chouteau M, Keating P (2010). 3d stochastic inversion of gravity data using cokriging and cosimulation. *Geophysics*, 75(1):I1–I10.

Shamsipour P, Schetselaar E, Bellefleur G, Marcotte D (2014). 3d stochastic inversion of potential field data using structural geologic constraints. *Journal of Applied Geophysics*, 111:173–182.

Sharpe R, Mirza A, Regis J (2014). *Titan 24: three lines of deep dcip and mt at the lalor deposit*.

Silverman BW (2018). *Density estimation for statistics and data analysis*. Routledge.

Sinclair AJ, Blackwell GH (2006). *Applied mineral inventory estimation*. Cambridge University Press.

Skjervheim JA, Evensen G, Aanonsen SI, Ruud BO, Johansen TA et al. (2005). Incorporating 4d seismic data in reservoir simulation models using ensemble kalman filter. *SPE Annual Technical Conference and Exhibition*, Society of Petroleum Engineers.

Smith M, Dimitrakopoulos R (1999). The influence of deposit uncertainty on mine production scheduling. *International Journal of Surface Mining, Reclamation and Environment*, 13(4):173–178.

Smith NJ (1950). The case for gravity data from boreholes. *Geophysics*, 15(4):605–636.

Straubhaar J, Renard P, Mariethoz G, Froidevaux R, Besson O (2011). An improved parallel multiple-point algorithm using a list approach. *Mathematical Geosciences*, 43(3):305–328.

Strebelle S (2002). Conditional Simulation of Complex Geological Structures Using Multiple-Point Statistics. *Mathematical Geology*, 34(1):1–21. DOI:10.1023/A:1014009426274.

Strébelle S, Journel AG (2000). Sequential simulation drawing structures from training images.

Tarantola A (2005). *Inverse problem theory and methods for model parameter estimation*. SIAM.

Taylor C (2014). Mine scale description of the mineralization at the lalor deposit, snow lake, manitoba, canada. *Proceedings from Exploration for Deep VMS Ore Bodies: The HudBay Lalor Case Study*, pages 1–3.

Thomas M, Walker J, Keating P, Shives R, Kiss F, Goodfellow W (2000). Geophysical atlas of massive sulphide signatures, bathurst mining camp, new brunswick, geological survey of canada, open file 3887; and new brunswick department of natural resources and energy. *Minerals and Energy Division, Open File*, 4:105.

Tikhonov AN, Arsenin VI (1977). *Solutions of ill-posed problems*. volume 14. Winston, Washington, DC.

Tirdad S, Gloaguen E, Bouchedda A, Dupuis JC (2019). Three-dimensional stochastic assimilation of gravity data in lalor volcanogenic massive sulphide, manitoba, canada. *Canadian Journal of Earth Sciences*, 56(5):556–568.

Tjelmeland H, Eidsvik J (2005). Directional Metropolis : Hastings Updates for Posteriors with Nonlinear Likelihoods. *Geostatistics Banff 2004*. Leuangthong O, Deutsch CV (éditeurs), Springer Netherlands, numéro 14 de Quantitative Geology and Geostatistics, pages 95–104.

Torres-Verdin C, Victoria M, Merletti G, Pendrel J (1999). Trace-based and geostatistical inversion of 3-D seismic data for thin-sand delineation: An application in San Jorge Basin, Argentina. *The Leading Edge*, 18(9):1070–1077.

Vallée M (2000). Mineral resource+ engineering, economic and legal feasibility= ore reserve. *CIM bulletin*, 93(1038):53–61.

Vargas HS, Caetano H, Mata-Lima H (2008). A new parallelization approach for sequential simulation. *geoENV VI–Geostatistics for Environmental Applications*, Springer, pages 489–496.

Verly G (1993). Sequential gaussian cosimulation: a simulation method integrating several types of information. *Geostatistics Troia'92*, Springer, pages 543–554.

Verly G (2005). Grade control classification of ore and waste: a critical review of estimation and simulation based procedures. *Mathematical geology*, 37(5):451–475.

Vries LMd, Carrera J, Falivene O, Gratacós O, Slooten LJ (2008). Application of Multiple Point Geostatistics to Non-stationary Images. *Mathematical Geosciences*, 41(1):29–42. DOI:10.1007/s11004-008-9188-y.

Wand M, Jones M (1995). Kernel smoothing chapman & hall. *Monographs on Statistics and Applied Probability, London*.

War SH (1988). The resistivity and induced polarization methods. *Symposium on the Application of Geophysics to Engineering and Environmental Problems 1988*, pages 109–250.

Wasylechko R, Bérubé P (2014). Borehole gravity over the lalor deposit. *BC Geophysical Society Lalor Lake Symposium*.

Webster R, Oliver MA (2007). *Geostatistics for environmental scientists*. John Wiley & Sons.

White D, Secord D, Malinowski M (2012). 3d seismic imaging of volcanogenic massive sulfide deposits in the flin flon mining camp, canada: Part 1—seismic results. *Geophysics*, 77(5):WC47–WC58.

Wu J, Boucher A, Zhang T (2008). A SGeMS code for pattern simulation of continuous and categorical variables: FILTERSIM. *Computers & Geosciences*, 34(12):1863–1876. DOI:10.1016/j.cageo.2007.08.008.

Wu X (2003). A 3-d finite-element algorithm for dc resistivity modelling using the shifted incomplete cholesky conjugate gradient method. *Geophysical Journal International*, 154(3):947–956.

Xu W, Journel A (1994). Dssim: A general sequential simulation algorithm. *Stanford Center for Reservoir Forecasting*.

Yang D, Fournier D, Kang S, Oldenburg DW (2018). Deep mineral exploration using multi-scale electromagnetic geophysics: the lalor massive sulphide deposit case study. *Canadian Journal of Earth Sciences*, 56(5):544–555.

Yang D, Oldenburg DW (2013). 3d conductivity models of lalor lake vms deposit from ground loop and airborne em data sets. *ASEG Extended Abstracts*, 2013(1):1–4.

Ying Z, Gomez J (2000). An improved deformation algorithm for automatic history matching. *Stanford Center for Reservoir Forecasting (SCRF)*.

Yrro BJF (2018). *Intégration de données électromagnétiques transitoires au sol et héliportées en Montérégie-Est par déformation graduelle*. Thèse de doctorat, École Polytechnique de Montréal.

Yungul S (1962). On: the role of the surface electrical methods of geophysical prospecting in the petroleum industry. *Geophysics*, 27(3):393–396.

Zhang T, Switzer P, Journel A (2006). Filter-Based Classification of Training Image Patterns for Spatial Simulation. *Mathematical Geology*, 38(1):63–80. DOI:10.1007/s11004-005-9004-x.